UCRL 8780

UNIVERSITY OF
CALIFORNIA

Ernest O. Lawrence

Radiation Laboratory

NUCLEAR REACTIONS OF LOW —Z ELEMENTS WITH 5.7 —Bev PROTONS: NUCLEAR STRUCTURE AND SIMPLE NUCLEAR REACTIONS

BERKELEY, CALIFORNIA

DISCLAIMER

UCRL-8780
Chemistry General

UNIVERSITY OF CALIFORNIA

Lawrence Radiation Laboratory
Berkeley, California

Contract No. W-7405-eng-48

NUCLEAR REACTIONS OF LOW-Z ELEMENTS WITH 5.7-Bev PROTONS: NUCLEAR STRUCTURE AND SIMPLE NUCLEAR REACTIONS

Paul A. Benioff

(Thesis)

July, 1959

Printed for the U. S. Atomic Energy Commission

Printed in USA. Price $2.75. Available from the
Office of Technical Services
U.S. Department of Commerce
Washington 25, D. C.

NUCLEAR REACTIONS OF LOW-Z ELEMENTS WITH 5.7-Bev PROTONS: NUCLEAR STRUCTURE AND SIMPLE NUCLEAR REACTIONS

Contents

NUCLEAR REACTIONS OF LOW-Z ELEMENTS WITH 5.7-Bev PROTONS: NUCLEAR STRUCTURE AND SIMPLE NUCLEAR REACTIONS

Paul A. Benioff
(Thesis)

Lawrence Radiation Laboratory and Department of Chemistry
University of California, Berkeley, California

July 1959

ABSTRACT

The first part of this work describes the results of 5.7-Bev proton bombardments of the target elements Be, C, N, O, F, Na, and Al. Production cross sections were obtained for many radioactive products with half lives between 1.2 minutes and 12 years. The p,pn cross sections for the targets C, N, O, F, and Na were found to be 29 ± 3 mb, 7.3 ± 0.7 mb, 33 ± 5 mb, 19 ± 2 mb, and 31 ± 5 mb respectively. Much of the variation in these values is shown to be due to the difference in the number of neutrons available for p,pn reactions in the different target nuclei. The cross sections for other types of reactions studied do not change as much over the range of target elements studied as do the p,pn cross sections. Extension of the excitation functions for the reactions studied up to 5.7 Bev shows that the cross sections seem to be fairly constant between 1 to 3 Bev and 5.7 Bev.

In the second part of this work a theory is developed to describe the observed magnitude and variation of the cross sections for simple nuclear reactions as exemplified by the p,pn reaction. At multi-Bev energies to which this treatment is restricted, the main contribution to the p,pn-reaction cross section comes from inelastic collisions between the incident protons and target neutrons, with all the p-n collision products escaping without further interaction. Approximations and assumptions used include the impulse approximation, 0° lab scattering angle for the inelastic p-n collision products, classical trajectories for the incident and scattered particles, and a quantum-mechanical treatment of the target nucleons. The multi-Bev n-p cloud-chamber data was used to determine the average total exit cross section for the

inelastically scattered particles. The only neutron shells in the target nucleus contributing to the p,pn reaction are those for which the instantaneous knocking out of a neutron creates a product-neutron hole state stable to particle emission. The resultant integrals, evaluated on the IBM-701 computer for the independent particle harmonic-oscillator shell model, give the p,pn reaction cross sections as a function of the nuclear density distribution and the number of available shells.

For the low Z nuclei where the available shells can be unambiguously determined, the results give a half central density radius parameter, r_o, of about 1.2 fermis compared to 1.02 fermis for the charge half radius from the electron-scattering work. Use of the requirement that r_o be less than 2 fermis allows one to set the minimum number of shells available for some targets. For example, the Zn^{64}, Cu^{65}, and Cu^{63} p,pn cross sections require that the 1f7/2 neutrons be available, or, equivalently, that a 1f7/2 neutron hole state (across a major shell) in the product nucleus have less than 8 to 9-Mev excitation energy. The Ce^{142} p,pn and p,2p reaction cross sections suggest that Ce^{142} consists of a Ce^{140} core with at most a small surface, and a diffuse surface generated by the two 2f7/2 neutrons. The results also show that the energy associated with nuclear rearrangement to particle stable product states must be less than 8 to 9-Mev. In several cases, the upper limit can be lowered considerably (to 1.5 Mev and 0 Mev in the cases of O^{16} and N^{14} respectively).

NUCLEAR REACTIONS OF LOW-Z ELEMENTS WITH 5.7-Bev PROTONS: NUCLEAR STRUCTURE AND SIMPLE NUCLEAR REACTIONS

Paul A. Benioff
(Thesis)
Lawrence Radiation Laboratory and Department of Chemistry
University of California, Berkeley, California

July 1959

Part I

NUCLEAR REACTIONS OF LOW-Z ELEMENTS WITH 5.7-Bev PROTONS

I. INTRODUCTION

The understanding of the structure of the atomic nucleus over the past several years has proved so elusive that many different avenues of approach, both theoretical and experimental, have been developed. The theoretical approaches have led to the development of the statistical model, the optical model, and shell model, the collective model, etc.[1] The experimental approaches have included the study of the scattering of and nuclear reactions initiated by various particles incident on nuclei. Most work on nuclear reactions has been divided into the study of either the angular distribution of reaction products, or the total production cross section for different types of reactions. These studies are carried out with the types and energies of particles available on the existing accelerators. As soon as an accelerator of higher maximum energy or different particle type is available, many of the experimental studies are repeated where feasible to see if a new type of reaction sets in, or to investigate the energy dependence of the various processes studied.

This study is an example of the latter type of experiment. It was decided to repeat various measurements of spallation cross sections done at lower incident-proton energies (3 Bev and lower) on selected target nuclei at the Bevatron with a proton energy of 5.7 Bev. In the first section, the experimental method and results will be presented, and results will be analyzed to investigate the energy dependence of various spallation cross sections. In the second section, a theoretical treatment of certain types of "simple" nuclear reactions, as exemplified

by the p,pn reactions, will be presented. The target nuclei chosen were Be, C, N, O, F, Na, and Al.[2] These elements were chosen because of the relative simplicity of analysis of the bombarded targets (no chemistry was necessary). Also by measuring the spallation cross sections for several neighboring elements, the dependence of the various reaction cross sections on the atomic weight of the target can be investigated.

II. EXPERIMENTAL METHOD AND APPARATUS

The experimental results are obtained from several bombardments of foils or powders of suitable compounds of the different elements. Each bombardment consists of placing the appropriate weighed foil or powder of the elements to be studied in a target holder and then bombarding the target in the internal proton beam of the Bevatron. After bombardment, the foils or powder are removed from the holder and placed on cards for counting. Each foil or powder is then counted several times in a gamma-ray pulse-height analyzer. The resulting decay curves of the different peaks are then resolved and supplementary data (counter efficiency, foil weight, etc.) are used to determine the different cross sections.

A. Target Holder

A diagram of the target holder is given in Fig. 1. The front end has a channel cut into the lucite and a threaded hole for help in aligning and securing the foils to the holder. The back end of the holder is designed for rapid attachment to and removal from the pneumatic target plunger on the Bevatron.

A diagram of the powder-target holder is given in Fig. 2. The hole in the back is used to attach this supplementary holder in the channel of the target holder in Fig. 1. The powder and monitor foils are placed in the front end of the powder holder.

B. Counter

Most of the samples were gamma counted by a 1- by 1-1/2-inch NaI (Tl) crystal and Dumont 6292 phototube used with a preamplifier, amplifier, and 50-channel pulse-height analyzer. Later the 50-channel analyzer was replaced by a faster 100-channel analyzer with a magnetic-core memory. The crystal and phototube were mounted on a sample holder with several shelves so that the sample-to-crystal distance could be varied. The whole detector assembly was surrounded by two inches of lead.

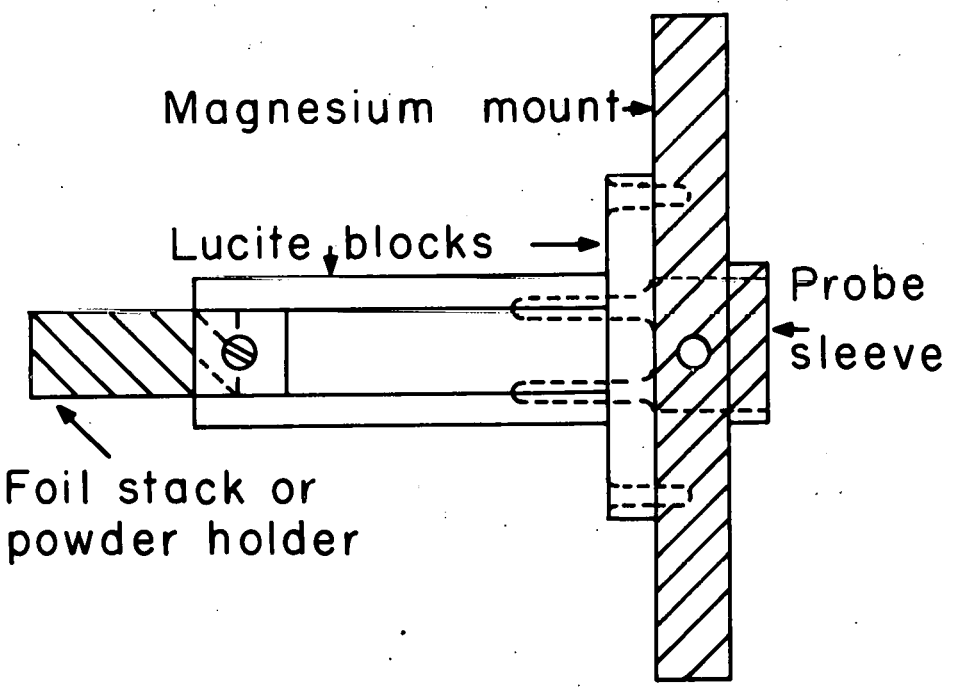

Fig. 1. Bevatron target-holder assembly.

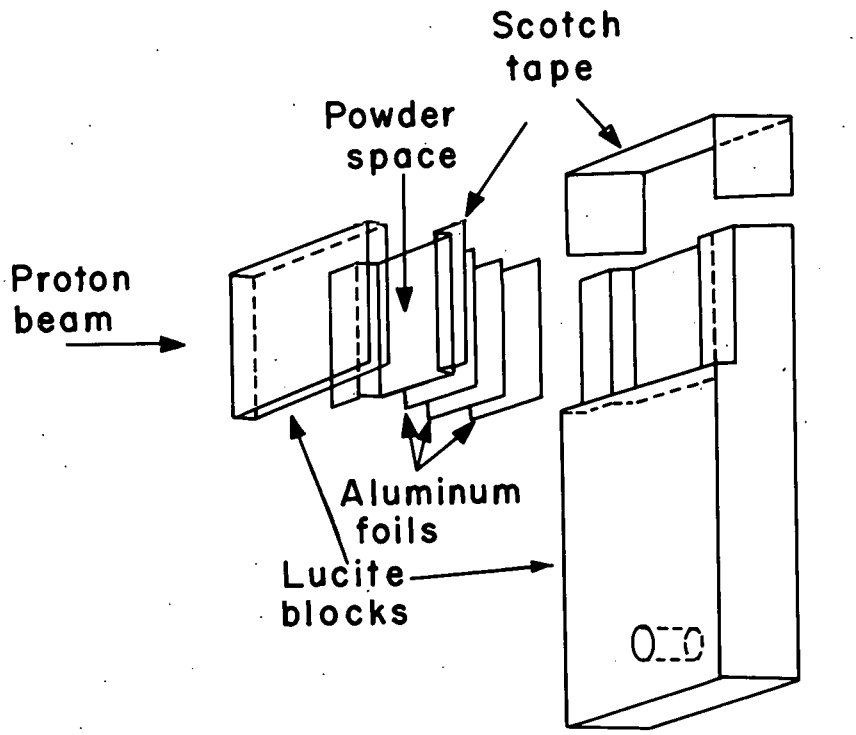

Fig. 2. Powder target holder.

C. Mounting of Target Material

For each bombardment the target foils and powder were arranged in order of increasing atomic weight, with the proton beam entering the lowest-atomic-weight side of the foil packet. This was done so that contamination from spallation products recoiling out of the target foil and secondary neutron and proton contributions to the beam could be held to a minimum. The majority of secondary products come out in the forward direction and the amount of secondary neutrons and protons emitted per nuclear reaction increases with increasing atomic weight of the target nucleus.[3] Guard foils were used in front of and behind each type of experimental foil to keep recoiling spallation products of one target element from contaminating the adjacent target foil. The guard foils also served to protect the target foil sandwiched in between from product-recoil loss, because as much product recoiled in from the guard foils as recoiled out of the target foil. Secondary neutrons and protons are not stopped in this manner, however. The best way to minimize formation of spallation products by secondaries is to keep the target thickness as low as possible. It has been shown that the secondary neutron contribution can be kept to less than 10% if the target thickness is held below 2 to 3 gms/cm^2.[4] The maximum target thickness used in these experiments was about 800 mg/cm^2. This included the thickness of the powder as well as the holder and other foils.

The appropriate 1/2-inch-wide foils were cut from sheet material for the foil holder. The leading edges of the foils were aligned and then secured with cellophane tape. After mounting the foils unto the target holder the whole assembly was ready for bombardment.

It was soon found that the powder holder made a convenient device for aligning the leading edges of the foil stack. Consequently, for bombardments with or without powders, foils were cut to fit the width of the compartment in the holder but to extend out beyond the leading edge. After taping the foils securely in the bottom of the chamber (down-beam side) with cellophane tape, the leading edges were trimmed flush with the end of the holder by means of a razor blade.

Whenever posders were used as target materials they were first dried at 110°C and kept in a desiccator. The holder was filled by tamping the powder into the space between the foil stack at the bottom of the holder and the cover. After any excess powder was scraped off the end was sealed with cellophane tape and the whole assembly was ready for mounting and bombardment.

D. Length of Bombardment and Sample Preparation

The length of time of bombardment varied greatly because it depended on the half life of the isotope being studied. For short-lived isotopes such as 2-1-min O^{15} and 10-min N^{13}, the bombardment times were 1 to 2 min at whatever beam intensity was available. After bombardment, the target holder was removed immediately from the Bevatron, the foils were separated and mounted without weighing, and the intensity measurements of the 0.51-Mev annihilation radiation were begun immediately. For determination of the short-lived activities, 1.2-min O^{14} and 2.1-min O^{15}, the samples were counted as quickly as possible after the end of bombardment. The minimum time delay between the end of bombardment and the begining of the first count was 5 to 6 minutes. This time delay was sufficiently short to see the 1.2- and 2.1-min activities. The resolution of these activities is described in more detail later.

For longer-lived activities, the bombardment times varied from 2 min to 1 hour. After bombardment, the foils were separated and weighed, and their areas were measured. Then they were mounted on aluminum cards for counting. The powder was weighed and mounted on an aluminum card with a small depression in the middle to contain the powder. Cellophane tape was placed over the powder to keep it in place. The powder thickness in mg/cm^2 was determined from the dimensions of the target holder and the powder weight. The samples were then covered with a sufficient thickness of stainless steel to annihilate the positrons immediately above the sample. Both the geometry correction factors (due to the point of origin of the 0.51 Mev gamma rays in the steel instead of the sample) and loss by gamma absorption in the steel were negligible.

E. Counting

The intensity of gamma rays within a certain energy range was then determined for each sample under known geometry conditions. This was done by calibrating the energy scale of the pulse-height analyzer with a standard whose decay scheme is well known, e.g., Na^{22}. For this work the particular channel range was determined which included all the counts resulting from photoelectric interactions in the crystal caused by the gamma rays resulting from the Na^{22} positron annihilation. The same channel range plus a few adjacent channels on the high-energy side were used to measure the 0.51-Mev activity level of the samples. The activity level of the adjacent channels above was determined in order to measure contributions to the activity level in the 0.51-Mev channel range which arise from other than simple photoelectric interaction processes. These contributions arise from several other types of interactions:

(a) Compton interactions in the crystal from gammas emanating from the sample with greater than 0.51 Mev energy.

(b) General background. This includes cosmic radiation, stray activity, and natural activity in the materials around the counter, spurious pulses, etc.

(c) Any interactions of the type where one of the two gammas from the positron annihilation undergoes a Compton interaction in the crystal and the backscattered gamma from a Compton interaction of the other gamma is captured photoelectrically in the crystal. The sample mount and the housing are the main places where the backscattered gamma would be produced.

(d) Annihilation of the positron in flight. In this case the energy of the gamma would include with the rest-mass energy one half of the kinetic energy of the positron at the time of annihilation. The loss from this source of annihilation gammas from the main peak is quite small, of the order of 1%.[5]

The correction for these four contributions was applied by determining the activity per channel in the channels adjacent to the peak on the high-energy side and subtracting this activity level from each channel in which the main photopeak occurs. The validity of such a subtraction is based on the assumption that the activity level of the channel under the peak from the above contribution is the same as it is in the channels immediately above the peak. An examination of the Na^{22} pulse-height spectrum indicates that the above assumption is valid for the first contribution mentioned. However, for the next three contributions the activity level will vary with the energy. Examination of background spectra shows that the count rate per channel increases with decreasing energy. The activity level as a function of energy coming from the other two contributions is undetermined, but is probably not too far from being constant. The contribution from these last two causes to the high-energy channels adjacent to those under the peak was determined by taking the pulse-height spectrum of a fairly intense source of a pure positron emitter such as C^{11} and was found to be about 1% for the worst case (smallest source-to-crystal distance). Thus even if the activity level does vary with energy, the correction will be some fraction of 1%, which is quite small enough to be neglected. For fairly active samples in which the background was a small fraction of the total activity, the correction for the variation of background-count rate with energy was neglected as it was less than 1%. For samples with a low count rate, the correction was included by obtaining background spectra and determining the variation in count rate per channel over the channel range desired.

For counting short-lived activities, the samples obtained from a given run were set up in a rotating series. Each sample was counted for 1 min, the data were recorded, and the sample was then removed and the next one was counted for 1 min, etc. As the count rate decreased, the counting time was increased, if necessary to total a minimum of 2000 counts per determination. In this way a decay curve was built up which contained a sufficient number of points to determine the 10-min N^{13} fairly well and also the 2.1-min O^{15}, which was seen as a tail on top of the 10-min N^{13} + 20-min C^{11} decay.

For the long-lived activities, the count rates were quite low — from 2 to 20 counts per minute (cpm). These samples were counted for long periods of time (about 10 hr) on the pulse-height analyzer, and then a background was run for the same length of time. The background-per-channel count rate was subtracted from the sample-per-channel count rate, and if any net activity remained in the few channels immediately above the peak, it was averaged and subtracted from the peak. An average of four points, or enough to give a net count rate with a fairly small standard deviation were taken for each sample.

Before the actual decay curves were drawn two more corrections to the data were made if necessary: For some samples with high count rates on the 50-channel pulse-height analyser, a dead time correction had to be applied. This correction of 7% per 100 cpm was added to the observed count rate.[6] If C is the corrected count rate and B is the observed count rate then we have

$$C = B + 7 \times 10^{-4} B^2 . \qquad (1)$$

In a few other cases the sample count rate for some isotopes was sufficiently low so that the duration of counting time was an appreciable fraction of the isotope half life. A correction for decay during counting was then applied as follows:

Let A = count rate at the time at which the count is started,

C = total number of counts (sample and background) obtained during time t,

Bg = total number of background counts obtained during time t from a separate run,

and λ = decay constant for the isotope in question.

Then we have

$$A = \frac{(C - Bg)\,\lambda}{1 - e^{-\lambda t}} . \qquad (2)$$

After the corrections were applied to the data, the decay curve for the gamma-ray peak in question was plotted, and the components of different half lives were resolved.

F. Resolution of Product Activities

1. Aluminum.

The target element with the most products, which was bombarded in this work, was aluminum. The decay curve of the 0.51-Mev peak contained contributions from Na^{22}, Be^{7}, Na^{24} (pair production by the high-energy gammas external to the crystal and capture of one of the annihilation gammas in the crystal) F^{18}, C^{11}, N^{13}, and (if the sample was counted soon enough after bombardment) O^{15} and Ne^{24}.[7] Samples which were bombarded for only a few minutes in order to see the O^{15} did not have detectable amounts of Na^{22} or Be^{7} so that the only "long-lived" component was Na^{24}. The 0.51-Mev decay curve was resolved by first subtracting out the Na^{24} contribution. The next component which could be easily subtracted out was the 118-min F^{18} as the resultant tail contains F^{18} only (usually several hundred cpm). Because the C^{11} ($t_{1/2}$ equals 20.4 min) and N^{13} ($t_{1/2}$ equals 10.0 min) have such similar half lives they cannot be resolved by the usual method. For the separation of these two isotopes, the portion of the decay curve left after the Na^{24} and F^{18} subtraction and more than 30 min after the end of bombardment was chosen. This curve was analyzed by a method developed by W. F. Biller.[8] This method depends on the fact that at any time t after the end of bombardment, the total activity C is given by

$$C = A_o e^{-\lambda_1 t} + B_o e^{-\lambda_2 t}.$$

Multiplying through by $(e^{r\lambda_1 t})$ $(\lambda_1 > \lambda_2)$ gives

$$Ce^{\lambda_1 t} = A_o + B_o e^{(\lambda_1 - \lambda_2)t}. \qquad (3)$$

For each point, C and t are known, so that a plot of $Ce^{\lambda_1 t}$ vs $e^{(\lambda_1-\lambda_2)t}$ gives a straight line with a slope B_o and intercept A_o. Decay

curves $A_o e^{-\lambda_1 t}$ and $B_o e^{-\lambda_2 t}$ are then constructed. If these two curves are added together and the total subtracted from the portion of the curve taken less than 30 min after bombardment, a short half-life component is found of 2 to 3 min. It is assumed that this component represents a sum of 2.1-min O^{15} and 3 min Ne^{24}, and consequently the method described above is used to separate the two isotopes. The values obtained for O^{15} and Ne^{24} are not very accurate, because of all the previous subtractions that have been made. Also, these isotopes have decayed considerably before the countings are begun. Consequently, the count rates obtained have a larger error associated with them than do the values for the other isotopes.

The Na^{24} count rate is determined by measuring the decay of the 1.38-Mev photopeak and subtracting any 1.28-Mev contribution from Na^{22} decay. This is determined by measuring the activity in the corresponding energy range after the Na^{24} has decayed.

The Na^{22} count rate is found by measuring the activity level in the 1.28-Mev photopeak. The activity level of the 0.51-Mev peak is taken at the same time as that of the 1.28-Mev peak. The spectrum of a pure Na^{22} standard is then determined, and the ratio of the integrated activity level in the 0.51-Mev peak to that in the 1.28-Mev peak is determined for the standard. This ratio in the sample is usually about twice that of the standard, and the excess is ascribed to Be^7 activity. A few decay points taken indicate that this excess does decay with the requisite half life for Be^7.

Magnesium-27 ($t_{1/2}$ = 9.6 min) was looked for in a couple of runs by taking decay points of the activity level in a few channels centered about 0.85 Mev. The decay curve had a small component of approximately the right half life. Because of the low count rate at this energy range, the values obtained for Mg^{27} are uncertain and hava a larger error associated with them than do the other isotopes.

A couple of targets which underwent long bombardments were sent to L. Currie who kindly analyzed them for tritium. These numbers are also included.

2. Sodium

The next-highest-atomic-weight target studied was sodium. This was bombarded as anhydrous $Na_2 CO_3$ in the powder holder. (The corrections for the contributions to the product activities from the carbon and oxygen are discussed later.) After bombardment, the powder was weighed and transferred to aluminum cards for counting. During this time, the powder was covered with cellophane tape so that the water pick-up would be small for the length of time the sample was counted. The decay curve was analyzed in exactly the same way as was the curve for aluminum except that Na^{24} and Mg^{27} were absent.

3. Fluorine

A 30-mil Teflon foil was used as a fluorine target. The Teflon was analyzed spectrographically and found to contain less than 1 ppn of Na, Mg, Al, Si, P, Ca, Fe, and Cu. It was assumed that these elements would be the major contaminations. The decay curve was analyzed in the same way as that for aluminum except that Mg^{27}, Na^{24}, Ne^{24}, and Na^{22} were not present.

4. Oxygen

Anhydrous oxalic acid was used as an oxygen target. A spectrographic analysis for the same elements as those looked for in Teflon yielded the same results, each element not detectable or present at less than 1 ppn. For those runs in which the cross-sections for short-lived activities were desired, the powder was placed on an aluminum card, covered with cellophane tape to prevent water pickup and immediately counted. The weighing of the powder was deferred until all the decay points needed were taken. The anhydrous acid was stored in a desiccator and removed only for packing into the holder. The decay data were resolved by the same methods as were used for fluorine targets.

5. Nitrogen

For a nitrogen target, the compound, 5 amino tetrazole (City Chemical Corp.) was used. A spectrographic analysis for the same elements

as were determined for fluorine yielded the same limits of detection results. The compound was obtained as the monohydrate and was dried in an oven at 110°C and then kept in a desiccator. The compound appeared to lose its water of hydrogen quite easily, because the crystals quickly changed to powder as heat was applied. This compound has one possible hazard -- some of the tetrazole derivatives are explosives.[9] It melts with decomposition at 203°C. After bombardment in the Bevatron it seemed to behave perfectly and did not discolor. The compound has a high ratio of nitrogen to carbon and hydrogen. Its formula is $CH_5 H_3$ or

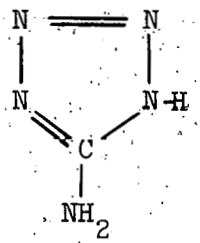

Bombardment of this compound even for more than 1 hr produced no visible change. The decay-curve resolution was done in the same manner as for oxalic acid targets.

6. Carbon

Carbon was bombarded as foils of polyethylene. Thick foils (50 mg/cm^2) were used for Be^7 cross-section determinations and thin foils (6 mg/cm^2) were used for C^{11} cross-section determinations. Again a spectrographic analysis of both foils for the elements Na, Mg, Al, Si, P, Ca, Fe, and Cu, gave less than 1 ppn for any one of them (i.e., they were not detected). The decay curves were analyzed also in the same manner as those for fluorine. One thick target with the aluminum monitor was sent to L. Currie[4] who kindly analyzed the sample for tritium.

7. Beryllium

One bombardment of a thick beryllium foil was done. Be^7 and C^{11} were the only two isotopes found. The foil was not analyzed for tritium. Analysis of the decay curves was quite simple because only two components were present.

G. Cross-Section Ratio Determination

After the counts per minute of all the isotopes produced in the different target foils in a given run were obtained, the ratio of each cross section to that of a selected monitor reaction was calculated. This was done by first determining the disintegrations per minute (dpm) for each isotope by dividing the counts per minute by the counting efficiency for the radiation in question. These efficiencies and counter geometry as a function of sample-to-crystal distance were already determined.[10] The geometry was redetermined by D. Barr of this laboratory.[11] He calibrated a Na^{24} source by beta-gamma coincidence counting and used it to determine the geometry of each shelf in the sample holder. His results agreed to within 2% of the values in the previous work.

The number of atoms per cm^2 of target material was determined from the dimensions of the foil or in the case of powders, of the space in the powder holder, and the weight of the material. For the powders which would absorb water such as Na_2CO_3 (anhydrous), the weighing was done as quickly as possible to avoid uptake of water. During the weighing no visible change in the weight due to water uptake was observed.

The correction for decay during bombardment was often complicated by the fact that during all but the shortest runs the beam would go off several times during a run. These interruptions were always temporary and were corrected in a few minutes. For long-lived activities (Na^{22}, Be^7, and sometimes Na^{24}), the decay during these interruptions was negligible and was neglected. For the short-lived activities, this decay was not negligible. Consequently, a long bombardment with interruptions was treated as a series of short bombardments with appropriate decay factors applied to correct each member of the series to the end of the run. This factor was equal to

$$T = \sum_{i=1}^{n} \left(1 - e^{-\lambda t_{2i-1}}\right) e^{-\lambda t_{2i}} + \left(1 - e^{-\lambda t_{2n+1}}\right), \qquad (4)$$

where n = number of interruptions

λ = decay constant of the isotope in question

(t_{2i-1}) = duration of the ith short bombardment

t_{2n+1} = duration of the last short bombardment

t_{2i} = time elapsed from the end of the ith short bombardment to the end of the last short bombardment.

In order to be exact, a factor should be included in the above sum to account for the change in beam intensity from one to another of the short bombardments comprising a run. However, a check by use of a pulse integrator which gave the number of protons in each pulse showed that within 2 min of running time, the variation from pulse to pulse averaged itself out.

The equation for calculation of the production cross section, σ, of A disintegrations per minute of an activity with decay constant, λ, and length of bombardment t, from a target with N atoms/cm^2 with a beam intensity of φ particles/min is

$$A = \varphi\sigma N(1-e^{-\lambda t}) \tag{5}$$

For interrupted bombardments, the factor T given by Eq. (4) is substituted for the exponential term, giving

$$A = \varphi\sigma NT.$$

This equation may be rearranged to give

$$\varphi\,\sigma = \frac{A}{NT} \tag{6}$$

where φ and σ are the unknowns in this equation. In each bombardment the activities in the monitor foil were determined in the same way as are the activities in the other foils and powder. The above equation is of exactly the same form for the monitor reaction: A, N, and T are different; φ is the same. Instead of determining φ from the monitor cross section, φ was removed by dividing the expression for $\varphi\sigma$ for the unknown activity by $\varphi\sigma$ for the monitor resulting in the

cancellation of φ. The result was expressed as a ratio of the production cross section of the particular activity to that of the monitor. The reason for using this method rather than calculating σ directly for each run was that the monitor cross section was not known until the work was well along. It was decided to keep the data in this form for all the bombardments and activities and convert to cross sections only at the end of the work.

For many of the activities in the powder targets and Teflon, the ratio determined in the above manner for the production cross section was a weighted average of the contributions from each element present. Thus in $Na_2 CO_3$, for instance, C^{11} is produced from the carbon and oxygen as well as the sodium and the production-cross-section ratio found was a weighted average of the three individual ratios. The correction for the contributions of the other elements occurring was made as follows: The N appearing in Eq. (6) represented the total number of all atoms/cm^2 contributing to the particular cross section. (For $Na_2 CO_3$ N represented the number of Na+C+O atoms per cm^2 in the target.) The resultant averaged production-cross-section ratio, $\sigma/\sigma_{F^{18}_{Al}}$, is given by

$$\frac{\sigma}{\sigma_{F^{18}_{Al}}} = \frac{N_{Na}\,\sigma_{Na} + N_C\,\sigma_C + N_O\,\sigma_O}{\sigma_{F^{18}_{Al}}} . \qquad (7)$$

For $Na_2 CO_3$, we find $N_{Na} = 1/3$, $N_C = 1/6$, $N_O = 1/2$.

The ratio $\sigma_C/\sigma_{F^{18}_{Al}}$ for the product in question was determined from bombardments of polyethylene, and $\sigma_O/\sigma_{F^{18}_{Al}}$ was determined from bombardments of oxalic acid powder. The ratio $\sigma_C/\sigma_{F^{18}_{Al}}$ was used to correct for the carbon content of oxalic acid.

III. RESULTS

In the manner described in the previous paragraphs, a whole series of ratios of production cross sections to the monitor cross section were obtained for each bombardment. Almost all of the ratios were determined more than once, and a few were determined many times.

A. Data Rejection

On examining the results it was found that, in some cases, the group of determinations of a given cross-section would have a reasonable spread except for one datum which was quite different. If this particular determination could not be rejected because of some known experimental error, a statistical rejection criteria was applied to the group to see if the outlying datum could be rejected. This test was applied by division of the difference between the outlying datum and the determination closest to it in magnitude by the range of the data set (largest minus smallest datum). This number is compared to another number, Q, whose magnitude depends on the number of determinations in the set and the confidence level of rejection.[12] If the former number is larger than the latter, the outlying observation is rejected. Otherwise it is retained. The confidence level of the rejection is 90%. Out of all the cross-section ratios determined, only five had an outlying datum that could be rejected by the above test.

B. Standard Deviation

For each product from each target element, the results after applying the above rejection test were averaged, and the standard deviation computed. For those few products with more than ten determinations, the standard deviation, S, was computed in the usual way, i.e.,[13]

$$S = \left(\sum_{i=1}^{n} \frac{(x_i - \bar{x})^2}{n - 1} \right)^{1/2} ,$$

where $\bar{x}$ is the average of the individual ratios, x_i, and n is the number of determinations of a given ratio. For the bulk of the products,

ten or less determinations were made, so another method, more accurate than the above formula, was used to determine S.[14] This method consists of finding the range of determinations in each data set and multiplying it by a number K' to get the standard deviation. The value of K depends on the number of samples in a set. Table I contains the literature values of Q and K for different set sizes.[12,14]

Table I

Values of the rejection-criteria factor and standard-deviation factor for different sample sizes

Sample size	Rejection factor $Q_{0.90}$	Standard-deviation factor K
2	-	0.89
3	0.94	0.59
4	0.76	0.49
5	0.64	0.43
6	0.56	0.40
7	0.51	0.37
8	0.47	0.35
9	0.44	0.34
10	0.41	0.33
∞	0	0

C. Monitor Reaction Cross Section

For most spallation work the cross section for the reaction $Al^{27}(p,3pn)Na^{24}$ has been used as a standard, and its excitation function is well known. This reaction is chosen because of the convenient half-life (15-hr) and beta-decay characteristics. However, for this work many of the irradiations were too short to use Na^{24} and also it was desired to use a source of annihilation radiation for direct comparison with the many positron emitters of interest to this study. For these reasons, F^{18} formed in the reaction $Al^{27}(p,X)F^{18}$ was chosen as a monitor. Use of this reaction as a monitor removes the counting-efficiency

correction for many determinations, because F^{18} is a positron emitter (97% of the F^{18} decays are by positron and 3% by electron capture).[7] The counting-efficiency correction, however, must be made to determine the F^{18}/Na^{24} production-cross-section ratio, because the energy of the Na^{24} gamma counted, 1.38 Mev, is higher than the F^{18} positron-annihilation gamma energy, 0.51 Mev. The inclusion of this correction gave a value for the F^{18}/Na^{24} production-cross-section ratio of 0.732 ± 0.063 (standard derivation). The production cross section for the reaction $Al^{27}(p,2pn)Na^{24}$ for 5.7-Bev protons was taken to be 10.5 millibarns (mb).[11] Recent accurate work gives the cross sections for the above reactions as 10.4 ± 0.6 mb at E_p = 2.0 Bev and 10.0 ± 0.6 mb at E_p = 3.0 Bev.[15] These results combined with lower-energy work are stated to be consistent with a constant cross section of 10.7 ± 0.6 mb for a proton energy range of 0.3 to 3 Bev. A preliminary absolute value for the cross section for the reaction $C^{12}(p,pn)C^{11}$ at 4.1 Bev has been determined to be 30.5 ± 4.1 mb.[16] In this work the ratio of the cross sections for the reactions, $C^{12}(p,pn)C^{11}$ and $Al^{27}(p,X)F^{18}$, $\sigma_{C^{11}}/\sigma_{F^{18}}$ was found to be 3.83. (See Table II below). Combining this with the $\sigma_{F^{18}}/\sigma_{Na^{24}}$ ratio given above and the 10.5 mb production cross section for Na^{24} from aluminum gives $\sigma_{C^{12}(p,pn)C^{11}}$ equal to 29.4 ± 3.3 mb. This value is in quite satisfactory agreement with the value of 30.5 ± 4.1 mb. The error limit on the value of 10.5 mb will be taken to be 0.6 mb in agreement with the results at lower energies. The standard deviation taken here to be one half the error limit, is then 1/2 (0.6 mb) = 0.3 mb.[13]

D. Final Results

Table II contains the results of the 5.7-Bev proton bombardments. The two tritium determinations were done by L. Currie and one of the Na^{22} determinations from the aluminum target was done my M. Kalkstein. The first column lists the target elements studied. The reaction type for each product is given in column 2. The "X" appearing in some entries, refers to any group of emitted particles which conserves charge and nucleon number. Cross sections were determined for all the radioactive

Table II

Summary of experimental results

Target	Reaction type	Product	Number of determinations, n	Cross-section ratio, $\langle \frac{\sigma}{\sigma_o} \rangle$	Standard deviation, S	Cross section, σ mb	Standard error, S_1	Error limit, E_σ
Be (impurities)		C^{11}	1	0.0057	-	0.044	-	-
	(p,p2n)	Be^7	1	1.92	-	15	-	-
C	(secondary)	F^{18}	2	0.0013	0.0003	0.01	0.0014	0.003
	(p,pn)	C^{11}	13	3.83	0.44	29	1	3
	(p,pnα)	Be^7	5	1.45	0.16	11	0.6	1.5
	(p,X)	H^3	1	1.62†	-	17	-	-
N	(secondary)	F^{18}	2	0.00064	0.00015	0.0040	0.0007	0.0014
	(p,pn)	N^{13}	3*	0.94	0.02	7.3	0.2	0.7
	(p,2p2n)	C^{11}	6	1.75	0.58	13	1.8	4
	(p,X)	Be^7	3*	1.90	0.18	14	0.8	2
O	(secondary)	F^{18}	2	0.0074	0.0025	0.06	0.014	0.03
	(p,pn)	O^{15}	3	4.34	0.53	33	2.2	5
	(p,p2n)	O^{14}	3	1.42	0.34	11	1.5	3
	(p,2p2n)	N^{13}	5	0.82	0.31	6	1.1	2
	(p,pnα)	C^{11}	7	1.52	0.42	12	1.2	3
	(p,X)	Be^7	2	1.38	0.50	10	2.6	5
F	(p,pn)	F^{18}	10	2.49	0.19	19	0.6	2
	(p,p2nα)	N^{13}	3	0.193	0.052	1.5	0.2	0.5
	(p,X)	C^{11}	3*	0.70	0.06	5.4	0.3	0.7
	(p,X)	Be^7	6	1.20	0.22	9.2	0.7	1.6
Na	(p,pn)	Na^{22}	2	4.01	0.35	31	2.0	5
	(p,pnα)	F^{18}	2	1.35	0.06	10	0.4	1
	(p,X)	Be^7	2	1.71	0.20	13	1.1	2
Al	(p,pπ+)	Mg^{27}	2	0.017	0.014	0.1	0.07	0.1
	(p,4p)	Ne^{24}	2	0.21	0.11	1.6	0.6	1.2
	(p,pnα)	Na^{22}	6	1.53†	0.28	17	1.3	3
	(p,X)	F^{18}	15	0.732†	0.063	7.68	0.17	0.57
	(p,X)	O^{15}	2	0.59	0.33	4.5	1.8	3.6
	(p,X)	N^{13}	5*	0.216	0.042	1.7	0.2	0.3
	(p,X)	C^{11}	8	0.77	0.13	6.0	0.4	0.9
	(p,X)	Be^7	4*	0.767†	0.049	8.3	0.3	0.9
	(p,X)	H^3	1	4.21†	-	45	-	-

*An outlying datum has been rejected from this set.

†This is the number of product atoms produced per number of target atoms per square centimeter divided by σ_o for $Al^{27}(p,3pn)Na^{24}$.

products given in column 3. The fourth column gives the number of bombardments made to determine the cross-section ratio for the listed product. The statistical rejection criteria described previously was applied to each set, and any outlying datum which could be rejected was not included. The asterisks denote sets from which an outlying datum was rejected. In these cases n excludes the rejected datum. The arithmetic average of the n determinations of the cross-section ratio; designated $\left\langle \frac{\sigma}{\sigma_o} \right\rangle$ is given in column 5. The values marked with the superscript "†" are the number of product atoms produced per number of target atoms per square centimeter divided by the same quantity, σ_o, for the $Al^{27}(p,3n)Na^{24}$ reaction. These samples were not counted until all the F^{18} activity was gone. All the other values are based on the F^{18} production cross section from aluminum. The fifth column lists the standard deviation of an individual determination associated with the average. For most of the ratios, this number was directly determined either by use of Table I or by the usual equation. For those ratios for which a correction due to contributions to the activity from other atoms in the molecule had to be made, the standard deviation was obtained by the usual rules for combining standard deviations, i.e.,[13]

$$C\ (A \pm \sigma) = CA \pm C\sigma$$

$$A \pm \sigma_1 + B \pm \sigma_2 = C \pm (\sigma_1^{\,2} + \sigma_2^{\,2})^{1/2} .$$

The standard deviation of the cross-section ratio for the contribution to be removed was obtained from the appropriate entry in column 5 and divided by $\sqrt{n}$ to obtain the standard error of the mean.[13] This number was used as the standard deviation of the cross-section ratio of the contributing activity. For example, to find the C^{11} cross section ratio from fluorine in Teflon $(C\,F_2)_n$, the contribution from the carbon must be accounted for. If X is the contribution to the C^{11} cross-section ratio from fluorine, then we have

$$X \pm \sigma_x = \left[\frac{3}{2}\,y - \frac{1}{2}\,(3.83)\right] \pm \left[\left(\frac{3}{2}\,\sigma_y\right)^2 + \left(\frac{0.44}{2\sqrt{13}}\right)^2\right]^{1/2} , \qquad (8)$$

where $y \pm \sigma_y$ is the observed cross-section ratio with its standard deviation for C^{11} produced in Teflon and 3.83 ± 0.44 is the cross-section ratio and standard deviation for C^{11} produced in polyethylene.

The seventh column lists the production cross sections for the given reactions. The cross sections are obtained from the ratios given in column 5 and 10.5 mb for $Al^{27}(p,3pn)Na^{24}$ or 7.68 mb for $Al^{27}(p,X)F^{18}$ whichever is appropriate. The standard errors of the mean cross sections are given in column 8. This number, S_1, gives the contribution of all the random errors in this work. For the results based on F^{18} as a monitor we have

$$S_1 = \sigma \left[\left(\frac{S}{\left\langle \frac{\sigma}{\sigma_o} \right\rangle} \right)^2 \frac{1}{n} + \left(\frac{0.17}{7.68} \right)^2 \right]^{1/2} ,$$

and for the few results[13] based on Na^{24},

$$S_1 = \frac{10.5}{\sqrt{n}} \, S .$$

The individual standard deviation, S, is given in column 3.

Column 9 gives the error limit, E_σ, associated with the given cross section. Besides the random errors, S_1, this includes the error in the $Al^{27}(p,3pn)Na^{24}$ monitor-reaction cross section and an estimate of systematic errors due to the possible experimental bias. This latter category includes such items as the small amount of water pickup in powder samples during weighing, the slight geometry effect of positron annihilation in the steel disks on top of the sample, systematic errors in the method used to obtain the integrated count rate under a gamma peak on the pulse-height analyzer, etc. Individually each of these errors is less than 1% and they may work in opposite directions. Somewhat arbitrarily a fractional error limit of 6% has been taken to represent the contribution of these sources. Since the standard deviation is taken as one half the error limit we get[13]

$$E_\sigma = 2\,\sigma \left[(0.03)^2 + \left(\frac{0.3}{10.5} \right)^2 + \left(\frac{S_1}{\sigma} \right)^2 \right]^{1/2} \qquad (9)$$

as the error limit to be associated with the given cross section. For those cases which exclude an outlying datum E_σ has the 90% confidence limit associated with it.

IV. DISCUSSION

Among the many different methods that can be used to systematically evaluate the experimental spallation data, three appear to be the most widely used. The first consists of studying the dependence of the cross section for a particular type of reaction (e.g. the p,pn reaction) on various parameters of the target and product nuclei. The second method consists of a study of the energy dependence of the cross section for a particular reaction and target element. The third is a study of the dependence of the cross section on nuclear-reaction and product parameters for a given target element. The first two methods will be used here, as they appear to be most suited for low Z target elements. The third is usually used for higher Z targets. First, cross sections for particular types of reactions for different target and product nuclei will be discussed (secondary reactions are included). The excitation functions will be given for most of the cross sections determined in this work.

A. Secondary Reactions

The cross section for the production of C^{11} from Be^{9} contains contributions from the secondary reaction $Be^{9}(\alpha,2n)C^{11}$ and the primary reactions, $O^{16}(p,X)C^{11}$ and $C^{12}(p,pn)C^{11}$. Literature values for the oxygen and carbon content in beryllium metal (hot pressing from beryllium powder) are 0.65% and 0.06% respectively.[17] Applying these values to the beryllium target used in this work and using the appropriate entries in Table II allows one to estimate a C^{11} production cross section of 0.093 mb from carbon and oxygen. This is more than the observed cross section of 0.044 mb, so one may conclude that the observed cross section probably consists mainly of contributions from impurities.

The cross sections for F^{18} production from 5.7-Bev proton bombardment of polyethylene and 5 amino tetrazole, 10 ± 3 μb and 4 ± 1.4 μb respectively, cannot be explained as being due to impurities. If one assumes a 10-mb cross section for F^{18} production from the impurities,

500 ppm total impurities would be required, which is much more than was found. Crude estimates of F^{18} production by the most likely secondary reactions give cross sections for F^{18} production from carbon and nitrogen as 0.04 μb and 0.1 μb respectively. These numbers are also much too small to account for the observed cross sections.

The foil stacks, from which these cross sections were determined after bombardment, contained thick Teflon foils which were separated from the polyethylene by a 5 mg/cm^2 polyethylene guard foil and from the 5 amino tetrazole by a 5 mg/cm^2 $(CH_2)_n$ guard foil and one layer of cellophane tape. It is possible that some of the F^{18} recoiled or migrated into the carbon or nitrogen target. The lower cross section for the nitrogen target, which had thicker guard foils, supports this possibility. Consequently, the experimental cross sections should be taken as upper limits.

The oxygen target shows the first real evidence of F^{18} production by nuclear reactions, because the contributions for F^{18} recoils and migration should be the same as for the carbon and nitrogen targets whereas the observed cross section is 60 ± 30 μb. The principal reactions leading to F^{18} production from oxygen targets would be $O^{16}(\alpha,d)F^{18}$; $O^{16}(H^3,n)F^{18}$; $O^{16}(He^3,p)F^{18}$ and the primary reaction $O^{18}(p,n)F^{18}$. The contribution from the $O^{18}(p,n)F^{18}$ reaction can be shown to be small. At 400 Mev, the cross section for the reaction $B^{11}(p,n)C^{11}$ is 1.5 mb,[18] and at a proton bombarding energy of 420 Mev, F^{18}-production cross section from oxygen targets is 0.083 mb.[19] If the reaction $O^{18}(p,n)F^{18}$ is taken to be the main source of F^{18}, then the observed cross section, corrected for the abundance of O^{18} in oxygen,[7] becomes 40 mb. The difference between the $B^{11}(p,n)C^{11}$ amd $O^{18}(p,n)F^{18}$ reaction cross section is too great to be ascribed to differences in the target element. Consequently, the bulk of the 40 mb must come from secondary reactions on O^{16} and, as a first guess, the $O^{18}(p,n)F^{18}$-reaction cross section will be taken to be 1.5 mb at 420 Mev. This cross section will be taken to be the same at 5.7-Bev bombarding energy. The value of 1.5 mb gives a contribution of 3 μb from the $O^{18}(p,n)F^{18}$ reaction in natural oxygen.

The cross section for the three secondary reactions is given by

$$\sigma = \sigma_1 \sigma_2 R$$

where σ_1 is the production cross section for the secondary bombarding particles, σ_2 is an average secondary-reaction cross section, and R is an average range over which the secondaries are effective in producing the product. The tritium-, He^3-, and alpha-production cross sections will be taken as 30 mb,[4] 50 mb, and 400 mb[20] respectively (assuming the H^3:He^3:He^4 ratio for oxygen is between that for beryllium and aluminum and not too different at 5.7 Bev from its value at 335 Mev). The Q values for the three reactions $O^{16}(t,n)F^{18}$, $O^{16}(He^3,p)F^{18}$, and $O^{16}(\alpha,d \text{ or } pn)F^{18}$ are 1.7 Mev, 2.0 Mev, and -16.3 Mev, respectively.[21] Consequently, the entire range of the H^3 and He^3 ions contributes to production of F^{18}, but for alphas only that part of the range in which the alpha energy is greater than 16.3 Mev contributes to the reaction. The values of 7 Mev for H^3 and 28 Mev for He^3 as rough average initial energies[4,20] yield ranges in air of 40 mg/cm^2 and 100 mg/cm^2 respectively.[22] The conversion of these figures into atoms of oxalic-acid oxygen per square centimeter in the target and the use of 100 mb for the (t,n) and (He^3,p) reaction cross sections[23] (the He^3 reaction cross section is taken equal to that for H^3 reaction) gives, from the preceding equation, contributions of 4 μb for the reaction $O^{16}(t,n)F^{18}$ and 7 μb for the $O^{16}(He^3,p)F^{18}$ reaction. From a published energy spectrum of alphas produced from light nuclei in film by 1-Bev protons, it is found that about 10% of the alphas produced have energies above 16 Mev.[24] Taking the whole 10% as produced at 24 Mev, the range in air necessary to slow a 24-Mev alpha to 16 Mev as 30 mg/cm^2,[25] and a guess of 100 mb for the reaction cross section gives a contribution of 3 μb for the reaction $O^{16}(\alpha,d)F^{18}$. Because the oxalic acid was bombarded under the same conditions with respect to guard foils and position in the foil stack as the 5 amino tetrazole, the maximum F^{18} contribution from possible recoil and migration will be taken as 5 μb. The addition of all these contributions, which are thought to be upper limits, gives a total estimate of 22 μb. It is difficult to say whether this is significantly lower than 60 ± 30 μb. More work would be necessary to decide this question.

B. p,pn Reaction

The most noticeable feature of the p,pn-reaction cross sections is their large variation for the different target elements. Bombardments by Burcham, Symonds, Warren, and Young with 980-Mev protons also show the same variation.[26] In this 980-Mev work it is suggested that the variation may be correlated with the level structure of the product nuclide and that the deposition energy in the product nuclide must be less than the excitation energy of the first particle-emitting level. The same fluctuation of the (p,pn) cross section for different target elements is shown by recent work with 0.3 to 3 Bev protons.[27] This work also suggests a correlation of the p,pn cross section with the separation energies of the most loosely bound particles in the products and with nuclear shell structure. These general ideas continue to be borne out by the data in Table II. In a later section, a theoretical approach to the p,pn and other types of "simple" reactions through the use of a combination of the shell and optical models will be developed. Here a further correlation can be developed by using the ideas already brought forth. The separation energy of the least-bound particle in the product can be used to determine which of the uppermost neutron shells in the nucleus contribute to the p,pn reaction. Only those shells would be allowed that left the residual nucleus with insufficient energy to emit another nucleon. Consequently, it might be expected that, for a given energy and over a restricted atomic-weight range of targets, the total p,pn cross section divided by the number of "available" nucleons, where known, might be constant.[28] For some of these light elements the excitation energy of nucleon holes in the "buried" shells can be determined fairly unambiguously from data in the literature.

A careful energy analysis of p,2p reactions on several low-Z elements with 185-Mev protons has demonstrated the scattering of protons from protons in the buried shells.[29] For C^{12} the 1p3/2 - 1s1/2 shell spacing was shown to be 16 Mev. This is more than the binding energy (7.5 Mev) of an alpha particle in C^{11}. Consequently, the 1s1/2 nucleons are unavailable, and only the four 1p3/2 neutrons are available for the p,pn reaction. The case of N^{14} is unambiguous because

only the ground state of N^{13} is bound:[21] all the other levels have much larger particle-emission widths than gamma-emission widths. This means that only the 1p1/2 neutron of N^{14} can contribute. For N^{15} the 1s1/2 and 1p3/2 proton-hole states are more than 15 Mev and 6 Mev above the ground state. Since N^{15} and O^{15} are mirror nuclei and the Coulomb energies are small, these excitation energies should be similar to those for the corresponding neutron-hole states in O^{15}. This means that in O^{16} the 1s1/2 neutrons are unavailable but the 1p3/2 (and 1p1/2) neutrons are available because the O^{15} proton binding energy is 7.3 Mev. The availability of the 1p3/2 level is supported by other studies of the O^{15} level structure.[30]

Determinations of the available neutron levels in F^{19} from the excited state configurations of F^{18} and the binding energy of the least-bound particle (4.41 Mev for an alpha and 5.61 Mev for a proton)[21] is not as easy as in the previous cases because less is known about F^{18}-level structure. However, isotopic spin, parity, and spin requirements can be used (neglecting collective effects) to help decide if the known excited states can be "buried-shell" hole states. For example, the parent 1p1/2 neutron hole F^{18} states of the ground state of F^{19} can have values of the isotopic spin, T, equal to 1 or 0, negative parity and values of the spin, I, equal to 1 or 0. The probability of producing any one of these states with specific values of T and I is given by the appropriate fractional percentage coefficients. All the F^{18} excited states below and including the 5.60-Mev state have T = 0 except two, which have T = 1. However, these two, at 1.08 and 3.07 Mev have positive parity.[21,31] Neither the isotopic spin nor the parity of the adjacent 5.67-Mev level are known. If the isotopic-spin selection rules hold, it probably has T = 0 as it is formed by He^4 bombardment of N^{14}.[21] The higher levels are known to be particle emitting.[21] The above data on the F^{18} excited states indicate that all the parent 1p1/2 neutron-hole F^{18} states with T = 1 are particle-emitting states as all the particle-stable F^{18} states with T = 1 have positive parity. This means that the 1p1/2 neutrons are unavailable whenever a

T = 1 F^{18} parent state is produced. It is not possible to decide at present from the F^{18} level scheme whether the parent states with T = 0 are particle emitting or not. Consequently the two 1p1/2 neutrons in F^{19} appear to be at least partially unavailable and may be completely unavailable. In order to have a number to work with, it will be assumed here that 1p1/2 neutrons are completely unavailable. The 1p3/2 and 1s1/2 neutrons should also be unavailable, because as 1p3/2 and 1s1/2 hole states would have even higher excitation energies than the 1p1/2 hole state.

Much less is known about Na^{22} levels. All the excited states below 3.5 Mev should have T = 0 by the isotopic spin selection rules because they are directly populated by the $Mg^{24}(d,\alpha)Na^{22}$ reaction.[32] No states have yet been found between 3.5 and 7.5 Mev (the proton binding energy in Na^{22} is 6.74 Mev. The spin, parity, and emission width of the 7.5-Mev state are not given. In the absence of further information it will be assumed here that the 1p1/2 neutrons are unavailable.

The discussion in the previous paragraphs has shown that the number of available neutrons for p,pn reactions can be taken as four 1p3/2 neutrons for carbon, one 1p1/2 neutron for nitrogen, four 1p3/2 and two 1p1/2 neutrons for oxygen, two 1d5/2 neutrons for F^{19}, and four 1d5/2 neutrons for Na^{23}. Table III has been prepared using these numbers of available neutrons. Columns 1 and 2 list the target element and the product nuclide. The third and fourth columns list the p,pn reaction cross section in millibarns and the number of available neutrons. The tentative nature of the values given for the number of available neutrons for F^{19} and sodium is indicated by the parentheses. The fifth column gives the p,pn reaction cross section per available neutron σ_i. It is immediately seen that σ_i is much more constant than is $\sigma_{p,pn}$, indicating that there is indeed some correlation between the number of available neutrons and $\sigma_{p,pn}$. The variation outside of the error limits remaining indicates that, as would be expected, σ_i varies with the atomic weight of the target and with the shell quantum numbers of the available neutrons.

Table III

p,pn cross sections per available neutron for low-Z elements

Target	Product	$\sigma_{p,pn}$(mb)	Available neutrons	p,pn cross section per available neutron σ_i
C	C^{11}	29 ± 3	4	7.2 ± .8
N	N^{13}	7.3 ± .7	1	7.3 ± .7
O	O^{15}	33 ± 5	6	5.5 ± .8
F	F^{18}	19 ± 2	(2)	10 ± 1
Na	Na^{22}	31 ± 5	(4)	8 ± 1.0

A very plausible mechanism for the p,pn reactions which accounts for the lack of variation in σ_i is that the incident proton collides with one of the available neutrons in the nucleus, and the proton, neutron, and any mesons produced leave without further interaction in the nucleus. This would mean that the total p,pn cross section would be approximately equal to some constant times the number of available neutrons, which is just what is observed. One would expect contributions to the cross section to be small from proton-neutron collisions in which the proton (or neutron) is left in the nucleus with enough energy to excite the nucleus to a proton- (or neutron-) emitting state. This is due to the small probability of such nucleon-nucleon collisions leaving one particle behind with a kinetic energy such that the nucleus will emit one but not two particles. More will be said about these considerations in the second section.

C. p,p2n Reactions

Cross sections for only two examples of this type of reaction were determined. For the reactions $Be^9(p,p2n)Be^7$ and $O^{16}(p,p2n)O^{14}$ the cross sections are 15 mb and 11 ± 3 mb, respectively. This type of reaction is not so easy to interpret as the p,pn reaction, as one would expect two

main contributing mechanisms. One of these would consist of the incident proton knocking out a neutron from a "buried shell", which leaves the residual nucleus in a sufficiently excited state to emit another neutron (the 1s shell in C^{12} is a possible example). The other mechanism consists of a proton knocking out a neutron available for the p,pn reaction and then one of the collision products knocking out another neutron from a shell, which leaves the residual nucleus with insufficient energy to emit another particle. It is difficult to estimate the relative contribution of these mechanisms to the observed cross sections.

D. p,2p2n Reactions

Two examples of this reaction were included, namely, the cross sections for the reactions $N^{14}(p,2p2n)C^{11}$ and $O^{16}(p,2p2n)N^{13}$ equal to 13 ± 4 mb and 6 ± 2 mb, respectively. The contributing mechanisms for this reaction are numerous. Besides one, two, or three successive collisions followed by emission of two, one, or no particles, respectively, from the excited nuclear state, deuterons can be emitted. The initial collision can be either with a neutron or a proton, etc. It appears from the above two cross sections that the fact that N^{13} has only one bound state, whereas C^{11} has several, is influencing the cross section. This can be seen from a general study of the data in Table II, i.e., from any given target element the N^{13}-production cross sections are always less than those for C^{11} or O^{15}.

E. p,pnα Reactions

Cross sections for four examples of this type of reaction were determined. For the reactions $Al^{27}(p,pn\alpha)Na^{22}$, $Na^{23}(p,pn\alpha)F^{18}$, $O^{16}(p,pn\alpha)C^{11}$, and $C^{11}(p,pn\alpha)Be^{7}$ cross sections of 17 ± 3 mb, 10 ± 1 mb, 12 ± 3 mb, and 11 ± 1.5 mb, respectively, were found. Contrary to the p,pn reactions, these values are all fairly uniform. There does not appear to be any correlation with the number of bound levels in the products, i.e., Be^{7} has two, C^{11} has seven or eight, F^{18} has ten or eleven, and Na^{22} has more than eleven.[21,31,32] Division of the total

cross sections by the same number of available neutrons as was taken for the p,pn reactions gives cross section contributions per available neutron of 2.1 ± 0.3, 2.5 ± 0.3, 2.0 ± 0.5, and 2.8 ± 0.4 mb/neutron, for aluminum, sodium, oxygen, and carbon targets, respectively. There are probably eight neutrons available for Al^{27} because the $1d_{5/2}$ neutron shell is closed.[33] It is seen that these values are almost constant within the error limits. The fact of the constancy of these numbers is of doubtful use, however, because there are even more mechanisms leading to the final product than in the previous case. The writing of this reaction as a p,pnα reaction is not meant to imply that after a proton-neutron collision an alpha particle is emitted for all the reactions leading to the p,pnα product. The alpha may be emitted as single nucleons by knock-on collisions or deexcitation, or deuterons, tritons, or He^3 may be emitted. Because of the large alpha-particle binding energy, it is possible that the proton-neutron collision followed by excitation by the collision products of an alpha-emitting mode of the nucleus with or without any further nucleon-nucleon collisions is a likely mechanism.

There are several other types of reactions each represented in Table II by one or two examples. Again the large number of pathways from target to product as well as the small number of examples for each reaction type precludes any definite conclusion about the likelihood of the possible mechanisms.

This work extends the cross-section measurements for spallation reactions on low-Z target elements up to a proton kinetic energy of 5.7 Bev. It is, consequently, worthwhile to extend the excitation functions to 5.7 Bev and look for any interesting energy-dependent effects on the cross sections.

F. Excitation Functions

Figures 3 to 10 inclusive, give the energy dependence of the cross section for the various reactions studied in this work and include literature data. The excitation functions are plotted for a

proton energy greater than 100 to 300 Mev. Each point has an error limit associated with it which was taken from the literature. For the points which were obtained from the literature as ratios of product-to-monitor cross sections and combined with newer monitor cross sections, the error limits do not include the (relatively small) error on the monitor cross section. The points without any error limit given are either the result of only one bombardment (for this work) or had no error limit given in the literature. The smooth curve drawn through each set of points is only meant to serve as a rough guide, and in a few cases, e.g., $Be^{9}(p,p2n)Be^{7}$ has hardly any meaning. For reactions written as target (p,X), product X refers to any combination of nucleons and fragments emitted that conserves charge and nucleon number.

1. Beryllium. Figure 3 gives the excitation function for the reaction $Be^{9}(p,p2n)Be^{7}$ from the literature data and this work.[19,34] Except for the Bev point from this work, the cross section appears to be decreasing strongly with increasing energy. More work is definitely needed to see if the minimum around 3 to 400 Mev is real.

2. Carbon. The excitation functions for the reactions $C^{12}(p,pn)C^{11}$ and $C^{12}(p,pn\alpha)Be^{7}$ obtained from the literature data[15,16,19,26,35-41] and this work are given in Fig. 4. As can be seen the $C^{12}(p,pn)C^{11}$ reaction has been fairly extensively studied. The excitation function for this reaction appears to go through a slight minimum in the 1 to 2-Bev energy range. The $C^{12}(p,pn\alpha)Be^{7}$ excitation function is remarkably flat over a wide energy range.

3. Nitrogen. Figure 5 gives the literature data[26,27] and the results of this work for spallation reactions on nitrogen. The existence of a minimum in the $N^{14}(p,pn)N^{13}$ excitation function is not definite because of the error limits on the data points. More work is necessary to clear up this point. The excitation function for the reaction $N^{14}(p,X)C^{11}$ appears to decrease in a uniform manner with increasing energy.

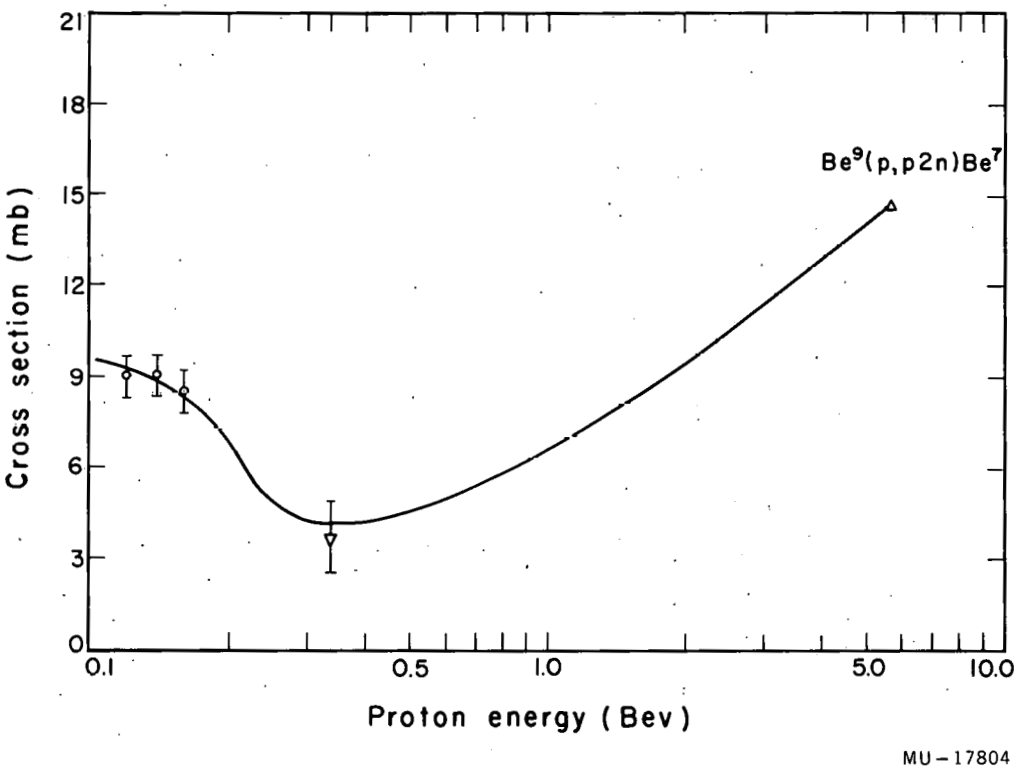

Fig. 3. $Be^{9}(p,p2n)Be^{7}$ excitation function. ○ and △ are the points from references 34 and 19, respectively; ▽ is from this work.

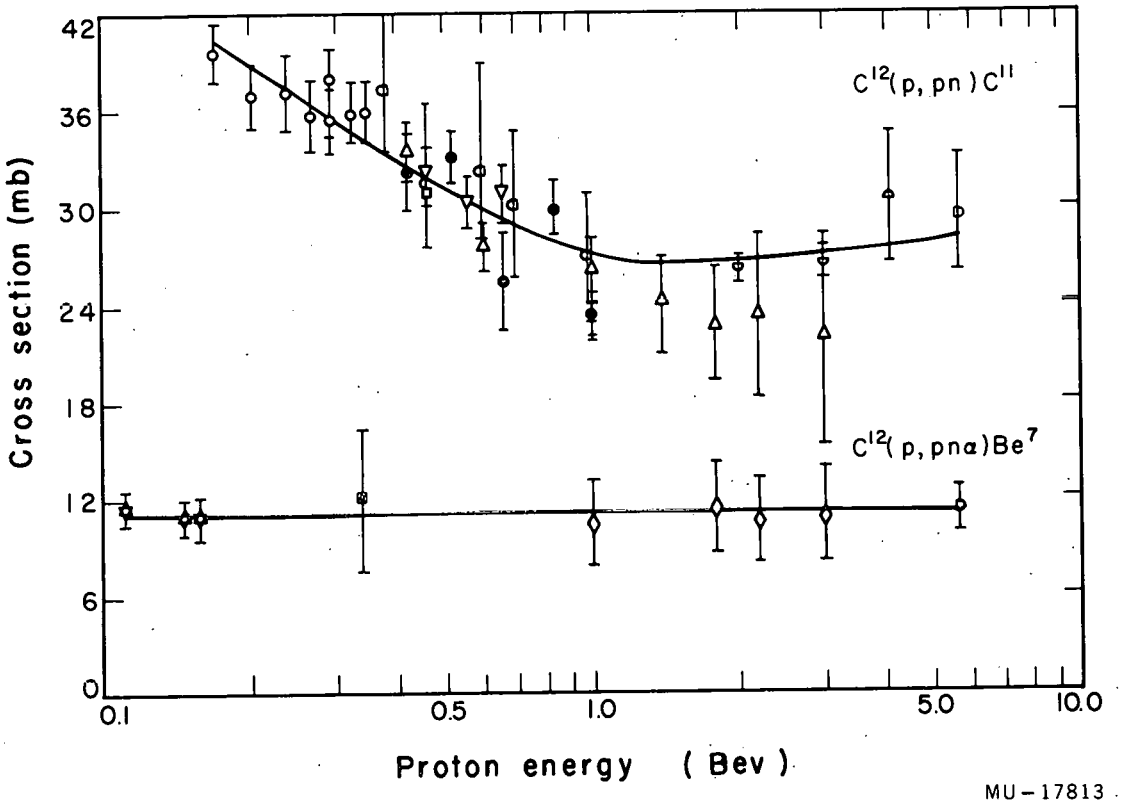

Fig. 4. $C^{12}(p,pn)C^{11}$ and $C^{12}(p,pn\alpha)Be^{7}$ excitation functions.

= reference	15	= reference	35	= reference	39
= "	16	= "	36	= "	40
= "	19	= "	37	= "	41
= "	26	= "	38	= this work	

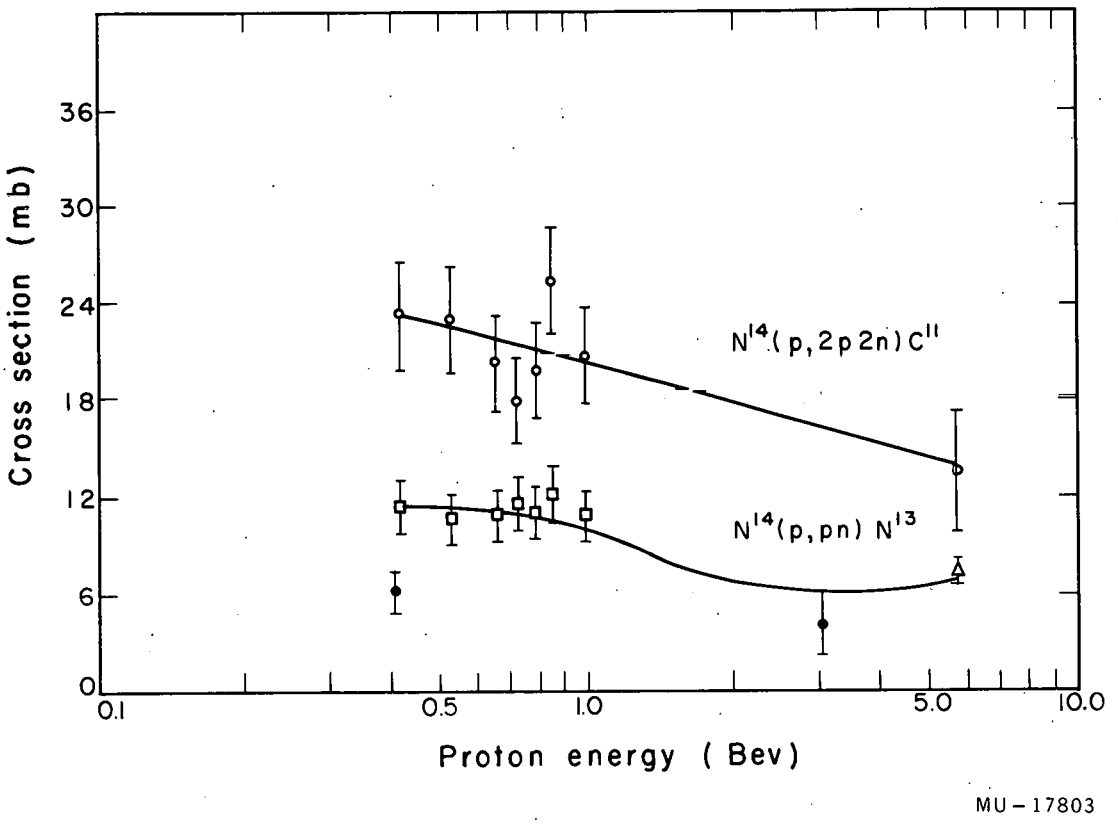

Fig. 5. $N^{14}(p,2p2n)C^{11}$ and $N^{14}(p,pn)N^{13}$ excitation functions. ○,□ = reference 26, ● = reference 27, and Δ,D = this work.

4. Oxygen. The spallation data for oxygen from this work are combined with the literature data[19,26] to give in Fig. 6 the excitation function for the reactions $O^{16}(p,pn)O^{15}$ and $O^{16}(p,X)N^{13}$. The p,pn excitation function does not appear to show the same minimum as do the nitrogen and carbon points. However, there is no data in the 1 to 5-Bev region where the minimum would exist, if present. The general slope of both excitation functions in Fig. 6 seems to be less than that of the data for nitrogen and the $C^{12}(p,pn)C^{11}$ reaction. The points for the reaction $O^{16}(p,X)C^{11}$ which are not shown reveal almost the same magnitude and energy dependence as do those for N^{13}.[19,26]

5. Fluorine. The most noticeable feature of the fluorine data in Fig. 7 is the scatter of the points, especially for the p,pn reaction.[19,26,27] The points for the p,pn reaction appear to go through a minimum at 1 Bev and a maximum at 3 Bev. There are no known reasons why the result from this work should be lower for the p,pn reaction than the other work. The Teflon foil used in this work was thicker (165 mg/cm^2) than the foil used by Markowitz et al.[27] (2.7 mg/cm^2) or Symonds et al.[26] (51.5 mg/cm^2). Also as mentioned before, the aluminum monitor foils were placed on the down-beam side of the foil stack rather than the up-beam side as was done by Markowitz et al.[27] Secondary reactions by slow nucleons in the monitor foil can not be the reason, because the cross section for the monitor reaction $Al^{27}(p,X)F^{18}$ was determined under the same conditions. If the monitor reaction cross section were affected by secondaries influencing the $Al^{27}(p,3pn)Na^{24}$ cross section, the F^{18} monitor cross section would be low. This does not seem to be the case (See Fig. 8). Also the $Al^{27}(p,X)F^{18}$ monitor reaction should be relatively free from secondary influence.

No points are given for N^{13} production from F^{19} because work done at a proton energy of 420 to 980 Mev gives only an upper limit of 0.4 to 0.6 mb.[26] Nitrogen-13 activity was definitely resolved from the decay curves for fluorine targets bombarded by 5.7 Bev protons to give a production cross section of 1.5 ± 0.5 mb (Table II). In view of the

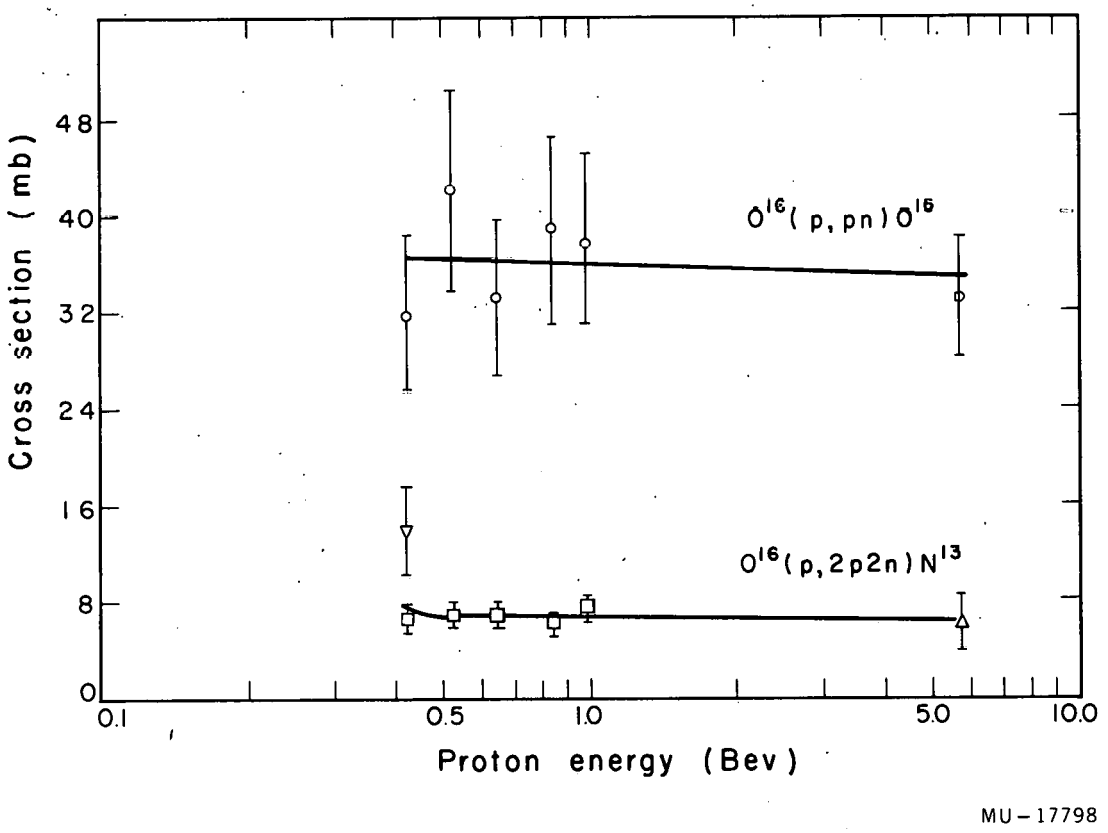

Fig. 6. $O^{16}(p,pn)O^{15}$ and $O^{16}(p,2p2n)N^{13}$ excitation functions.
▽ = reference 19, □, ○ = reference 26, △, ▯ = this work

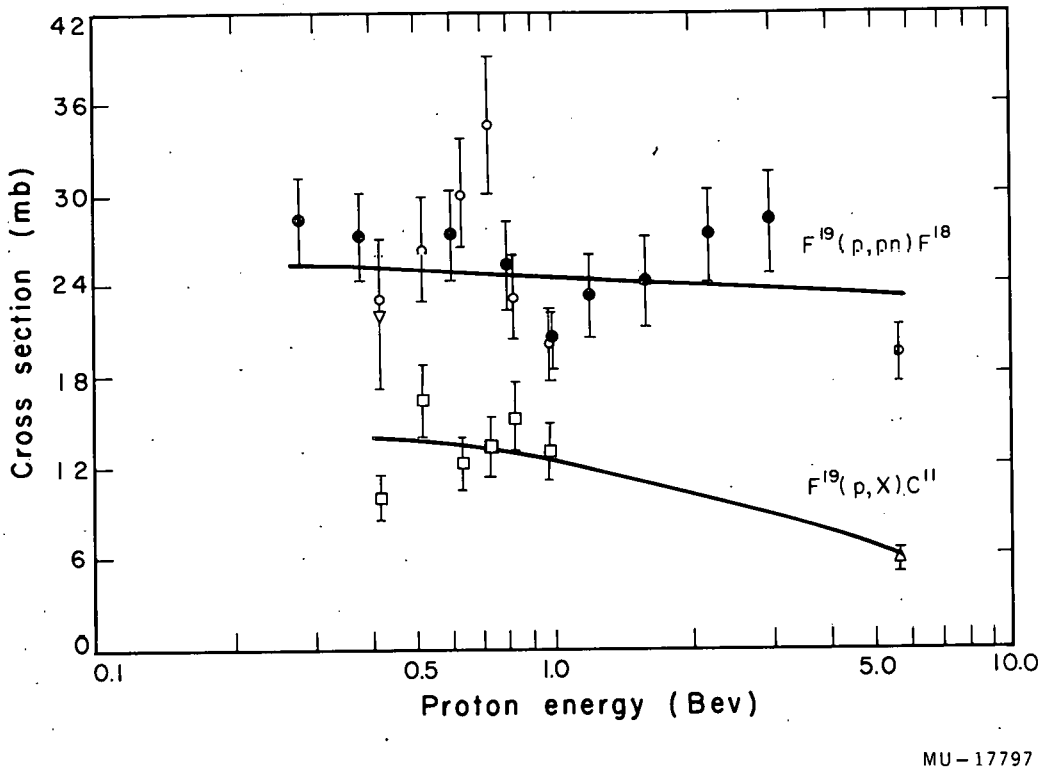

Fig. 7. $F^{19}(p,pn)F^{18}$ and $F^{19}(p,X)C^{11}$ excitation functions. ▽ = reference 19, □, ○ = reference 26, ● = reference 27, △, ▯ = this work.

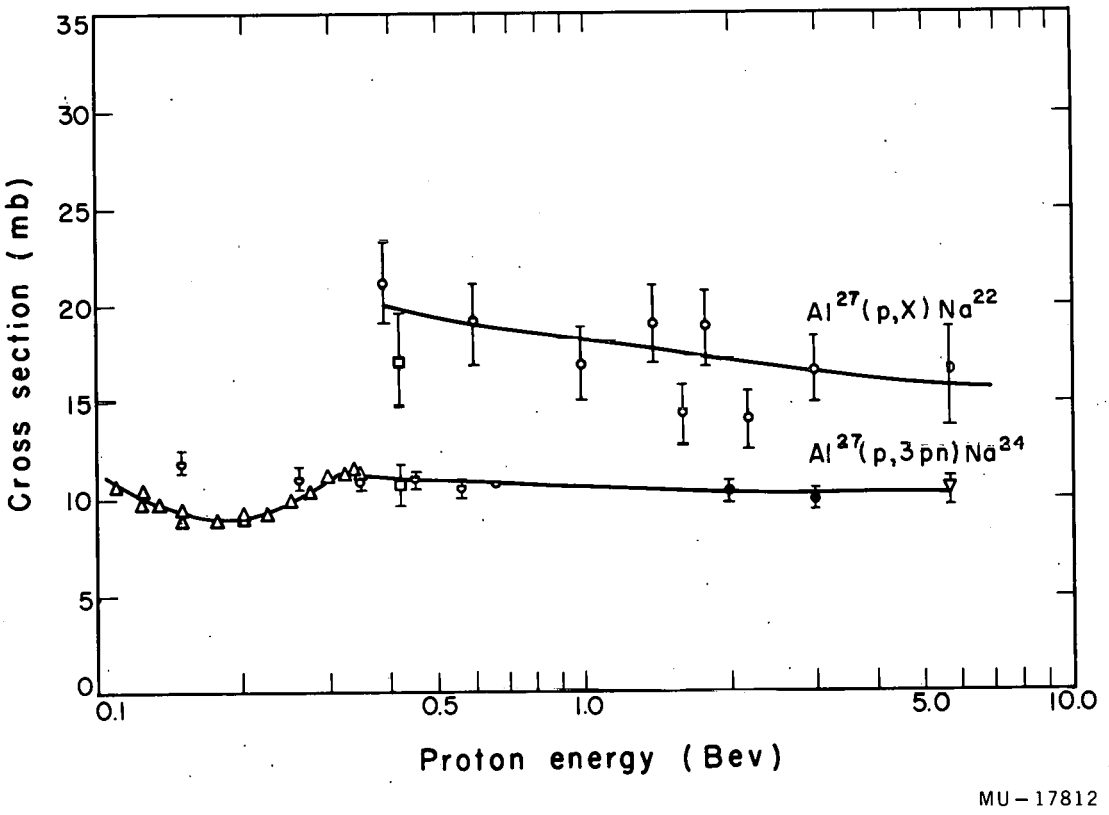

Fig. 8. $Al^{27}(p,3pn)Na^{24}$ and $Al^{27}(p,X)Na^{22}$ excitation functions.

● = reference 15 ⊽ = reference 40 D,Δ = this work

□ = " 19 Δ = " 42

◇ = " 36 ○ = " 43

independence or slight decrease of the excitation functions with increasing energy for most of the reactions studied, it is difficult to explain this opposite trend of the N^{13} data.

6. Sodium. No curves are given for sodium, because there appears to be no cross-section data at high energies in the literature.

7. Aluminum. Of the low-Z elements studied in this work, aluminum is the most extensively studied. Figure 8 gives the cross-section data for the often-used monitor reaction[15,19,36,40,42] $Al^{27}(p,3pn)Na^{24}$ and the reaction $Al^{27}(p,pn\alpha)Na^{22}$.[19,43] The excitation function for Na^{24} production is a combination of the graphs given by Cumming et al.[15] and Hicks et al.[42] and the 10.5-mb point at 5.7 Bev. This curve was then used to convert into absolute cross sections the literature values of ratios of various reaction cross sections to the monitor cross section for Na^{24} production from aluminum.[40,43] The data of Prokoshkin and Tiapkin for Na^{24} production, given as ratios of the cross section at a given proton energy to that at 660 Mev,[40] was converted by means of the above curve, and the resulting cross-section points were added. Ratios were also given for Na^{22} production. They were not included, because the Na^{22} excitation function in Fig. 8 is not reliable enough to use to convert these ratios into cross sections.

Inspection of Fig. 8 shows that the excitation function for Na^{24} production is flat above 0.5 Bev within the error limits, whereas the Na^{22} data show a decrease in value with increasing energy. The curious minimum in the $Al^{27}(p,3pn)Na^{24}$ excitation curve may be an expression of a possible increase in the cross section due to the onset of meson production,[39] although the work of Prokoshkin and Tiapkin does not show such a minimum.[40]

Figure 9 shows the excitation functions[19,39,43] for the reaction $Al^{27}(p,X)F^{18}$ and $Al^{27}(p,X)N^{13}$. No points are given for O^{15}, because at the time that the work in the literature was done, the existence of 3.4-min Ne^{24} was not known.[7] The points for F^{18} production taken from the works of Friedlander et al.[43] and Marquez[19] were increased by 3%

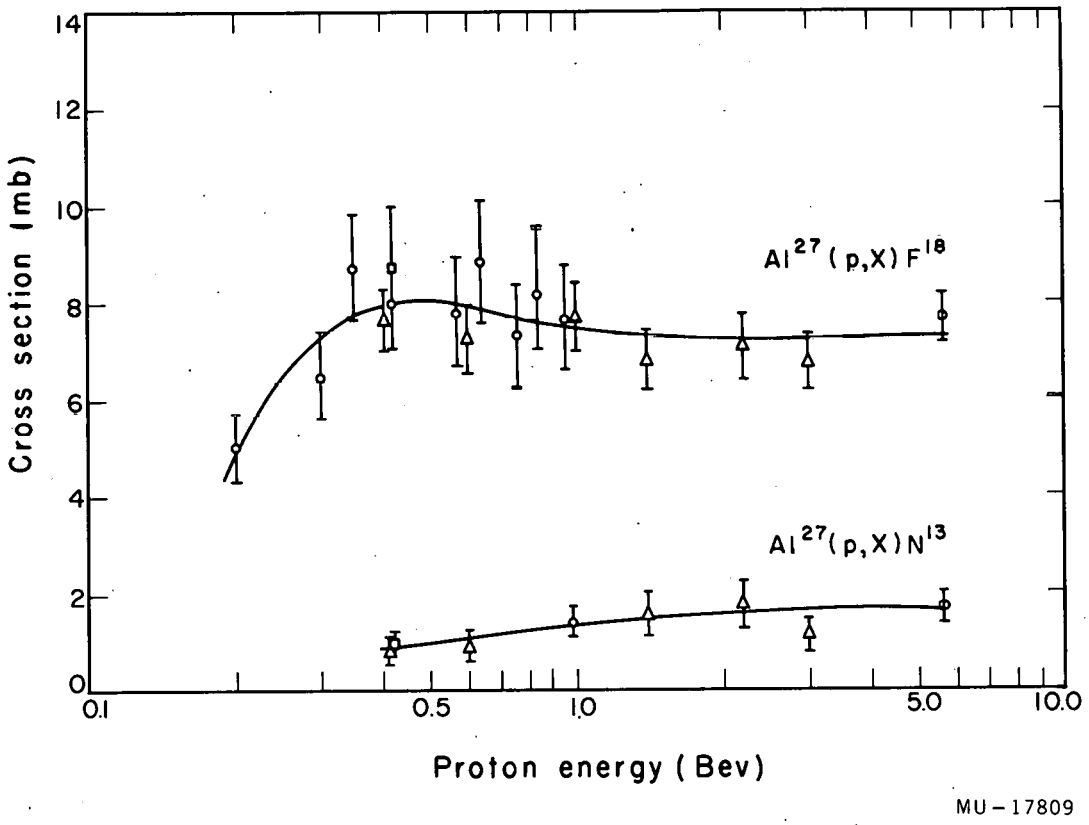

Fig. 9. $Al^{27}(p,X)F^{18}$ and $Al^{27}(p,X)N^{13}$ excitation functions.
□ = reference 19 △ = reference 43
○ = " 39 ◗ = this work

to account for the 3% electron-capture decay branch[7] in F^{18}. The F^{18} points above 1 Bev show little variation with energy, with the "usual" increase with decreasing energy below 1 Bev. Contrary to most of the data, the N^{13} points indicate an increase in cross section with increasing proton energy. N^{13} may be a sufficient number of mass units away from the target atomic mass that high-energy incident particles would be needed to cause the emission of the requisite number of nucleons, either singly or in chunks.

The points for C^{11} and Be^{7} production from aluminum in Fig. 10 show an even stronger increase with increasing proton energy.[19,39,43] Again, as has been suggested, the incident energy necessary to cause the required mass change may be high.[43] Because the rise in cross section continues into the Bev region, it seems quite possible that the increase in average number of mesons produced per nucleon-nucleon collision in the nucleus is important.

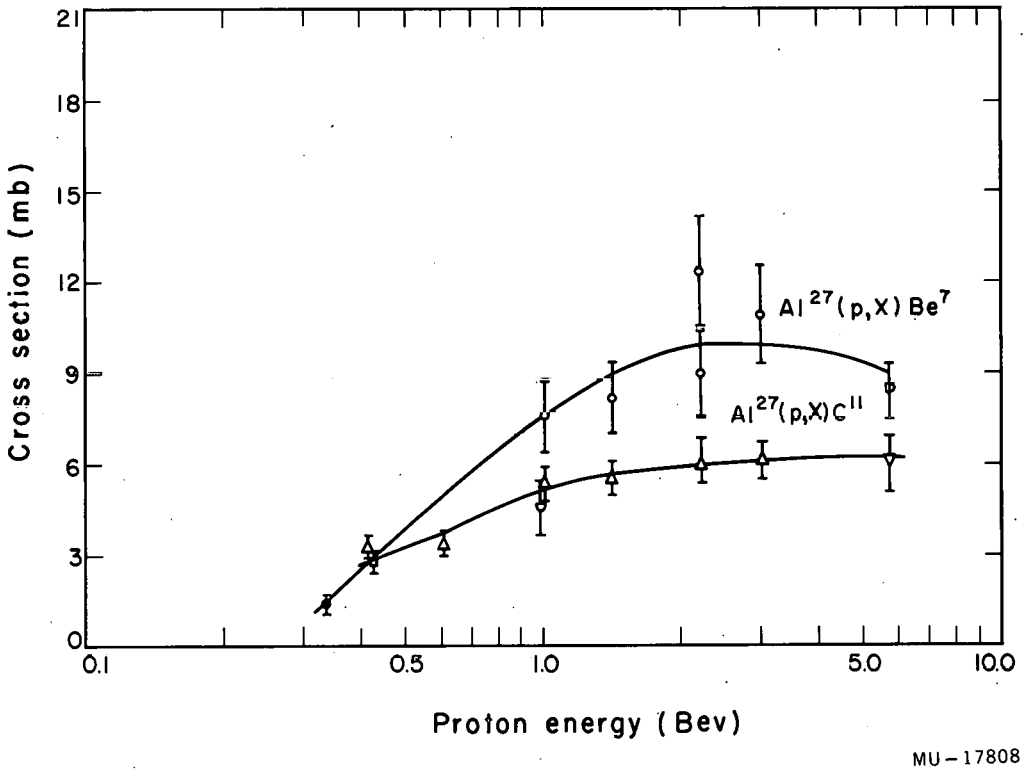

Fig. 10. Al^{27}(p,X)C^{11} and Al^{27}(p,X)Be^{7} excitation functions.
● , □ = reference 19 ○ , △ = reference 43
◒ = " 39 ◑ , ▽ = this work

V. SUMMARY

In general the spallation cross sections for 5.7-Bev protons incident on low-Z elements show no striking difference from those obtained on the same elements at 500 Mev and up. Some of the reactions, in particular those which lead to products 1 atomic mass unit (amu) away from the target, yield cross sections which vary quite a bit from element to element. Other reactions yield cross sections that are quite independent of the target atomic number. The excitation functions, when extended up to 5.7 Bev, exhibit no discontinuities or strong energy dependence. Most of them are either independent of or decrease somewhat with increasing bombarding energy in the Bev energy range. A couple of p,pn excitation functions seem to have a slight minimum in the 1 to 2-Bev energy region, but the minimum is within the error limits. There are also a few excitation functions that increase with increasing energy in the Bev region. These are all for products whose mass is at least 14 amu less than that of the target. It appears (See Table III) that there is a strong correlation between the magnitude of the p,pn cross section and the number of available nucleons in the target nucleus. In the next section an attempt will be made to develop a theory to explain the magnitude and variation of the p,pn and related cross sections.

NUCLEAR REACTIONS OF LOW-Z ELEMENTS WITH 5.7-Bev PROTONS: NUCLEAR STRUCTURE AND SIMPLE NUCLEAR REACTIONS

Part II

NUCLEAR STRUCTURE AND SIMPLE NUCLEAR REACTIONS

I. INTRODUCTION

In recent years a large number of cross sections for various types of spallation reactions has accumulated.[11,26,44-50] The Monte Carlo method[51,52] coupled with a Fermi gas model of the nucleus has been used to interpret the experimental results. At medium and high bombarding energies (hundreds of Mev and up) and for products whose mass is more than a very few atomic mass units less than that of the target, the existing calculations are in fair agreement with the experimental results.[11,52,53] However, for (p,pn) and (p,2p) reaction products whose mass is one unit less than that of the target, the calculated cross sections, when compared to experimental values, are low by a factor of two to three.[11,52,54] Also the calculations predict a smooth dependence of the cross section with the atomic mass of the target, whereas the experimental p,pn and p,2p cross sections show quite an erratic variation. It has been suggested that adding a diffuse nuclear boundary to the existing Monte-Carlo calculations would correct this discrepancy.[52] Possible shell-structure effects have been advanced as an explanation for the apparent irregularity in the experimental values.[26,27]

Because of the existing discrepancy, it was thought worthwhile to try a method of calculating p,pn cross sections based on the optical and shell models with a diffuse nuclear surface. Recent work has shown that such an approach is profitable, and proton scattering by protons in buried shells has been described.[29,55] Throughout the rest of this work the discussion is restricted mainly to p,pn cross sections because of the preponderance of p,pn over p,2p cross-section data in the literature. However, with minor changes, the theoretical results apply just as well to p,2p, $p,p\pi^-$ (including p,n), $p,p\pi^+$, and possibly p,p^* reaction cross-section data. In order to simplify certain aspects of the calculation, the theory is developed to be valid in the multi-Bev region of bombarding energies.

II. p,pn REACTION PATHS

A consideration of p,pn reactions indicates that there are several possible paths by which an isotope containing one neutron less than the target nuclei can be produced. If the proton-neutron collision is inelastic, the p,pn product can be formed as follows:

(a) All the collision products can escape without further interaction in the nucleus. The neutron must have been knocked out of a shell, which leaves the nucleus in an excited "hole" state stable to particle emission.

(b) A neutron can be left behind with an energy increase (about 8 to 16 Mev) such that the primary collision is followed by nuclear emission of only one neutron. The Coulomb barrier suppresses proton emission for all but the low-Z elements.

A proton-proton inelastic collision can also form the p,pn product by:

(c) Leaving a proton behind with an energy increase (also about 8 to 16 Mev) such that the primary collision is followed by nuclear emission of a neutron.

Elastic p-n and p-p collisions form the p,pn product by the same pathways as for the inelastic p-n collisions. Similar pathways also hold for the p,2p reaction cross section.

An estimate of the relative contribution of processes (a) and (b) can be made by reference to the experimental cloud-chamber data on p-n and p-p collisions. Out of 134 inelastic events caused by 1.72-Bev neutrons on hydrogen gas,[56] 86 events produced neutrons by the reaction (np , $np\pi^+\pi^-$). The rest of the events consisted of the reactions (np, $pp\pi^-$) and (np, $pp\pi^-\pi^o$). Only two out of the 86 events, which are the only ones that can contribute to the p,pn cross section by process (b) produced protons with an energy as low as 40 Mev. The lowest-energy neutron had a kinetic energy as low as 74 Mev. A study of 201 inelastic events caused by 3.8 ± 2.4-Bev neutrons on protons[57] showed that there were 35 $pp\pi^-$ events, 97 $pn\pi^+\pi^-$ events, 34 $pn\pi^+\pi^-\pi^o$ .... events (the dots refer to other possible neutral pions), and 35 events of various types that produce between two and five pions. The 131 $pn\pi^+\pi^-$ and $pn\pi^+\pi^-\pi^o$.. events provided only one proton with a kinetic energy less than 20 Mev.

These results can be used in the following manner: For 1.72-Bev neutrons on hydrogen, no protons from 86 events were found with kinetic energies in the 8- to 16-Mev range. For the 3.8-Bev neutrons on hydrogen, one proton from 131 events had a kinetic energy within the 8- to 16-Mev range. These numbers are for high-energy neutrons on protons. For high-energy protons incident on neutrons, these same results should hold if neutrons are exchanged for protons in the $pn\pi^+\pi^-$ and $pn\pi^+\pi^-\pi^o$ events only. These numbers give a relative contribution from process (b) which is $\leq 2\%$ of process (a).

The relative contribution of process (c) is more difficult to estimate, as there are no laboratory-system scatter diagrams for inelastic p-p collisions in the literature. However, one can use the n-p scatter-diagram data by assuming that the energy and angular distributions for the scattered particles in the $pp\pi^-$ and $pp\pi^-\pi^o$ reactions from n-p collisions can be used for the $pn\pi^+$ and $pn\pi^+\pi^o$ reactions from p-p collisions respectively. An analysis of 2.75-Bev p-p events[58] shows that slow protons are produced in $pn\pi^+$ and $pn\pi^+\pi^o$ events (the neutrons have high momentum). Since the majority of two-prong inelastic events are $pn\pi^+$ and $pn\pi^+\pi^o$ types, the fraction of the inelastic events from 6.2-Bev p-p collisions[59] which are two-pronged, 0.32, was assumed to apply to $pn\pi^+$ and $pn\pi^+\pi^o$ events only. Out of 35 $pp\pi^-$ events from 3.8 ± 2.4-Bev neutrons on hydrogen, three produced protons with kinetic energies between 8 and 16 Mev. The above assumptions and the assumption that a p-p collision in a nucleus is equally probable to a p-n collision gives the value of the relative contribution of process (c). This is $\leq 0.32 \times 3/35 = 3\%$ of process (1). Consequently, the relative contribution of processes (b) and (c) is $\leq 5\%$ of process (a) and can be neglected.

III. APPROXIMATIONS

A. Impulse Approximation

At high incident energies the impulse approximation should be valid:[60] i.e., the wavelength of the incident proton is sufficiently short that the proton may be considered to interact with only one nucleon at a time in the nucleus. The effect of the rest of the nucleons is the provision of a potential well and resultant momentum distribution for the particular target nucleon considered. Also the time it takes the incident nucleon to cross the nucleus is so short that the nucleus would not have time to rearrange itself or affect the course of the elementary collision. The exclusion principle has a negligible effect on the elementary nucleon-nucleon collision, as the amount of momentum space forbidden is negligible compared to the volume available. The incident proton can then be considered to have "snatched" a nucleon from the nucleus so fast that the only effect is to leave the target nucleus in an excited nucleon-hole state.[61] If the products of the elementary collision get out of the nucleus without further interaction, and the resultant excited state of the nucleus is not a particle-emitting state, the product nucleus contributes to the p,pn or p,2p cross section.

B. Zero-Degree Scattering-Angle Approximation

Another approximation which greatly simplifies the calculations is that, for inelastic n-p and p-p collisions, the particles are scattered at zero degrees in the laboratory system. The validity of this approximation can be seen from an examination of the free n-p and p-p collision data. Cloud-chamber data taken for 1.72-Bev-average-energy neutrons on hydrogen[56] show that three-fourths of the doubly produced mesons have a median laboratory scattering angle of 36 degrees. The nucleons associated with these mesons have a median laboratory scattering angle of 17 degrees. Singly produced mesons and the associated nucleons have median laboratory scattering angles of 34 degrees and 20 degrees respectively. Inelastic events produced by 3.8-Bev-average-energy neutrons on hydrogen[57] show that one half the particles are emitted within 20 degrees laboratory of the primary

beam, and two thirds within 30 degrees of the primary beam. Roughly one-half of the inelastic events emit all particles within 35 degrees of the forward direction, and there are only a few events which emit two or more particles at an angle greater than 35 degrees. Three-fourths of the charged particles produced by 5.3-Bev p-p collisions emerge within 20 degrees of the incident beam.[62] Other work indicates a median laboratory scattering angle of 32 degrees for neutral pions produced by 6.2-Bev proton-nucleon collisions.[63] Cosmic-ray work indicates that for higher incident energies, the median laboratory scattering angle is as small as, or smaller than, the values given above.[3,64]

Contrary to the case for inelastic collisions, the approximation of a zero-degree scattering angle for the products is definitely invalid for n-p and p-p elastic collisons. The $\cos^n\theta$ angular dependence taken to be the same in the forward c.m. hemisphere for p-n as for p-p collisions, (Appendix I) ensures that at high energies ($n \gg 1$)[65,66] either one or the other of the nucleons has a very high probability of being scattered at large angles (close to 90 degrees) and having a low energy in the laboratory system. At 5.7 Bev, the energy and scattering angle of the target particle in the laboratory system corresponding to the angle in the c.m. system at which most nucleons are emitted (the maximum of $\cos^n\theta \sin\theta$ were $n = 36$)[65,66] is 39 Mev and 80 degrees (Appendix I). The same cosine dependence of the scattering angle ensures that the other nucleon is scattered at almost zero degrees in the laboratory system.

The invalidity of the zero-degree laboratory scattering-angle approximation for elastic p-n and p-p collisions is one of the reasons the ensuing treatment is restricted to multi-Bev bombarding energies where the elastic fraction of the total collision cross section is low. Since the contribution to the p,pn cross section from elastic p-n collisions can be only crudely estimated, restriction of the bombarding energy to the multi-Bev region minimizes the error in this estimation.

C. Use of Classical Trajectories

Another helpful approximation depends on the fact that at Bev energies the wavelength of the incident nucleon is small compared to

nuclear dimensions ($\lambda\!\!\!^{-}$ is 0.03 fermis for a 6-Bev nucleon). Consequently, the incident nucleon may be considered to have a classical trajectory in the nucleus. The particles scattered in the inelastic p-n or p-p collision in the nucleus will also be assumed to have classical trajectories ($\lambda\!\!\!^{-}$ is 1.1 and 0.4 fermis for 100-Mev pions and nucleons respectively).[51] On the other hand, all the target nucleons have insufficient momentum, especially in the surface region, to be treated classically and will be treated quantum mechanically.

D. Other Approximations

The use in this work of the high-energy cloud-chamber scatter-diagram data depends on the assumption that the energy and angular distributions of the scattered particles for free n-p collisions can be "inverted" to describe p-n collisions and then lifted into the nucleus with only small resultant changes. The inversion can be accomplished by exchanging the forward c.m. hemisphere for the backward c.m. hemisphere. The angular and energy distributions of the scattered particles in the nucleus will be affected by a number of factors such as the Pauli exclusion principle, motion of the target nucleon, etc. It will be shown later that most of the contributions to the p,pn reaction come from the nuclear surface where the effect of these factors is small.

IV. THEORY

A. Development

By the use of the previously discussed approximations, the contribution to the p,pn cross section from inelastic p-n collisions [process (a)] can be found. Consider a cylindrical coordinate system whose origin coincides with the center of a nucleus and in which a proton is coming in parallel to the z axis. Then, for a given p-n inelastic interaction which produces 2 nucleons and t-2 mesons, the probability per unit path length, $P_{t,k}$, that the incident proton gets to a point r,z,φ without interacting, collides with the kth nucleon, and all the collision products escape without further interaction is

$$P_{tk} = \exp\left(-\sigma_1 \int_z^\infty \rho(R)dy\right) \exp\left(-\sum_{i=1}^{t} \sigma_i \int_{-\infty}^{z} \rho'(R)dy\right) \sigma_2 P_k (r\ z\ \varphi). \quad (10)$$

The first exponential factor gives the probability that the proton gets to r,z,φ without colliding with any nucleons, and the second exponential gives the probability that all the collision products escape (with 0^o scattering angle) without further interaction. The increment of path length, dy, is along the path of the incident and emergent particles. Here $\sigma_2 P_k (r\ z\ \varphi)$ is the probability per unit path length that the incident proton collides inelastically with the kth nucleon at r z φ. The inelastic p-nucleon interaction cross section is σ_2, and $P_k (r\ z\ \varphi)$ is the normalized probability per unit volume of finding the kth nucleon at r, z, φ. The term $\rho(R)$ ($R^2 = r^2 + y^2$, where y is equivalent to z) gives the total nuclear density distribution in the target nucleus and $\rho'(R)$ is the same as $\rho(R)$ except that the kth nucleon has been removed from the total nucleon density distribution, because after the collision it is one of the collision products. The total interaction cross section for the incident proton with a target nucleon is σ_1. The σ_i are the free nucleon-nucleon and pion-nucleon total collision cross sections, and the sum is over all the t particles produced in the particular type of p-nucleon interaction under consideration. The integrals in the exponents

give the total number of nucleons per unit area along the path lengths of the incident and emergent particles. The two exponential terms are the equivalent of factors used in the optical model to give the damping of the incident and emergent particle waves.[67]

If the target nucleus is in a uniform beam of bombarding protons, the cross-section contribution, σ_{tk}, to single collision processes from the kth nucleon is obtained by integrating P_{tk} along the path length and then weighting the result by $rdrd\varphi$ and integrating over all r and φ. This gives

$$\sigma_{tk} = \int_0^{2\pi} d\varphi \int_0^{\infty} r dr \int_{-\infty}^{\infty} \exp\left(-\sigma_1 \int_z^{\infty} \rho(R)\, dy\right) \exp\left(-\sum_{i=1}^{t} \sigma_i \int_{-\infty}^{z} \rho'(R)\, dy\right) \sigma_2 P_k (r\ z\ \varphi)\, dz. \tag{11}$$

The constant σ_2 can be moved outside the integrals. If one sets σ_{tk} equal to $\sigma_2 M_{tk}$, then σ_2 can be ignored at this stage. An average of Eq. (11) over the inelastic collision types (different values of t) and energy spectrum of the scattered particles (different values of each σ_i) gives the result

$$M_k = \overline{M_{tk}} = \int_0^{2\pi} d\varphi \int_0^{\infty} r dr \int_{-\infty}^{\infty} \exp\left(-\sigma_1 \int_z^{\infty} \rho(R)\, dy\right) \exp\left(-\bar{\sigma} \int_{-\infty}^{z} \rho'(R)\, dy\right) P_k (r\ z\ \varphi)\, dz\ , \tag{12}$$

where $\bar{\sigma}$ is an appropriate average of $\sum_{i=1}^{t} \sigma_i$, and M_k may be regarded as the fractional availability of the kth nucleon in the nucleus for single-collision processes.

The factor P_k is given by

$$P_k = \int \Psi_A^* \Psi_A\, d\tau\ , \tag{13}$$

where Ψ_A is the antisymmetric nuclear wave function. Because the integrand in Eq. (12) depends only on the space coordinates of the kth nucleon, the integration in Eq. (13) is over the spin coordinates of all the nucleons and the space coordinates of all nucleons except those of the kth. If the nucleus is regarded as an assembly of independent particles, Ψ_A is equal to the normalized Slater determinant. Substitution of this determinant into Eq. (13) and performance of the integrations over the coordinates of all nucleons (kth excluded) gives

$$P_k = \frac{1}{A} \sum_q \int_{\text{spin space}} \psi_q^* (\tau_k) \psi_q (\tau_k) \, d\alpha \, . \qquad (14)$$

The $\psi_q (\tau_k)$ represents the single-particle wave functions of the kth nucleon, and q stands for a set of quantum numbers needed to specify a nucleon completely. The sum is over all A sets of q, where A is the number of nucleons in the nucleus. The experimental evidence indicates that nucleons in the nucleus show strong spin-orbit coupling.[68] Consequently, if the $\psi_q(\tau_k)$ represent individual-particle wave functions that are spin-orbit-coupled, they must be transformed so that the space and spin coordinates appear explicitly. This is done by use of the Clebsch-Gordan coefficients to give[69]

$$\psi_q (\tau_k) = \sum_{n,\ell} C(\ell s j; m_\ell, m_j - m_\ell) \, T_{n\ell j} (R_k) \, Y_{\ell m_\ell} (\theta_k \varphi_k) \, \chi_{s, m_j - m_\ell} \qquad (15)$$

where $T_{n\ell j} (R_k)$ is the radial part of the wave function, $Y_{\ell m_\ell} (\theta_k \varphi_k)$ is a normalized spherical harmonic, and $\chi_{s, m_j - m_\ell}$ is the spin function. For a given m_j, the sum over m_ℓ is restricted by the requirement that m_j equal $m_\ell + m_s$, where m_s is either + 1/2 or - 1/2.

A given term in the q sum in Eq. (14) refers to a specific single-nucleon state with quantum numbers n, ℓ, j, m_j. There are $(n+p)_{n\ell j}$ terms in

the q sum which differ only by m_j, where $(n+p)_{n\ell j}$ is the number of nucleons in the $n\ell j$ shell (the subscript n is the principal quantum number). Because each nucleon in a given shell may assume any one of the m_j values, an average over the m_j values must be taken. The target nucleus is bombarded in an essentially field-free region as far as its alignment is concerned, so that each one of the m_j states in equally probable. Substitution of Eq. (15) into Eq. (14), breaking up the sum into a sum over $n\ell j$ shells, and averaging over the m_j values using the operator

$$\frac{1}{2j+1} \sum_{m_j=-j}^{j}$$

gives the result

$$P_k = \frac{1}{A} \sum_{n\ell j} \sum_{m_j m_\ell} \frac{(n+p)_{n\ell j}}{2j+1} \; C^2(\ell s j; m_\ell, m_j - m_\ell)$$

$$T^2_{n\ell j}(R_k)\, Y^*_{\ell m_\ell}(\theta_k \varphi_k)\, Y_{\ell m_\ell}(\theta_k \varphi_k) \,. \qquad (16)$$

The equal probability that m_j assume any value between -j and j allows m_ℓ to assume all of its values between $-\ell$ and ℓ. The m_j sum can be done by use of standard procedures[69] for manipulating Clebsch-Gordan coefficients to give

$$P_k = \frac{1}{A} \sum_{n\ell j} \sum_{m_\ell=-\ell}^{\ell} \frac{(n+p)_{n\ell j}}{2\ell+1} \; T^2_{n\ell j}(R_k)\, Y^*_{\ell m_\ell}(\theta_k \varphi_k)\, Y_{\ell m_\ell}(\theta_k \varphi_k) \,.$$

Use of the spherical-harmonic addition theorem,[70]

$$\sum_{m_\ell=-\ell}^{\ell} Y^*_{\ell m_\ell}(\theta_k \varphi_k)\, Y_{\ell m_\ell}(\theta_k \varphi_k) = \frac{2\ell+1}{4\pi}$$

gives

$$P_k = \frac{1}{4\pi A} \sum_{n\ell j} (n+p)_{n\ell j}\, T^2_{n\ell j}(R_k) \,. \qquad (17)$$

Substituting Eq. (17) into Eq. (12) and summing over all nucleons gives for the fractional availability, M, of all the nucleons in the nucleus for single collisions ($R_k^2 = r_k^2 + z_k^2$)

$$M = \frac{1}{4\pi A} \sum_{k=1}^{A} \sum_{n\ell j} (n+p)_{n\ell j} \int_0^{2\pi} d\varphi \int_0^{\infty} r dr \int_{-\infty}^{\infty} \Big[\exp\left(-\sigma_1 \int_z^{\infty} \rho(R)\, dy\right)$$

$$\exp\left(-\bar{\sigma} \int_{-\infty}^{z} \rho'(R)\, dy\right) T^2_{n\ell j}\,(r_k^2 + z_k^2)\Big]\, dz. \qquad (18)$$

In Appendix II it is shown that Eqs. (17) and (18) hold also for j-j-coupled shell-model wave functions. The k sum may be done immediately, as each term is identical, which removes the 1/A. Likewise the φ integration may be done, as the integrand is azimuthally symmetric.

The part of M which contributes to the p,pn reaction by processes of type (a) is obtained by limiting $(n+p)_{n\ell j}$ to neutrons only and limiting the sets $n\ell j$ to those for which the sudden removal of a neutron with quantum numbers $n\ell j$ leaves the nucleus in an excited state stable to particle emission. This gives, for $M_{p,pn}$,

$$M_{p,pn} = \sum_{\substack{\text{allowed} \\ n\ell j \text{ values}}} n_{n\ell j}\; M_{n\ell j} \,. \qquad (19)$$

The fractional availability per neutron in the $n\ell j$ shell for single-collision processes, $M_{n\ell j}$ is given by

$$M_{n\ell j} = \frac{1}{2} \int_0^{\infty} r dr \int_{-\infty}^{\infty} \Big[\exp\left(-\sigma_1 \int_z^{\infty} \rho(R)\, dy\right)$$

$$\exp\left(-\bar{\sigma} \int_{-\infty}^{z} \rho'(R)\, dy\right) T^2_{n\ell j}\,(r^2+z^2)\Big]\, dz \,. \qquad (20)$$

The availability, $M_{n\ell j}$, for target protons is also given by Eq. (20) if the correct value of $\bar{\sigma}$ and form of $T_{n\ell j}\,(r^2+z^2)$ are inserted.

Equation (20) holds for a variety of potential-well shapes, such as the square, harmonic-oscillator, exponential wells, etc. In this work the harmonic-oscillator well will be used for two reasons. First, it gives a finite gradient to the nuclear surface, something which has been postulated to explain the difference between the calculated and observed p,pn cross sections.[27.52.54] Second, solutions to the Schrödinger equation can be obtained in an analytic form. This simplifies the numerical evaluation of Eq. (20). An additional simplification is introduced by the fact that for the harmonic-oscillator well, inclusion of a spin-orbit coupling term in the wave equation changes only the eigenvalues and not the wave functions. For this reason, the j subscript will be dropped from M and T in Eq. (20) from now on.

The normalized radial harmonic-oscillator wave functions for the first three radial shells are[71]

$$T_{n\ell} = \left(\frac{\beta^3 \, 2^{\ell+2}}{\pi^{1/2} \, (2\ell+c)!!} \right)^{1/2} B_n \left(\beta^2(r^2+z^2)\right)^{\ell/2} \exp\left(- \frac{\beta^2(r^2+z^2)}{2} \right) , \quad (21)$$

where c and B_n are a numerical constant and simple polynominal, respectively, both depending on n. Equation (21) is normalized to give 2 upon integration over the r and z coordinates. This is necessary to remove the factor of 1/2 brought in from the removal of the spherical harmonics. This factor of 2 appears because of the change from spherical coordinates used in the addition theorem to cylindrical coordinates used in Eqs. (20) and (21). The validity of this argument can be shown by removing the exponential factors from Eq. (20), substituting Eq. (21) into Eq. (20), and integrating over the r and z coordinates to get unity.

The density term $\rho\,(r^2+y^2)$ is obtained from Eq. (21) by putting y = z and

$$\rho\,(r^2 + y^2) = \frac{1}{4\pi} \sum_{n\ell} (n_{n\ell} + p_{n\ell}) \, T^2_{n\ell}/4\pi \, , \quad (22)$$

where $n_{n\ell}$ and $p_{n\ell}$ are the neutron- and proton-shell occupation numbers for the target nucleus. For a given n and ℓ, $n_{n\ell}+p_{n\ell}$ is the number of nucleons in the two shells obtained by setting $j = \ell + 1/2$ and $j = \ell - 1/2$. The $1/4\pi$ comes from the normalization requirement that we have

$$\int_{\text{all space}} \rho\,(r^2+y^2)\,d\tau = A\ ,$$

where A is the number of nucleons in the target nucleus, and $\rho\,(r^2+y^2)$ is obtained from Eq. (22) by subtracting one from that value of $n_{n\ell}$ whose subscripts are the same as those on $M_{n\ell}$.

Equation (22) was used for the nuclear-density distribution rather than the simpler

$$\rho\,(R) = \rho^{o}\left[\exp\left(\frac{R-c}{\alpha}\right)+1\right]^{-1}$$

obtained for most target nuclei from the electron-scattering results[72] for two reasons. One is that a single model is used by which the complex dependence of Eqs. (20), (21), and (22) on β can be removed, and the other is that there is only one adjustable parameter β rather than three -- β, c, and α. This also ensures a consistent nucleus whose total density distribution is built up out of the distributions of the individual nucleons.

The substitutions $u = \beta r$, $v = \beta v$, $w = \beta y$, simplify the complex β dependence remarkably. Making these substitutions and putting Eqs. (22) and (21) into Eq. (20) gives

$$M_{n\ell} = \frac{2^{\ell+1}}{\sqrt{\pi}\,(2\ell+c)!!}\int_{0}^{\infty} u\,du \int_{-\infty}^{\infty}\left\{B_n^{\,2}\,(u^2+v^2)^{\ell}\right. \tag{23}$$

$$\left.\exp\left[-u^2-v^2-\frac{\sigma_1\beta^2}{\pi^{3/2}}\int_{v}^{\infty}\rho(u^2+w^2)\,dw-\frac{\bar{\sigma}\,\beta^2}{\pi^{3/2}}\int_{-\infty}^{v}\rho'(u^2+w^2)\,dw\right]\right\}dv\ ,$$

where

$$\rho\,(u^2+w^2) = \sum_{n\ell}\,(n_{n\ell}+p_{n\ell})\,\frac{2^{\ell}\,B_n^{\,2}}{(2\ell+c)!!}\,(u^2+w^2)^{\ell}\,e^{-u^2-w^2}\ , \tag{24}$$

and $\rho'\,(u^2+w^2)$ bears the previously mentioned relationship to $\rho\,(u^2+w^2)$. The following table gives the values of $B_n^{\,2}$ and c for the different values of n:

n	c	B_n^2
1	1	1
2	3	$2\{\ell+3/2-(u^2+[v^2 \text{ or } w^2])\}^2$
3	5	$2\{(\ell+5/2)(\ell+3/2)-(2\ell+5)(u^2+[v^2 \text{ or } w^2])+(u^2+[v^2 \text{ or } w^2])^2\}^2$.

The double factorial stands for the product of all the odd integers $\leq 2\ell+c$.

For ease in interpreting the results, the harmonic-oscillator spring constant β in the exponents of Eq. (23) can be written as

$$\beta^2 = \frac{g}{A^{1/3}} , \tag{25}$$

where g is given by

$$g = \frac{0.847}{r_o^2} , \tag{26}$$

and r_o is the half central-density radius constant. Equations (25) and (26) are derived in Appendix III. As is discussed there, Eq. (26) is only approximately correct and gives values of r_o which are in error by from +3% for F^{19} to -9% for Ce^{142} when compared to values of r_o obtained in an exact manner.

B. Integral Evaluation

Equation (23) can not be integrated analytically, so it was integrated using Simpson's rule by means of the IBM-701 electronic computer. The interval size for Simpson's rule and the upper limits of integration were chosen such that the accuracy of $M_{n\ell}$ was less than or equal to 1%. The accuracy and program testing are helped considerably by noting that if both w integrations are removed, we obtain $M_{n\ell} = 1$. Also the u and w integrations of $\rho(u^2+w^2) + \rho'(u^2+w^2)$ with the limits, v, on the w integration replaced by infinity and all the multiplicative constants replaced by $2/\sqrt{\pi}$ gives $M_{n\ell} = 2A-1$. Using both these checks, it was found that replacing the upper u limit by b and the other infinite limits by (b^2-u^2), where b ranged from 4 for C^{12} to 5 for U^{238}, gave results for the checks accurate to about 1/2%. In order to obtain this accuracy, it was necessary for the Simpson's-rule program to divide the range of

the u integration into 32 intervals. Because the checks, each of which consisted of two integrations, gave results accurate to 1/2%, it was felt that adding a third integration would give results accurate to 1%. The time it took the machine to compute a single value of $M_{n\ell}$ ranged from 8 min for C^{12} to 40 min for U^{238}, with most of the medium-weight nuclides requiring 30 min per case. The computer was also programmed to print out the values of the integrand of the u,v integration given in Eq. (23) and the values of u and v. This was done to find out by means of contour plots what part of the nucleus contributed most to $M_{n\ell}$.

C. Input Parameters

For any given computation there are the three input parameters, σ_1, σ, and g. The value of σ_1 was taken to be 30 mb.[66] This is slightly lower than the preliminary experimental value of 32 ± 3 mb of the total n-p collision cross section for neutrons of 4.5-Bev average energy.[73] This difference will be corrected for later.

The average total exit cross section, $\bar{\sigma}$, was determined by first finding the distribution of the values of $\sum_{i=1}^{t} \sigma_i$ from the experimental laboratory scatter diagrams of the high-energy n-p inelastic collisions in the following manner: The analysis of inelastic events caused by 3.8 ± 2.4-Bev neutrons on protons[57] shows that 83% of the events consist of the reactions $pn \rightarrow pp\pi^-$ (18%), $pn \rightarrow pn\pi^+\pi^-$ (48%), and $pn \rightarrow pn\pi^+\pi^-\pi^o$ (17%). The rest of the events (17%) consist of small amounts of several types of two-, three-, and four-meson producing events. Because there are so many different types of these events, the 17% will be neglected and the inelastic events will be assumed to consist only of the three main types of events given above (with their percentage occurrence increased by 100/83). The analysis further shows that in the c.m. system the intensity distribution of the emitted protons from the $pp\pi^-$ reaction is strongly peaked forward and backward, and that of the pions is peaked forward. The neutron and negative-pion intensity is peaked forward for the $pn\pi^+\pi^-$ reaction, while the intensity for the protons and positive pions is peaked in the backward direction. For the $pn\pi^+\pi^-\pi^o$ reactions, the proton distribution is peaked in the forward direction, and the pion distributions are

isotropic. The momentum distribution in the laboratory system for each of the various particles emitted for each type of inelastic event[57] was divided into several sections, and the number and midpoint kinetic energy of the particles in each section was tabulated. From the published pion-nucleon and nucleon-nucleon excitation functions,[44,52,74] a cross section, σ_i, was associated with the midpoint energy for the given type of particle passing through nuclear matter that is assumed to be half neutrons and half protons. By the use of the fact that forward and backward c.m. distributions correspond to high and low kinetic-energy laboratory distributions, "events" were reconstructed. For the $p,p\pi^-$ reaction, a proton and π^- out of the highest energy range were combined with a proton in the lowest energy range, the three values of σ_i were found, and the three particles were removed from the distribution. This process was repeated until all the particles were used up. Similarly for the $pn\pi^+\pi^-$ events, a neutron and π^- each from their respective highest-kinetic-energy section were combined with a proton and π^- each from their respective lowest-kinetic-energy section, and the four values of σ_i were found, etc. Scatter diagrams were not available for the neutrons and π^o's from the $pn\pi^+\pi^-\pi^o$ reaction. Somewhat arbitrarily the π^+'s and π^o's were considered to have the same forward peaking in the c.m. system, and the π^- distribution was taken to be peaked in the backwards c.m. direction. Then a proton and π^+ and $\pm^o$ from their respective highest-kinetic-energy sections were combined with a π^- and neutron in their respective lowest-kinetic-energy sections, and the five values of σ_i were found, etc.

The distribution of values of σ_i is not affected by the previously discussed "inversion" of the n-p scattering data to give p-n data. The correction on σ_1 due to the exclusion principle can be roughly estimated by finding what the maximum nucleon kinetic energy, T_m, is at the point $R_m = (u^2+v^2)^{1/2}/\beta$ for which $M_{n\ell}$ is a maximum, and by assuming, for the purposes of correction, that the nucleus is a degenerate Fermi gas. Use of the kinetic energy and particle type associated with each cross section, σ_i, and T_m in the published equations[75,76,77] gives the cross-section reduction factor. T_m may be determined from

$$T_m = [2(n-1)+\ell+3/2]\ \hbar\omega - \frac{\lambda \hbar^2 \omega^2}{4 m c^2} \begin{Bmatrix} \ell & j=\ell+1/2 \\ \\ -(\ell+1) & j=\ell-1/2 \end{Bmatrix} - \frac{1}{2} m \omega^2 R^2. \quad (27)$$

The first two terms on the hight-hand side[78,79] give the kinetic energy of the least-bound shell (with quantum numbers n and ℓ) relative to the lowest point in the well, and the last term gives the decrease in well depth relative to the lowest point. The nucleon mass is m, and λ equals 25.[79] Use of Eqs. (25) and (26) and of R_m for R gives T_m as a function of g. Values of R_m were chosen from contour plots of $M_{n\ell}$ for three cases, the 1d shell of F^{19}, the 1f shell of Cu^{65}, and the 1h shell of Ce^{142}. From the obtained distribution of the σ_1 (and $\sum_{i=1}^{t} \sigma_i$) $\bar{\sigma}$ was estimated to be 180 mb without including the exclusion-principle effect or meson absorption. Table IV gives values of T_m as a function of g for the three shells mentioned.

Table IV

	1d shell of F^{19}		1f shell of Cu^{65}		1h shell of Ce^{142}	
g	0.5	0.8	0.5	0.8	1.0	1.5
T_m (Mev)	13	15	10	11	12	16

The value of T_m was taken to be 12 Mev. With this value, the σ_i were now corrected and, for σ_i associated with mesons, the meson-absorption cross section was included. The σ_i values were then combined according to the "event reconstruction" mentioned to give a distribution of values of $\sum_{i=1}^{t} \sigma_i$ where t = 3, 4, and 5 for the $pp\pi^-$, $pn\pi^+\pi^-$, and $pn\pi^+\pi^-\pi^o$ reactions, respectively.

This distribution of $\Sigma\ \sigma_i$ must still be weighted by the value of $M_{n\ell}$ associated with each $\Sigma\ \sigma_i$. This was done by computing values of $M_{n\ell}$ for the three shells given in Table IV for values of $\bar{\sigma}$ ranging from 90 mb to 400 mb. Plots of $M_{n\ell}$ against $\bar{\sigma}$ were made and used to weight the $\Sigma\ \sigma_i$ distribution. This gave a final averaged value of $\bar{\sigma}$ equal to 168 mb, a

value which was found to be quite insensitive to changes in g and to be the same for each of the three shells for which $\bar{\sigma}$ was derived. This value was sufficiently close to the 180 mb previously chosen so that $\bar{\sigma}$ = 180 mb was also used for all the subsequent IBM-701 calculations. It turned out that correcting for this difference in $\bar{\sigma}$ is very easy, and such a correction will be included when the calculated $M_{n\ell}$ values and the experimental ppn cross sections are combined.

V. RESULTS

Table V gives a possible choice of neutron- and proton-shell occupation numbers, $n_{n\ell}$ and $p_{n\ell}$, for the target elements for which values of $M_{n\ell}$ were calculated. Except for those of uranium, the numbers were taken from Reference 33. The U^{238} occupation numbers were obtained from a Nilsson diagram for a deformed nucleus.[80] The 1d and 2s occupation numbers for F^{19} (and possibly Na^{23}) are open to question as one work places all three extra F^{19} nucleons in the 2s shell.[81] And another work keeps the occupation numbers given in Table V but shows that F^{19} may be deformed.[82] Using these numbers, values of $M_{n\ell}$ for several shells for several values of g for different isotopes were determined and contour plots obtained for some cases. For a few shells, values of $M_{n\ell}$ for different values of $\bar{\sigma}$ with g constant were obtained.

A. Contour Plots

Figures 11 through13 are contour plots for three cases -- the F^{19} id shell, the Cu^{65} if shell, and the Ce^{142} 2f shell of the integrand of Eq. (23), i.e., of

$$Q_{n\ell} = \frac{2^{\ell}}{(2\ell+c)!!} B_n^{\,2} (u^2+v^2)$$

$$\exp\left[-u^2-v^2-\frac{\sigma_1 g}{A^{1/3}\pi^{3/2}}\int_{v}^{\infty}\rho\,(u^2+w^2)\,dw\right.$$

$$\left.-\frac{\bar{\sigma} g}{A^{1/3}\pi^{3/2}}\int_{-\infty}^{v}\rho'\,(u^2+w^2)\,dw\right] \qquad (28)$$

for various values of $r = u/\beta$ and $z = v/\beta$. The contour lines connect points r,z which give values of $Q_{n\ell}$ from Eq. (28). The dashed circle is the locus of points for which the total nuclear density $\rho\,(u^2+v^2)$ from Eq. (24) (obtained by use of the same value of g as was used to

Table V

Occupation numbers for neutron and proton shells

Isotopes	Shell 1s	1p	1d	2s	1f	2p	1g	2d	1h	3s	2f	3p	1i	2g	1j	3d
C^{12}	2n 2p	4n 4p														
N^{14}	"	5n 5p														
O^{16}	"	6n 6p														
F^{19}	"	"	2n	1p												
Na^{23}	"	"	4n 3p													
A^{40}	"	"	10n 8p	2n 2p	2n											
Ni^{58}	"	"	10n 10p	"	8n 8p	2n										
Cu^{65}	"	"	"	"	12n 8p	4n 1p										
Nb^{93}	"	"	"	"	14n 14p	6n 6p	10n 1p	2n								
In^{115}	"	"	"	"	"	"	18n 9p	6n	2n							
I^{127}	"	"	"	"	"	"	18n 12p	6n 1p	10n							
Ce^{142}	"	"	"	"	"	"	18n 18p	10n	12n	2n	2n					
Os^{192}	"	"	"	"	"	"	"	10n 6p	22n 12p	2n	14m	6n	4n			
U^{238}	"	"	"	"	"	"	"	10n 10p	22n 16p	2n 2p	14n 2p	6n	18n 4p	6n	8n	2n

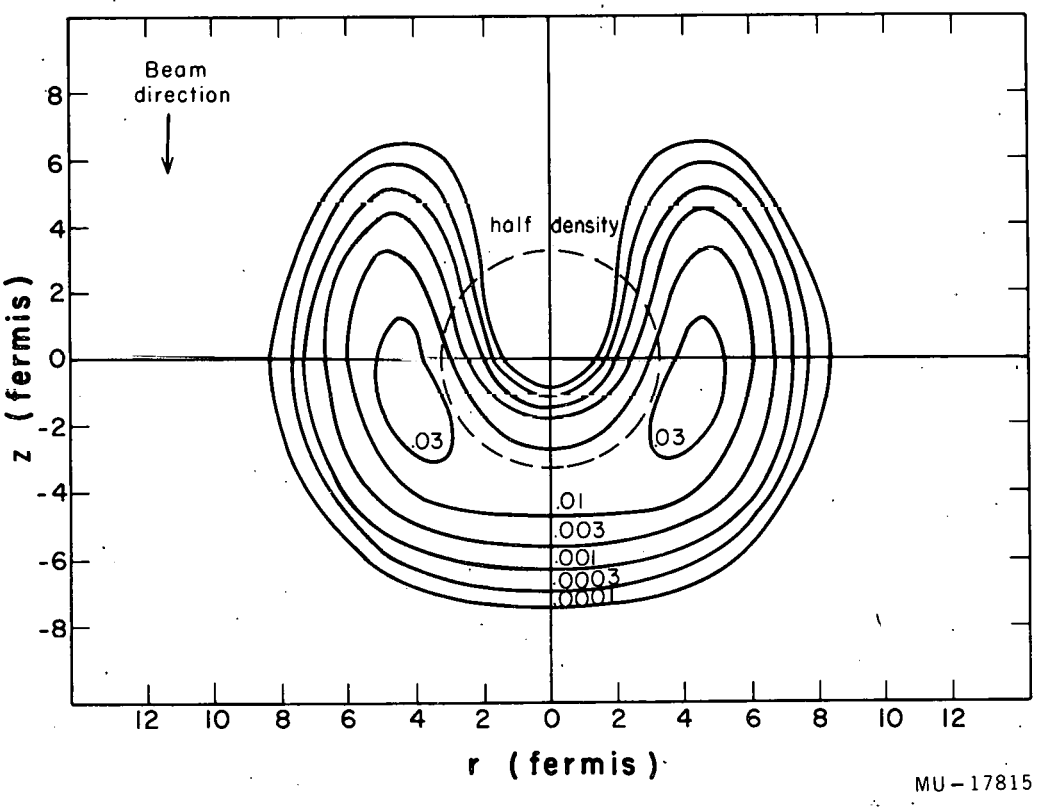

Fig. 11. Contour plot of the 1d shell of F^{19}, σ_1 = 30 mb, $\bar{\sigma}$ = 180 mb, g = 0.50. The broken line circle gives the half-central-density radius.

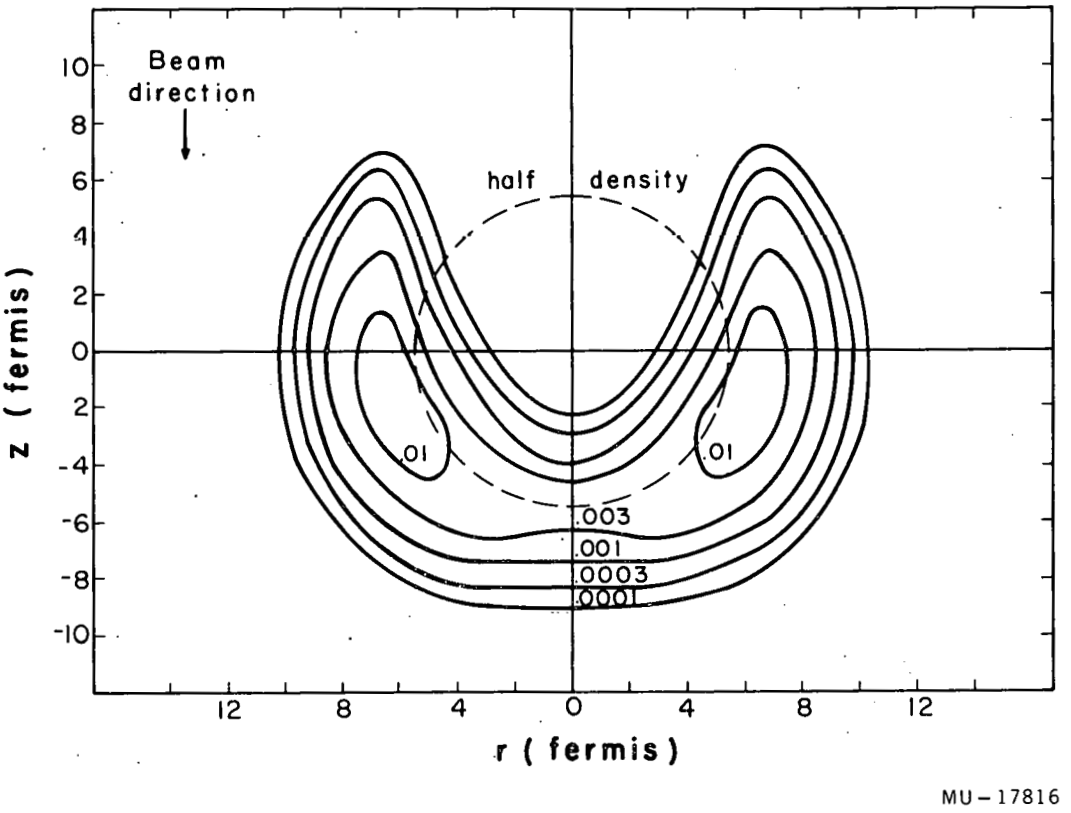

Fig. 12. Contour plot of the 1f shell of Cu^{65} σ_1 = 30 mb, $\bar{\sigma}$ = 180 mb, g = 0.50.

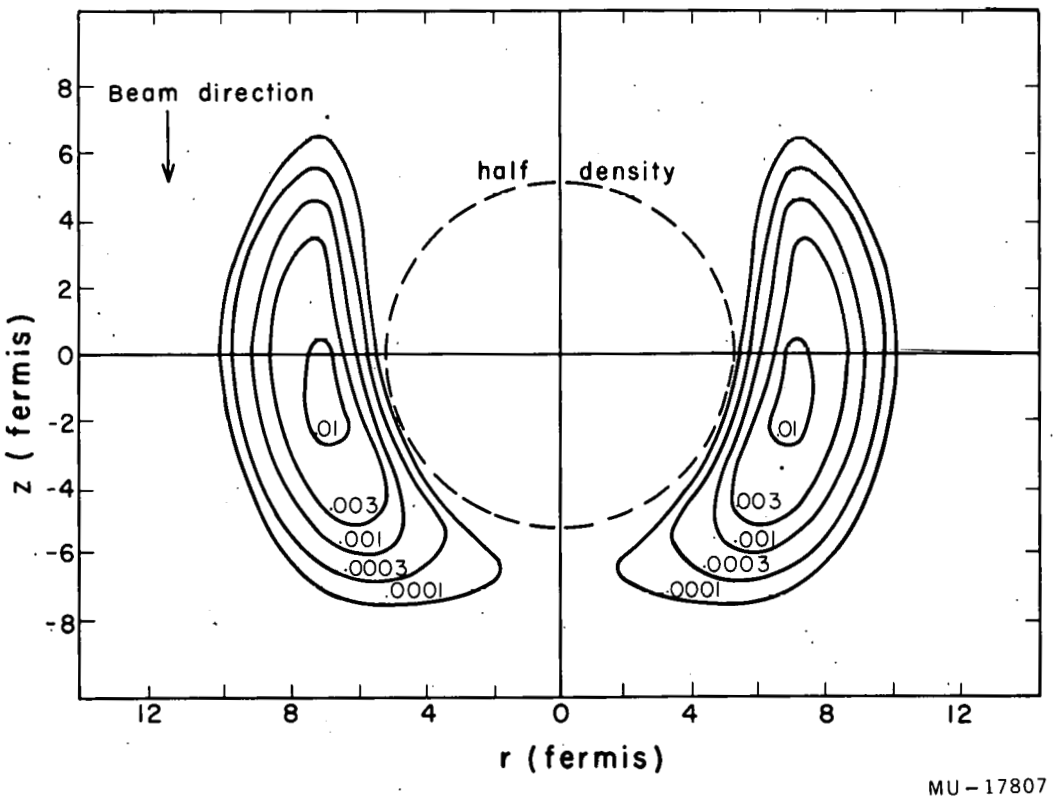

Fig. 13. Contour plot of the 2f shell of Ce^{142} σ_1 = 30 mb, σ = 180 mb, g = 1.00.

obtain the contour lines) is one half its value at the center of the nucleus. The three-dimensional "picture" is obtained by rotating the contour maps about the z axis.

It is immediately apparent from Figs. 11 to 13 that the main contribution to $M_{n\ell}$ comes from regions of the nucleus outside of the half-density circle. In fact for the 2f Ce^{142} shell the main contribution is quite far out from the half-density circle. Because the p,pn reaction is limited to the topmost few shells, these contour plots clearly indicate that the p,pn reaction is a surface reaction. This is why the errors introduced by "lifting" the free n-p scattering data into the nucleus are small. The contours indicate shapes ranging from two rounded peaks rising somewhat above a high pass for the F^{14} 1d shell to two high isolated peaks separated by a deep gorge for the Ce^{142} 2f shell. The secondary peak in Fig. 13 for the Ce^{142} 2f shell is not visible, as it is too far inside the nucleus and is suppressed by the exponent integrals in Eq. (28). The contours also show that most of the contribution to $M_{n\ell}$ comes from the downbeam side of the nucleus. This asymmetric distribution about the z = 0 plane comes from the fact that $\bar{\sigma}$ is much bigger than σ_1; the distribution becomes symmetric about the z = 0 plane as $\bar{\sigma}$ approaches σ_1.

B. $M_{n\ell}$ Results

Figures 14 and 15 are plots of $gM_{n\ell}$ for different shells of F^{19}, Cu^{65}, and Ce^{142} as a function of g, the spring constant parameter. The curves indicate that the following relation holds approximately:

$$gM_{n\ell} = \text{constant}. \tag{29a}$$

This equation turns out to be very useful for interpolation of values of $M_{n\ell}$ for other target elements to other values of g than the ones for which $M_{n\ell}$ was calculated. If desired, Figs. 14 and 15 can be used to correct values of $gM_{n\ell}$ for the slight g dependence. They show also that the values of $M_{n\ell}$ for the outermost shells are less affected by changes in g than are the inner shells.

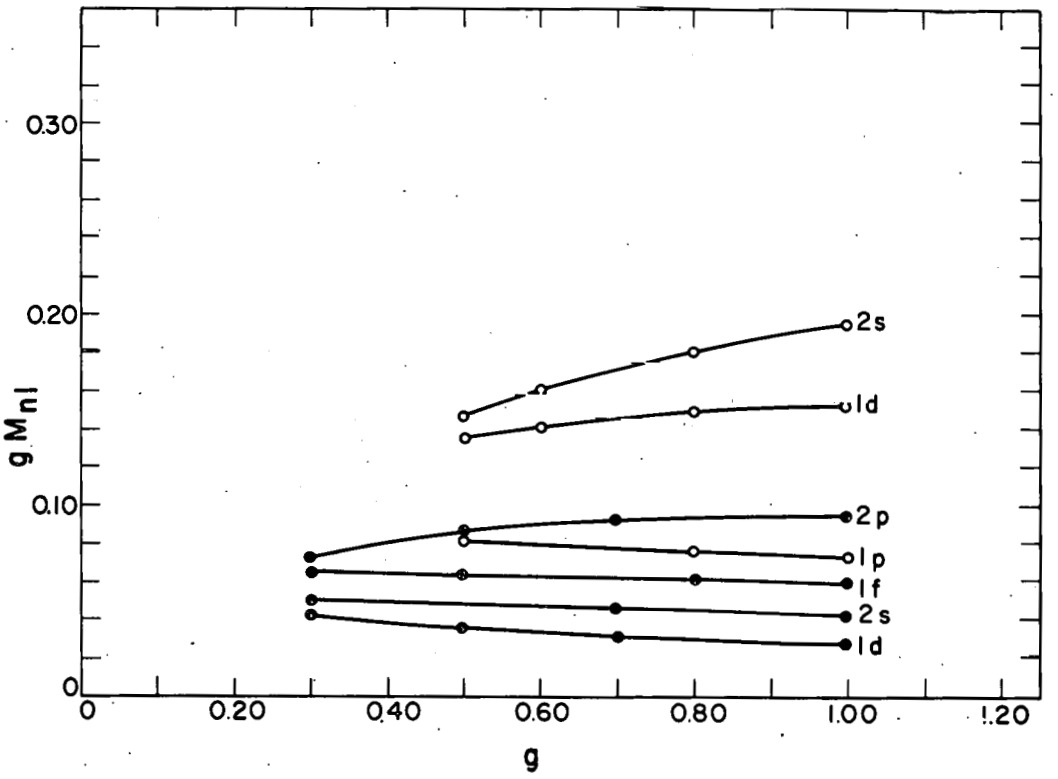

Fig. 14. gM_{nl} as a function of g, the nuclear density distribution parameter, for F^{19} and Cu^{65}. ○ refers to F^{19} shells and ● to Cu^{65} shells σ_1 = 30 mb, $\bar{\sigma}$ = 180 mb.

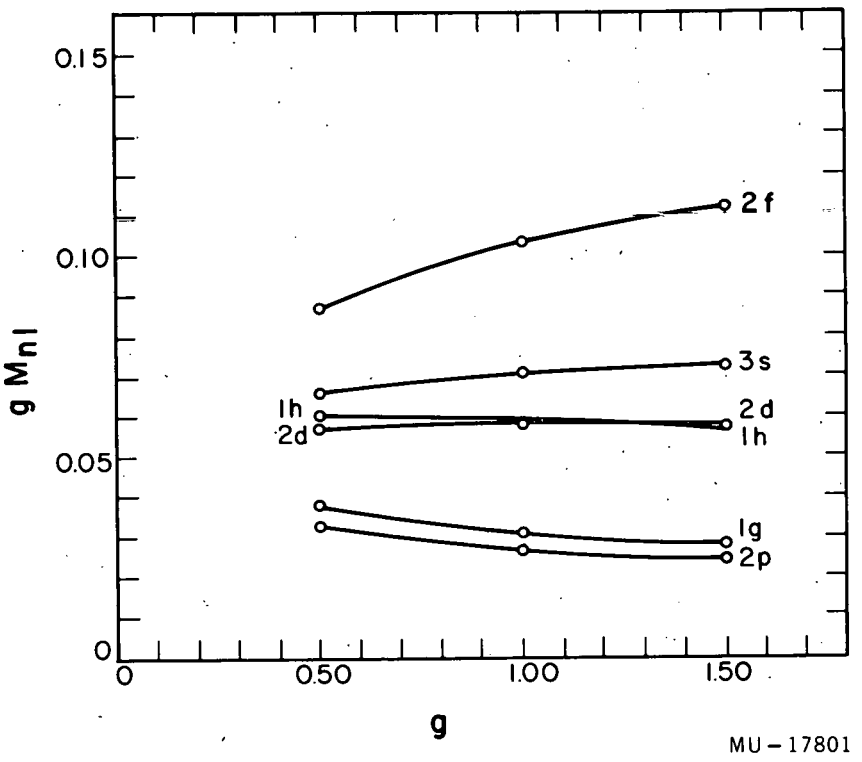

Fig. 15. gM_{nl} as a function of g for Ce^{142} shells.
σ_1 = 30 mb, $\bar{\sigma}$ = 180 mb.

Figure 16 shows the dependence of $M_{n\ell}$ for the F^{19} 1d shell, the Cu^{65} 1f shell, and the Ce^{142} 1h shell on $\bar{\sigma}$. It can be seen that the dependence of $M_{n\ell}$ on $\bar{\sigma}$ is not as strong as that on g. The dependence on $\bar{\sigma}$ can be well represented by

$$(\bar{\sigma})^{1/2} M_{n\ell} = \text{constant}. \tag{29b}$$

For these three shells as well as a few others, $M_{n\ell}$ was determined for $\sigma_1 = 50$ mb. The results show that, similarly, we have

$$(\sigma_1)^{1/2} M_{n\ell} = \text{constant}. \tag{29c}$$

It would be expected, from an examination of Eqs. (23) and (26) that the g dependence would be greater than the σ_1 or $\bar{\sigma}$ dependence because g occurs as a factor of both exponent integrals, whereas σ_1 and $\bar{\sigma}$ each occur as a factor of only one of the integrals. Also the points of maximum contribution to $M_{n\ell}$ obtained from the contour plots are points at which the two exponent integrals, each with their associated factors, would appear to be similar in value. Figure 16 contains the curves which were used to obtain the final average value of $\bar{\sigma}$ as was discussed previously.

Figures 17 and 18 show the dependence of $M_{n\ell}$ on the atomic weight A, of the target nucleus for two values of g, 0.50 and 1.00. These curves may be used for interpolating to target isotopes other than those for which $M_{n\ell}$ values were computed. The difference between the values of $M_{n\ell}$ due to different neutron and proton occupation numbers for isobaric target elements for any given shell would be expected to be small. This was shown by computing values of M_{1f} for Ga^{65} and Nd^{142} ($\sigma_1 = 30$ mb, $\bar{\sigma} = 180$ mb, $g = 1.00$). The value of M_{1f} for Ga^{65} (two less 1f 5/2 neutrons and two more 2p 3/2 protons than Cu^{65}) was found to be less than M_{1f} for Cu^{65} by 0.3%, and M_{1h} for Nd^{142} (no 2f 7/2 neutrons and two 2d 5/2 protons) was higher than M_{1h} for Ce^{142} by 1.2%. The effect of changing the configuration of the top three nucleons of F^{19} from $(1d5/2)^2\ (2s1/2)^1$ to $(2s1/2)^3$ was found by computing M_{2s} for both forms. The value of M_{2s} for the $(1d5/2)^2\ (2s1/2)^1$ configuration was lower than that for $(2s1/2)^3$ by 1.4% ($\sigma_1 = 30$ mb, $\bar{\sigma} = 180$ mb, $g = 0.50$).

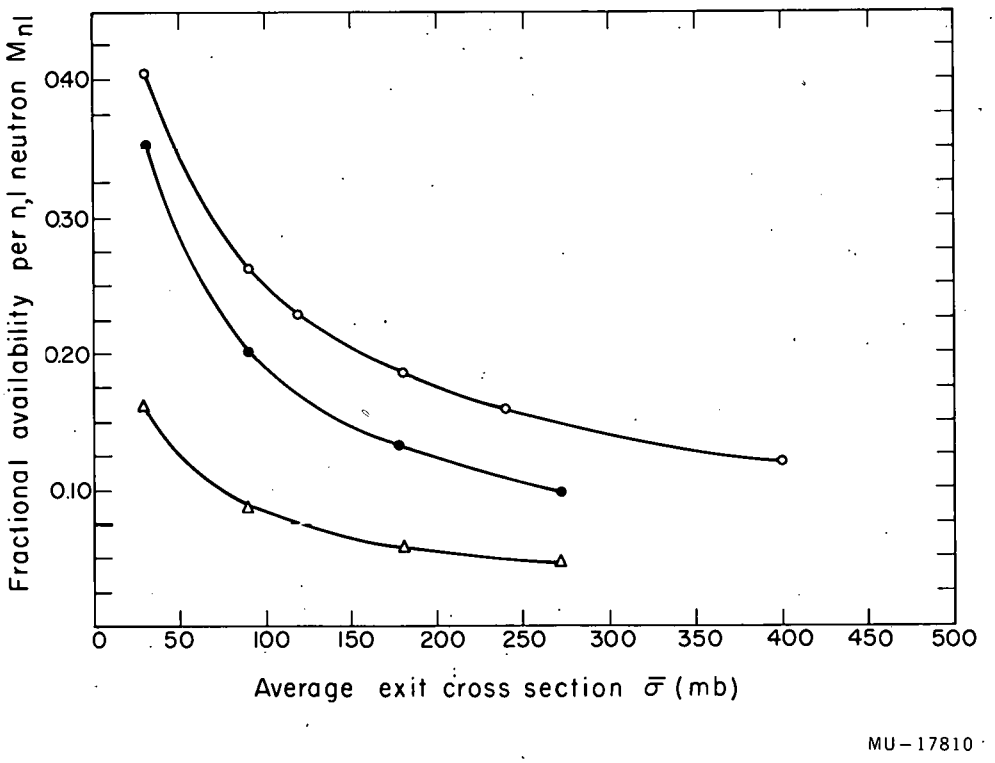

Fig. 16. M_{nl} as a function of $\bar{\sigma}$ the average total exit cross section

○ refers to the F^{19} 1d shell, σ_1 = 30 mb, g = 0.80,

● refers to the Cu^{65} 1f shell, σ_1 = 30 mb, g = 0.50,

△ refers to the Ce^{142} 1h shell, σ_1 = 30 mb, g = 1.00.

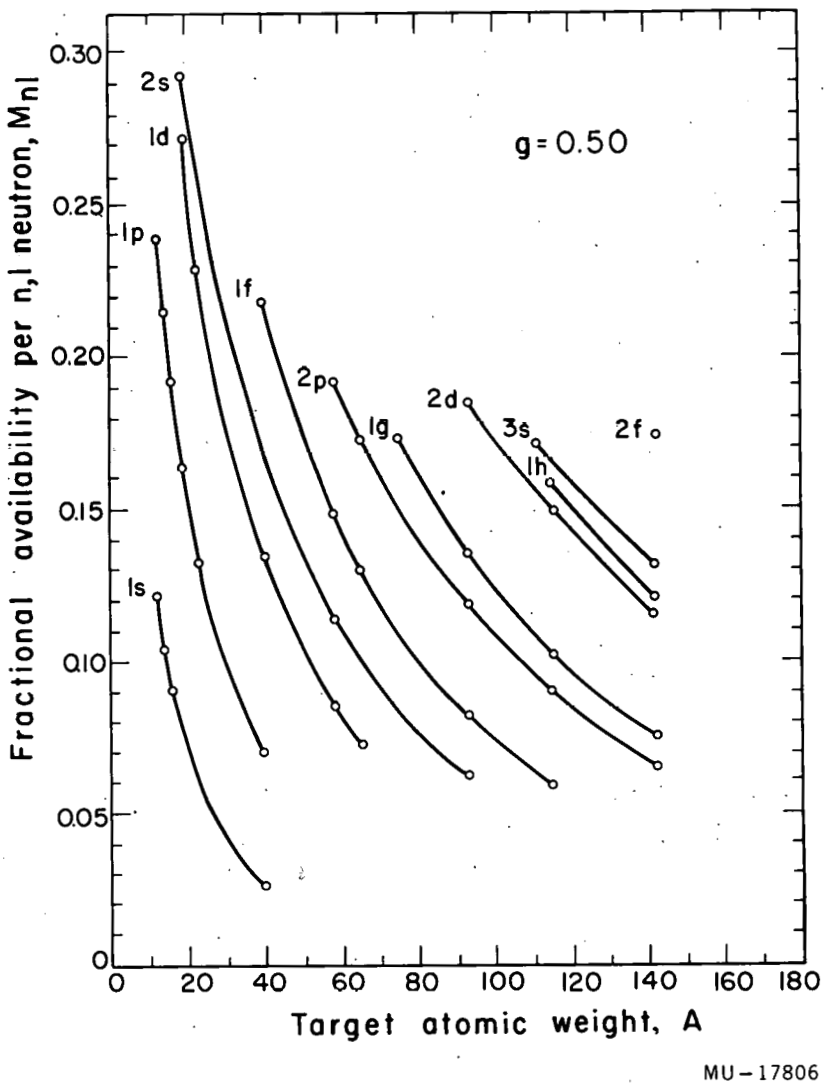

Fig. 17. The dependence of M_{nl} on A, the target atomic weight, for different shells; σ_l = 30 mb, $\bar{\sigma}$ = 180 mb, and g = 0.50.

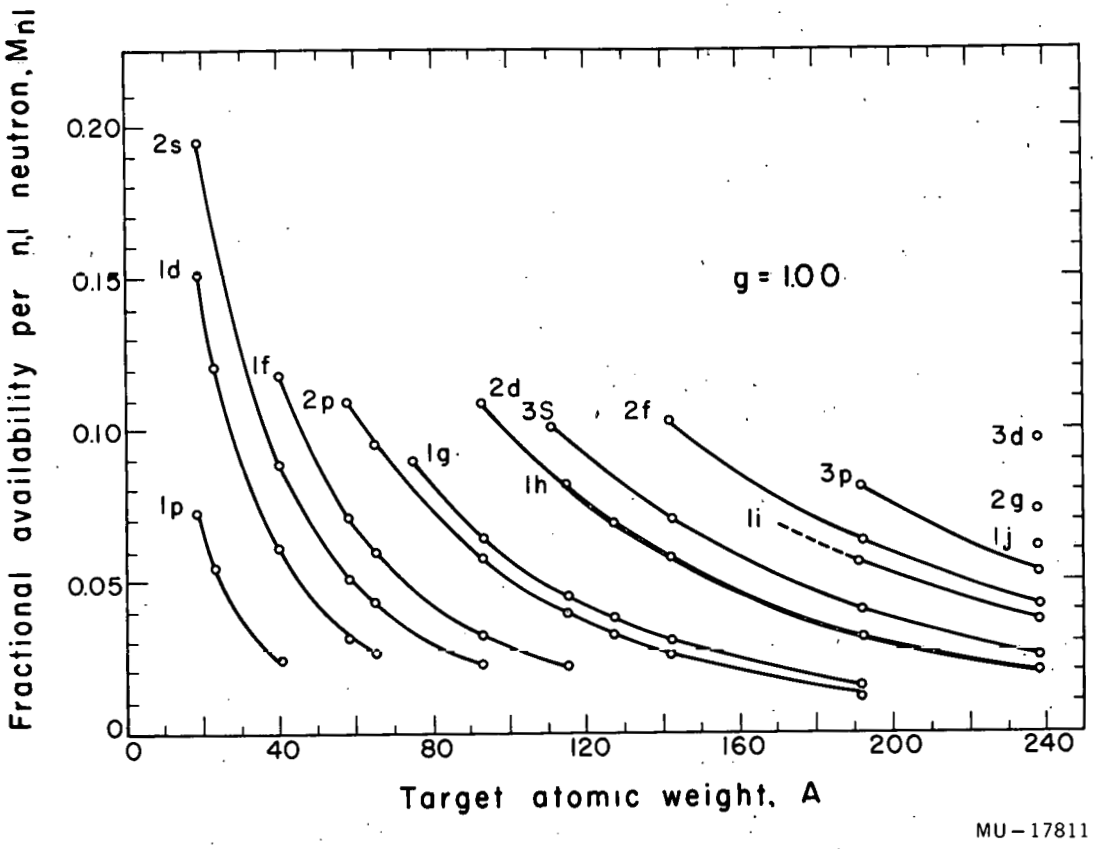

Fig. 18. The dependence of M_{nl} on A for different shells; σ_1 = 30 mb, $\bar{\sigma}$ = 180 mb, and g = 1.00.

The shell structure in Figs. 17 and 18 is quite evident in that for a given A there appears to be a close correlation between the values of $M_{n\ell}$ and the total energy of the n,ℓ shell in the potential well. The correlation is due to the fact that for a potential well with sloping sides, the mean square radius of a shell is larger the higher the shell is in the potential well. Here $M_{n\ell}$ would be expected to be larger for bigger values of the mean square radius, because the exponent integrals in Eq. (23) are smaller. In Figs. 17 and 18 the curves of $M_{n\ell}$ as a function of a target atomic weight were not extended beyond the point at which the shells are so far down in the well that their availability to the p,pn cross sections is highly improbable. This is the reason why all the curves appear to have a cutoff at the low $M_{n\ell}$ end.

C. Elastic p,pn Collision Contribution

Figures 13 to 18 coupled with Eqs. (19) and (29a), (29b), and (29c) allow one to determine the contribution of the elastic p-n collisions to the p,pn reaction cross section by process (a). As mentioned before, the contributions of processes (b) and (c) relative to (a) are less than 5% and will be consequently neglected. The evaluation of the contribution to the p,pn reaction cross section from elastic p-n collisions is more difficult than for inelastic collisions. This is due to the invalidity of the zero degree scattering-angle approximation used to derive Eq. (23). As has been previously shown, a much better assumption for the elastic collisions is to take the scattering angle to be 90° laboratory. To evaluate an expression like that of Eq. (23) which would have a double integral in the exponent and a more complex integrand would be prohibitively long in terms of machine time. Also the effect of the Pauli exclusion principle would have to be included specifically in Eq. (22) because the target neutron has a high probability of being scattered with relatively low energy. [For 5.7-Bev protons on free neutrons one-half the elastically scattered neutrons have kinetic energies of 60 Mev or less. See Appendix I, Eq. (A4)]. Consequently, the following approximate method will be used.

The p,pn cross section, σ_{ppn}, is equal to [see Eq. (19)]

$$\sigma_{ppn} = \sum_{\substack{\text{allowed} \\ \text{shells}}} (M_{n\ell}\, \sigma_{inel} + N_{n\ell}\, \sigma_{el})\, n_{n\ell} , \tag{30}$$

where the second term on the left gives the contribution from the part of the p-n collision which is elastic. A factor $N_{n\ell}$ similar to $M_{n\ell}$ for elastic p-n collisions can be approximated by

$$N_{n\ell} \simeq FM'_{n\ell} ,$$

where F is independent of the shell quantum numbers and target atomic weight. The term $M'_{n\ell}$ is given by Eq. (23) with $\bar{\sigma}$ set equal to σ_1 and accounts for the entrance, elastic collision, and exit of the incident proton which suffers negligible energy loss and angular deviation. The factor F is the amount by which $M'_{n\ell}$ should be reduced to account for the escape of the struck neutron. Use of Eq. (29b) gives the result

$$M'_{n\ell} = \left(\frac{\bar{\sigma}}{\sigma_1}\right)^{1/2} M_{n\ell} . \tag{31}$$

It can be seen from Fig. 16 that for $\bar{\sigma} \sim 180$ mb and $\sigma_1 \sim 30$ mb this equation is correct to within 10% when summation over the allowed shells in Eq. (30) is allowed for. Combining the above three equations and using $\sigma_{tot} = \sigma_{inel} + \sigma_{el}$ gives

$$\sigma_{ppn} = \sigma_{tot}\, \left[1 + f\, \left(F\, \left(\frac{\bar{\sigma}}{\sigma_1}\right)^{1/2} - 1\right)\right] \sum_{\substack{\text{allowed} \\ \text{shells}}} n_{n\ell}\, M_{n\ell} , \tag{32}$$

where f is the fraction of the total p,n cross section which is elastic.

The factor F can be estimated by dividing the spectrum of the energy gain of the struck neutron into three parts. If the struck nucleon gains less than 8 Mev, it can not escape from the nucleus, so that collision does not contribute to the p,pn reaction. If the struck

nucleon gains between 8 and 18 Mev, the collision will always contribute to the p,pn reaction because if it does not escape, the resultant excited nucleus will usually evaporate only one neutron. Finally, if the target nucleon gains 18 Mev or more it must escape. This division into three parts with boundaries of 8 and 18 Mev is not meant to be accurate. It does, however, allow F to be easily estimated.

The fraction of elastic 5.7-Bev p-n collisions that gives the struck neutron a gain of $\geq$ 18 Mev (similar to process (a) for inelastic p-n collisions) is calculated from Eq. (A4) (n = 36)[65,66] to be 0.79. For this fraction $M'_{n\ell}$ will be assumed to be reduced by roughly one half. This is arrived at by assuming that, similar to the inelastic collisions, most of the contribution to $N_{n\ell}$ comes from collisions in the nuclear-surface region. For an elastic surface collision, the struck nucleon has roughly a probability of one half to be going away from or towards a lot of nuclear matter. If it is moving towards most of the nucleus it will probably interact, because compound nucleus formation is likely for nucleons with kinetic energies of $\leq$ 50 Mev incident on nuclei.[83] If it is moving away from most of the nucleus, it is likely to escape without interaction. Various other effects such as the exclusion principle, reflection at the nuclear surface, production of the $\geq$ 18-Mev energy-gain neutron further inside the nucleus, etc., are ignored for this rough determination. Consequently, the contribution to F from this part of the elastic p-n collisions is $1/2(0.79) \approx 0.4$.

Elastic 5.7-Bev p-n collisions that give the struck neutron between 8 and 18 Mev (a process similar to process (b) have a probability of occurrence of 0.1 [Eq. (A4), Appendix I]. Since all of these collisions contribute to the p,pn case, as far as the struck neutron is concerned, the contribution to F is 0.1. There is a smaller contribution from a process similar to process (c) for the inelastic p-p case where a p-p collision occurs leaving a proton with a kinetic energy gain between 8 and 18 Mev. This contribution will be neglected, as the 0.1 given above which also holds for p-p collisions must be multiplied by factors that take account of the fact that the slow proton must not

leave and the p-p collisions with low nuclear excitation resulting are less likely than are p-n collisions for all but the low Z elements. Consequently, F is set equal to the sum of the first two contributions, which is 0.5.

D. p,pn Reaction Cross-Section Equations

The fraction of 5.7-Bev p-n collisions that are elastic is not known, so f will be taken from the 6.2-Bev p-p scattering data as equal to 0.24 ± 0.06.[65] As was mentioned before, $M_{n\ell}$ was calculated from Eq. (23) with a value of the total p-n collision cross section, $\sigma_1 = \sigma_{tot}$, equal to 30 mb. The value of $M_{n\ell}$ can be easily corrected for the change in σ_1 to 32 ± 3 mb for 4 ± 1.5-Bev neutrons on hydrogen.[73] Use of Eq. (29c) gives the result

$$M_{n\ell} \quad \text{for}(\sigma_1 = 32 \text{ mb}) \qquad = \qquad \left(\frac{30}{32}\right)^{1/2} M_{n\ell} \quad \text{for}(\sigma_1 = 30 \text{ mb})$$

The previously mentioned correction stemming from the fact that $\bar{\sigma}$ should be 168 mb instead of 180 mb can now be included by use of Eq. (29b). The values of $M_{n\ell}$ obtained from Figs. 17 and 18, when multiplied by $(30/32)^{1/2}\,(180/168)^{1/2}$, can consequently be used in Eq. (32). Substitution of the values given above for f and F ($\bar{\sigma} = 168$ mb and $\sigma_1 = 32$ mb) gives the result

$$\sigma_{ppn} = (33 \pm 3) \sum_{\substack{\text{allowed} \\ \text{shells}}} n_{n\ell}\, M_{n\ell} \text{ mb} \,. \tag{33}$$

Use of other 6.2-Bev p-p scattering data to determine f gives the same numerical constant in Eq. (33).[59] Even though F is determined quite roughly it can be seen from Eq. (32) that errors in F are scaled down roughly by the factor f. If F is changed to 1/4 or 3/4, the numerical constant in Eq. (33) changes to 29 mb and 38 mb respectively.

For 3-Bev data, the numerical constant in Eq. (33) can also be determined from Eq. (32) and experimental data. A determination of $\bar{\sigma}$

from the 1.72-Bev neutron-hydrogen collision work[56] in the same manner as for the 3.8-Bev neutron data including the exclusion principle for T_m = 12 Mev gives $\bar{\sigma}$ = 160 mb. The values of σ_1 will be taken to be 36 ± 3 mb. This value is a linear interpolation between the 1.4 Bev[74] and 4 Bev[73] n-p cross sections for a bombarding energy of 3 Bev. The fraction, f, of σ_1 which is elastic is taken from the 2.75-Bev p-p collision data to be 0.37 ± 0.04.[58] As before, F is approximately 0.5. Substituting these values into Eq. (32) and correcting by the previously discussed methods for the fact that $M_{n\ell}$ is calculated for $\bar{\sigma}$ = 180 mb and σ_1 = 30 mb gives for 3-Bev protons incident on nuclei

$$\sigma_{ppn} = (36 \pm 3) \sum_{\substack{\text{allowed} \\ \text{shells}}} n_{n\ell} M_{n\ell} \text{ mb} . \qquad (34)$$

E. Energy Independence of σ_{ppn} in the Bev Region

Equations (33) and (34) show that the theory developed here satisfies the requirement that the p,pn cross sections be independent of the bombarding energy in the Bev region. The decrease with increasing energy shown in these equations is less than 10% and is within the experimental error limits on the experimental p,pn cross sections. At first sight it seems surprising that the cross sections do not decrease with increasing energy, because the meson multiplicity, which affects $\bar{\sigma}$, is dependent on the bombarding energy. However, this dependence is not strong, as can be seen from the mean meson multiplicities of 1.8 and 2.2 for neutrons of 1.7-Bev and 4-Bev average energy, respectively.[56,57] The effect of the extra 0.4 meson at 4 Bev is further reduced by the fact that, as has been discussed, all the $\Sigma \sigma_i$ terms, which make up $\bar{\sigma}$, are weighted by $M_{n\ell}$. This weighting tends to suppress reactions with high meson multiplicity whose abundance is quite sensitive to the bombarding energy.

The p,pn cross section is also dependent on $\sigma_1^{1/2}$ as can be seen from Eqs. (29c) and (32). The square-root dependence and the relative

constancy of σ_1 in the Bev region (σ_1 equals 42.4 mb and 32 mb for 1.4 Bev and 4 Bev n-p reactions respectively[73,74]) help to give the independence of σ_{ppn} from the bombarding energy.

F. Inherent Uncertainties Due to Nuclear Model Chosen

Before the theoretical results are compared with experimental data it is worthwhile to stress the fact that the nuclear model used in the foregoing calculations does not represent real nuclei. One fault of the model used in the calculations is that the harmonic-oscillator well was used instead of the more realistic inverse exponential well. It is difficult to estimate how much the values of $M_{n\ell}$ would be changed if the inverse exponential well were used. Both the density-distribution terms and the radial wave functions in Eq. (21) et seq. would be affected. Furthermore, the degeneracy in the two values of $M_{n\ell}$ for different j but same $n\ell$ values would be removed.

Another fault is that some effects of nucleon-nucleon interactions, e.g., j-j coupling, have been neglected. Even though Eqs. (17) and (18) hold for j-j coupling, the radial wave functions and the density terms would be altered in a complex manner. This would induce further changes in $M_{n\ell}$. In addition to this effect, Eqs. (19), (30), and (32 to 34) would have to be altered under any nucleon-nucleon coupling scheme. This change arises because the sudden removal of a nucleon from a shell will leave the product nucleus in any one of several possible parent states. Any one of these parent states, when coupled to the $n\ell j$ nucleon, gives the ground state of the target nucleus. Since some of these parent states may be unstable to particle emission, a factor ≤ 1 should be included inside the $n\ell j$ sum of Eq. (19) and the sum should be extended over all $n\ell j$ shells of the nucleus. This factor is the sum of the squares of the appropriate fractional-parentage coefficients of all the parent states stable to particle emission. This factor tends to unity or zero as the nucleon-nucleon interaction becomes weaker and, in the limit of the independent-particle model, becomes equal to either 0 or 1, giving Eq. (19) et seq. For closed-shell target nuclei, Eqs. (19), (30), and (32 to 34)

are valid as they are, because there is only one possible parent state even with nucleon-nucleon coupling.

The difficulties mentioned above which are caused by differences between real nuclei and the model chosen here add an element of uncertainty to any comparison of theory with experiment. In spite of this, we shall proceed to see what can be learned from a simple independent-particle model while keeping the above discussion in mind.

VI. USE OF EXPERIMENTAL DATA WITH THEORY

Two variables are now left in Eqs. (33) and (34) -- which shells are available and the value of g (or r_o by Eq. (26), the nuclear-density-distribution parameter. A correct calculation of which shells are available, i.e., which neutron-hole states of the product nucleus have small particle-emission widths compared to the gamma-emission widths, is quite beyond the scope of this work. However, one can use the eigenvalues of a reasonable independent particle model as a guide to determine which shells are available and then use the p,pn cross sections with Eqs. (29a) and (33) or (34) and Figs. 17 or 18 to determine g or r_o. These values of r_o can be compared with values obtained by other experimental methods. Later another method of treating the data which considers both the shell availability and r_o as unknowns will be discussed.

A. Radius Parameter Determinations

The independent particle calculations of Ross, Mark, and Lawson,[84] which appear to be successful in predicting the experimentally observed shell filling, will be used here as a guide to determine the excitation energy of neutron-hole states in various shells. The availability of a shell is determined by subtraction of the excitation energy of the neutron-shell hole state from the highest particle-stable excitation energy of the product. Only if the result is greater than zero is the shell available.

The highest particle-stable excitation energy of the product is merely that excitation energy for which the total particle-emission width is roughly equal to its gamma-emission width. If a neutron is the least-bound particle, its binding energy is usually the highest particle-stable excitation energy. If a proton is the least-bound particle, an appropriate barrier correction must be added and the sum compared to the neutron binding energy. Except for a few cases, alpha particles need not be considered. Appendix IV gives a possible method of estimating the effective barrier.

Table VI lists the particle binding energies and highest particle-stable excitation energies for the p,pn products for which cross sections

Table VI

Particle binding energies and effective barriers

product	Product-nucleus particle binding energies (Mev) alpha	proton	neutron	Effective coulomb barrier (Mev) alpha	proton	Lowest particle emitting excitation of product nucleus (Mev)	Reference
C^{11}	7.55	8.70	13.11			~ 8.0 α	21
N^{13}	9.50	1.94	20.4		< 0.43	< 2.37 p	21
O^{15}	10.26	7.35	13.30		< 0.26	< 7.61 p	21
F^{18}	4.41	5.61	9.16			~ 5.4 α	21
Na^{22}	8.48	6.74	10.9	1.8	0.4	7.1 p	21,32,86
Fe^{53}		7.6±0.2	10.6±0.2		1.7	9.3 p	85
Mn^{54}		7.56±0.02	8.94±0.02		1.8	8.94±0.02 n	85
Ni^{57}		7.6±0.4	11.1		1.9	9.5 p	85
Cu^{62}		5.9±0.4	8.9±0.4		2.5	8.4 p	85
Cu^{64}		7.19±0.02	7.91±0.02		2.5	7.91±0.02 n	85
Zn^{63}	4.0	6.51±0.10	8.97±0.10	7.7	2.9	8.97±0.01 n	85
Mo^{99} + Nb^{99}_a	1.7	5.17	10.5	9.8	3.4	8.5 p	86,87
		9.72_a	7.89_a			7.9_a n	86,87
In^{114m}	3.4	6.36	7.0		5.9	7.0 n	86
I^{126}	1.6	5.94	6.87		5.6	6.9 n	86
Ce^{141}	1.65	8.41±0.07	5.44±0.07			5.44±0.07 n	86,88
La^{141}_a	0.4	7.62	6.76±0.07			5.76±0.07 n	86,88
Ta^{180m}	-0.89	5.47	6.21	18	8.3	5.2 n	86,87

[a] p,2p product.

are available for proton bombarding energies of 3 Bev or more. Column one gives the p,pn products for which cross sections were measured. Both the p,pn and p,2p products are included for the target Mo^{100}, because the experimental cross section is the sum of both. The subscript "a" refers to the p,2p product. The next three columns give the binding energies for the product nucleus. Error limits are given for the data taken from References 85 and 88 only. Error limits are not given in Reference 21, and a comparison of error limits given in References 85 and 86 indicates that it is inappropriate to use error limits on total binding energies to determine error limits on the last-particle binding energies. Columns five and six give the effective Coulomb barrier computed from the results of Appendix IV. For the nuclei with Z less than 9, no entries are needed, because the available shells can be better determined from the level schemes[21] and buried-shell nucleon scattering[29] (See Part I). For the entries with Z greater than 9, proton barriers were computed for those cases for which the proton binding energy was less than the neutron binding energy. A few alpha barriers were also determined. Column seven gives the lowest excitation energies at which particle emission from the product competes favorably with gamma decay. The particle to which this excitation energy refers is also given. This energy is determined by adding the barrier corrections in columns five and six to the binding energies in columns two to four and choosing the smallest of the resulting excitation energies. The centrifugal barrier can also be neglected for most cases, because it is small. A case will be discussed later for which this barrier should be included. The references from which the binding energies were obtained are given in column five.

Table VII gives the experimental p,pn reaction cross sections and the values of g and r_o derived from the cross sections, the number of available shells, and values of $M_{n\ell}$. Column one gives the p,pn product (p,2p product in the case of La^{141}). Column two gives the proton bombarding energies in Bev at which the cross sections in column three were determined. The cross sections at both 3 to 4 Bev and 5.7

Table VII

p,pn cross sections and nuclear-density-distribution parameters[a]

p,pn product	Proton bombarding energy (Bev)	p,pn cross section (mb)	Reference	Available shells	g	r_o
C^{11}	3.0	26.7±1	15	$1p^{3/2}$ (4)	0.65±0.06	1.14±0.05
	5.7	29±3	Part I	$1p^{3/2}$ (4)	0.55±0.07	1.25±0.08
N^{13}	3.0	4.0±2.4	27	$1p^{1/2}$ (2)	0.98±0.58	1.10±0.36
	5.7	7.3±0.7	Part I	$1p^{1/2}$ (2)	0.48±0.07	1.34±0.10
O^{15}	5.7	33±5	Part I	$1p^{1/2}$ (2) $1p^{3/2}$ (4)	0.58±0.10	1.21±0.09
F^{18}	3.0	28±4	27	$1d^{5/2}$ (2)	0.35±0.06	1.57±0.14
	5.7	19±2	Part I	$1d^{5/2}$ (2)	0.47±0.06	1.35±0.09
Na^{22}	5.7	31±5	Part I	$1d^{5/2}$ (4)	0.48±0.09	1.35±0.13
F^{53}	3.0	45±7	27	$1f^{7/2}$ (8) $2d^{3/2}$ (4) $2s^{1/2}$ (2)	0.72±0.13	1.10±0.10
Mn^{54}	6.2	44±10	89	$2p^{3/2}$ (2) $1f^{7/2}$ (8) $1d^{3/2}$ (4)	0.75±0.20	1.07±0.14
Ni^{57}	3.0	37±6	27	$2p^{3/2}$ (2) $1f^{7/2}$ (8) $1d^{3/2}$ (4)	0.91±0.17	0.98±0.09
Cu^{62}	3.0	66±14	27	$1f^{5/2}$ (2) $2p^{3/2}$ (4) $1f^{7/2}$ (8)	0.56±0.12	1.25±0.14
	5.7	46±7	11	$1f^{5/2}$ (2) $2p^{3/2}$ (4) $1f^{7/2}$ (8)	0.73±0.13	1.09±0.10
Cu^{64}	3.0	66±7	27	$1f^{5/2}$ (4) $2p^{3/2}$ (4) $1f^{7/2}$ (8)	0.62±0.07	1.17±0.07
	5.7	71±6	11	$1f^{3/2}$ (4) $2p^{3/2}$ (4) $1f^{7/2}$ (8)	0.53±0.06	1.27±0.07
Zn^{63}	3.0	68±11	27	$1f^{5/2}$ (2) $2p^{3/2}$ (4) $1f^{7/2}$ (8)	0.54±0.10	1.27±0.12
Mo^{99} Nb^{99}	3.0	72±12	27	$1g^{7/2}$ (2) $2d^{5/2}$ (6) $1g^{9/2}$ (10) / $1g^{9/2}$ (2) $2p^{1/2}$ (2) $1f^{5/2}$ (6) $2p^{3/2}$ (4)	0.99±0.18	0.94±0.09
In^{114m}	4.1	57±9	47	$1h^{11/2}$ (2)1.84 $1g^{7/2}$ (8)7.05 $2d^{5/2}$ (6)5.35	0.57±0.10	1.23±0.11
	6.2	63±10	47	$1h^{11/2}$ (2)1.84 $1g^{7/2}$ (8)7.05 $2d^{5/2}$ (6)5.35	0.48±0.09	1.35±0.12
I^{126}	4.0	59±15	48	$1h^{11/2}$ (10) $1g^{7/2}$ (8) $2d^{5/2}$ (6)	0.86±0.22	1.02±0.13
	6.2	45±11	48	$1h^{11/2}$ (10) $1g^{7/2}$ (8) $2d^{5/2}$ (6)	1.03±0.28	0.93±0.13
Ce^{141}	3.0	24±3	54	$2f^{7/2}$ (2) $2d^{3/2}$ (4) $3s^{1/2}$ (2)	0.86±0.15	1.00±0.08
La^{141}	3.0	4.2±0.6	54	$1g^{7/2}$ (8) $2p^{1/2}$ (2)	2.34±0.39	0.61±0.05
Ta^{180m}	3.0	47±12	27	$1i^{13/2}$ (8) $1h^{9/2}$ (10) $2f^{7/2}$ (8)	1.06±0.26	0.92±0.11
	5.7	46±12	45	$1i^{13/2}$ (8) $1h^{9/2}$ (10) $2f^{7/2}$ (8)	0.99±0.25	0.95±0.12

[a]The nuclear density distribution parameters, g and r_o, given in this table are partly based on the number of available shells determined from the shell spacings given by Ross, Mark, and Lawson[84] and the entries in Table VI. A different nuclear model than the one used by Ross, Mark, and Lawson, would give different shell spacings and consequently different values of g and r_o than are given here. (The value of g equals $\beta^2 A^{1/3}$, where β is the harmonic-oscillator spring constant, and r_o, the half-central-density radius parameter, equals $R/A^{1/3}$, where R is the nuclear radius at which the density is one half the central value.)

to 6.2 Bev are given, if available, to indicate the spread in the experimental data. Equation (34) was used for the 4-Bev data. The references to the experimental cross-section values are given in column four. Column five gives a possible choice of available shells determined, as has been discussed, from the eigenvalue calculations of Ross, Mark, and Lawson[84] and the highest particle-stable excitation energies given in Table VI. The target neutron occupation numbers are given in parentheses immediately below each shell. Values of g and r_o derived from the cross sections by the use of Eqs. (26), (29a), (33), or (34), and Figs. 17 or 18, are given in columns six and seven respectively. Figures 14 and 15 can be used to interpolate for errors made in using Eq. (29a) if desired. In this work, the only targets for which such an interpolation was made were F^{19} and Ce^{142}.

The values for g determined for the target In^{115} must be corrected for the fact that the measured p,pn cross section refers only to the isomer In^{114m} ($J = 5+$) and does not include contributions from In^{114} ($J = 1+$).[7] This correction can be determined by adding vectorially the j value of the neutron hole in a given shell, j_1, to the spin of the target nucleus j_2 to get resultant J's between j_1+j_2 and $|j_1-j_2|$. The fraction of each J state which decays to either one or the other of the isomers is found by considering the decay to proceed by emission for a gamma ray of the appropriate multipolarity and comparing by means of the published formulas[90] the lifetimes for such gamma decays. It turns out that, except for the state with a J value midway between the spins of the two isomers, the states decay essentially entirely into one or the other of the isomers. For a given neutron shell, the number of neutrons effective in producing one of the isomers is obtained by weighting each J state by the fraction decaying into the isomer and the statistical weight, 2J+1, summing over all allowed J states, and dividing by $\sum_J (2J+1)$. This final fraction is multiplied by the total number of neutrons in the shall. For In^{115}(p,pn) In^{114m}, the effective number of neutrons for each available shell was found by taking the ground-state spin of In^{115} to be 9/2+ (due to a $1g_{9/2}$ proton hole).[7] The effective number of neutrons so obtained for each

shell are given in column five, Table VII, to the right of the neutron occupation numbers. It is not possible to make such a correction for Ta^{180m} because the spins of the two isomers are not available. Consequently, values of g and r_o, computed as if the only product were Ta^{180m}, represent upper and lower limits respectively.

Figure 19 is a plot of the half-density radius parameter, r_o, given in Table VII, as a function of the target atomic weight. Points for 3 to 4 Bev, and 5.7- to 6.2-Bev data are denoted by triangles and circles respectively. The error limits given on each point are the experimental error limits only. The dashed lines connect half-density radius parameters as given by the electron-scattering results.[72] The solid lines connect a few radius parameters, r_o, calculated to be necessary to give the observed p,pn cross sections for nuclei containing a degenerate Fermi gas with a uniform density distribution. This is the nuclear model used in the Monte Carlo calculations.[52] The radius parameter, r_o, was calculated from the observed p,pn cross sections at 3 Bev by the use of the equations derived in Appendix V with σ_1 = 36 mb and $\bar{\sigma}$ = 150 mb. The value of $\bar{\sigma}$ was lowered by an estimated 10 mb from the value used in Eq. (34) to account for the greater effect of the exclusion principle for a square well.

A number of interesting points are revealed on examination of Fig. 19. The very large values of r_o needed for the uniform-density model (roughly 1.8 fermis) to reproduce the experimental p,pn cross sections, compared with the points for the harmonic-oscillator model, the electron-scattering results, and literature data obtained from total nuclear cross sections,[91] show that the p,pn reaction cross sections cannot be explained without the diffuse nuclear surface. This has already been suspected from the Monte Carlo calculations.[27,52] The values for the half-density radius parameters (1.0 to 1.3 fermis) determined from the harmonic-oscillator well lie fairly close to the half-density radius parameters (1.0 to 1.1 fermis) determined from electron scattering work. Other determinations of nuclear radii give values for r_o of 1.07 fermis (exponential-well half-denisty radius parameters)[92] and 1.25 fermis (square density distribution).[93]

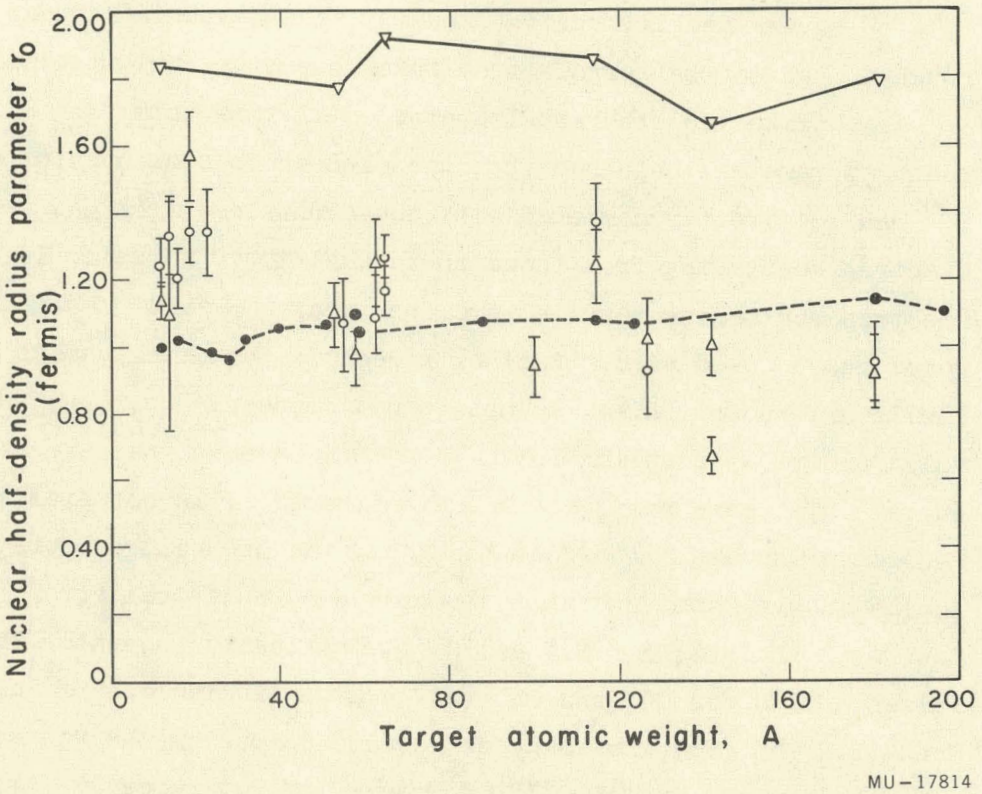

Fig. 19. The half-central-density radius parameter, r_o, as a function of target atomic weight. The points are obtained from experimental 3.0-Bev (△) and 5.7-Bev (○) p,pn-reaction cross sections (Eqs. 33 or 34), and the static level spacings of Ross, Mark, and Lawson.[84] The broken line connects values (●) of r_o obtained from the electron scattering results.[72] The solid line connects values (▽) of square-density radii, calculated from the formulae in Appendix V, necessary to give the observed p,pn cross sections. These square density radii are the ones which would have to be used in the Monte Carlo calculations to give agreement between experimental and calculated p,pn cross sections.

The agreement between these values of the half-density radii and the values found in this work is quite satisfactory, especially in the light of the discussed uncertainties contributed by the use of the harmonic-oscillator model. It is, of course, not correct to compare half-density radii directly with square-density radii. However, the comparisons made above are rough enough so that errors from this source are relatively small.

Unlike the other nuclei studied in this work, the half-density radius parameters obtained from the p,pn cross sections for C^{12}, N^{14}, and O^{16} can be directly compared with those obtained from the results of the electron scattering from these three nuclei. One reason is that the electron-scattering results were analyzed in terms of a harmonic-oscillator well, as was used here. Another reason is that the available neutron shells are known. Also, as has been discussed, Eqs. (33) and (34) are valid under j-j coupling for C^{12} and O^{16} because they are closed-shell nuclei. The same holds for N^{14} even though it is not a closed-shell nucleus. This is due to the fact that only the one neutron outside the closed shells is available. Finally, there is no numerical error made in using Eqs. (25) and (26) for C^{12} and O^{16}. This can be shown by substituting the values of $1/\beta$ for C^{12} and O^{16}, given as a_o in Table I of Reference 72, into Eqs. (25) and (26), solving for r_o, and comparing the values so obtained with those given in Table IV, Column 8, of Reference 72. No electron-scattering data is given for N^{14}, so the value of r_o for this nucleus is taken to be midway between that of C^{12} and O^{16}.

A direct comparison (See Fig. 19) between the values of r_o obtained in this work and the electron-scattering work shows that, for C^{12}, N^{14}, and O^{16}, the nucleon half-density radius parameters are larger than the charge half-density radius parameter by 0.1 to 0.5 fermis (exclusive of the 3-Bev N^{14} point because of its large error limit). This difference seems to be somewhat larger than the value of 0.1 ± 0.1 fermis obtained by other means for the differences between the half-nucleon and charge-density radii (the factor of $A^{1/3}$ is included in this value).[94] It is difficult to say where this discrepancy comes from. Perhaps the zero degree laboratory scattering-angle approximation or errors inherent in the method of computing $\bar{\sigma}$, as are discussed later, are the cause. It would seem that these error

sources are not sufficient to explain the above discrepancy. The crude method used to estimate the contribution from elastic p-n collisions may also be contributing errors.

It is interesting to note that on the basis of the available-shell assignments made, the p,pn radius parameters show a decrease with increasing A. Some of this decrease is probably due to the error associated with using Eq. (26). There also appear to be some irregularities associated with major shells; i.e., Fe^{54}, Mn^{55}, and Ni^{58} all have 28 or less protons and a smaller value of r_o than do Cu^{63}, Cu^{65}, and Zn^{64}, which have more than 28 protons. Similarly, In^{115}, which has between 28 and 50 protons, has a larger value of r_o than does I^{127}, Ce^{142}, or Ta^{181} with more than 50 protons. Molybdenum-100 causes some difficulty here, a difficulty which could be resolved by a study of more p,pn reactions around mass 100 uncontaminated by p,2p reactions. The low-Z elements again show a value of r_o similar to that of copper, zinc, and indium. Thus it appears as if nuclei with $20 < Z < 28$ protons and $Z > 50$ protons may have smaller half-density radius parameters than the other nuclei. Neutron major shells appear to have less effect, because Mn^{55}, Ni^{58}, Cu^{63}, Cu^{65}, and Zn^{64} all have more than 28 neutrons, and In^{115} and I^{127} have between 50 and 82 neutrons. It must be realized that these conclusions regarding shell effects on r_o are of a <u>most</u> tentative nature as they depend on the nuclear models used to determine the values of $M_{n\ell}$ and which neutron shells are available.

B. <u>Available-Shell and Radius-Parameter Determinations</u>

It is perhaps more profitable to consider both the availability of the shells and the radius parameter as unknowns. Then the p,pn cross sections can be used to determine, for each target isotope, values of r_o as a function of the shells selected to be available. This has been done by using Eqs. (26), (29a), (33), or (34), Figs. 17 and 18, and occasionally Figs. 14 and 15. The results are given in Fig. 20. The ordinate gives the half-density radius parameter, and the abscissa gives the neutron shells in the order in which they appear in the shell.[33,84]

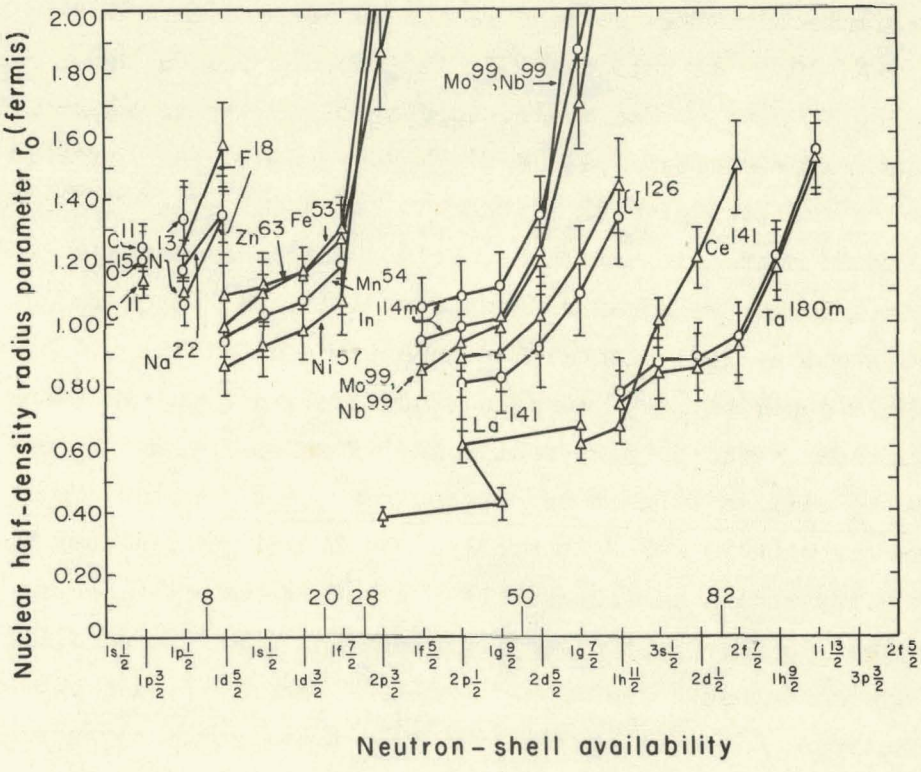

Fig. 20. The half-central-density radius parameter as a function of shell availability. The points are obtained from experimental 3.0-Bev (Δ) and 5.7-Bev (O)p,pn cross sections and Eqs. 33 or 34. The solid lines connect points belonging to the same product. The abscissa of each point gives the lowest shell considered available, i.e. all shells lower down in the potential well are considered unavailable, all the shells higher in the potential well up to the highest occupied neutron shell (represented by the right hand point of the series for each product) are also considered available. The heavy solid vertical lines on the abscissa represent major neutron-shell closures.

The "x coordinate" of each point is the last shell considered available: i.e., for that point all shells below are unavailable, and all shells up to the highest neutron-containing shells are available. The lines connect points for a given target in the order of the neutron (proton in the case of La^{141}) shell filling in the well. Other than this use, the lines have no meaning. This is due to the fact that either a whole shell is available or none of it is, so the finite series of points, one for each shell, gives the total number of points possible. The series of points for each target ends at the right, corresponding to only the topmost neutron-containing shell being available. Each series extends to the left all the way to the 1s1/2 shell (all the neutrons available). However, the series were terminated much earlier both to avoid cluttering the graph and at a point where the number of shells taken to be available was considered to be more than sufficient for any reasonable nuclear model. The x coordinates for the Mo^{99}, Nb^{99} points refer to the lowest available Mo^{100} neutron shell. The lowest available Mo^{100} proton shell for the first point on the left was taken as 1f7/2. The rest of the points were computed for a 2p3/2 proton shell as the lowest available. The Cu^{62} and Cu^{64} data were omitted to avoid clutter: points for these two elements would be similar to those for Zn^{63}. The major neutron shells are indicated along the abscissa of Fig. 20.

Except for the points for C, N, and O, Fig. 20 should be considered as only approximately representing the correct situation. Under any coupling scheme there would be more points than shells. This is because a given shell could be partly available, because some of the product parent states with a hole in the given shell may be particle-unstable. The position of the points might be somewhat different also if the wave functions corresponding to an inverse exponential well were used. It is to be hoped, though, that the general characteristics of Fig. 20 would be preserved if the correct model were used; accordingly the discussion will be limited to the general features of Fig. 20.

The series of points for each element all show the same characteristic of a decrease in r_o as more shells are made available. The steepness

of the initial portion on the right of each series is dependent on the number of nucleons in the topmost occupied shell. Iodine-127 and Ta^{181} have many neutrons and protons respectively in the topmost shells, whereas In^{115} has only two neutrons. For several elements, the series of points make it possible to put lower limits on the number of shells available. Thus for In^{114m} the large value of r_o required, if only the 1g7/2 and 1h11/2 shells are available, make it quite likely that a large part or all of the 2d5/2 neutron shell is also available. Similarly the unreasonable values of r_o required for Mn^{54}, Ni^{57}, Cu^{62}, Cu^{64}, and Zn^{63} if the 1f7/2 level is unavailable show that much of or all the 1f7/2 neutron shell is probably allowed. This is rather striking in that the 1f7/2-1f5/2 spacing more than crosses a major shell closure.

The upper limits on the number of shells available can not be set because of the flatness of the point series for each element. Conversely, by the same token, lower limits on r_o can be set which vary from about 1.0 fermi for the lightest elements down to roughly 0.6 fermi for Ta^{180m}. These lower limits would correspond to all the neutrons being available. It is evident from Fig. 20 that if the available shells correspond to some point in the flat region of the point series for each target element, then there appears to be a general decrease in the r_o values from 1.2 fermis for the light elements down to 0.8 fermi for the heavier elements. (Again these numbers are model dependent. However they should be less sensitive to details of the model than other quantities as they are almost independent of the number of available neutrons.) This decrease in r_o is much the same as the general trend observed in Fig. 19.

The considerations of the last two paragraphs show that some p,pn cross sections can be used to determine the availability of certain shells and, through the data in Table VI, upper or lower limits on the excitation energy of the neutron-hole states in these shells. It has already been shown how the zinc and copper p,pn cross sections were used to show that at least a considerable part of the 1f7/2 neutron shell is probably available. From Table VI it appears that the excitation energies of at least most 1f7/2 neutron-hole parent states, relative to the p,pn-product

ground state formed by the removal of a 1f5/2 neutron, are less than 8 Mev. The same results are obtained from the mangese and nickel cross sections for the p,pn-product ground states (removal of a 2p3/2 neutron). Similar considerations apply to the 2d5/2 hole state relative to the In^{114} ground state. Other, as yet unmeasured, p,pn cross sections would yield more similar upper limits. For example the p,pn cross sections of Nb^{93} or Ru^{96} would show whether the 1g9/2 neutron shell is available or not. From these results, limits on the excitation energies of many of the 1g9/2 neutron-hole parent states across the N = 50 major shell compared to removal of a 2d5/2 neutron can be set. The fact that the Mo^{100} result contains p,2p contributions makes it difficult to use it to draw conclusions about the 1g9/2-1g7/2 hole-state energy difference.

C. The Problem of Ce^{142}

The values of r_o given in Fig. 20 and obtained from the cross sections for the reactions $Ce^{142}(p,2p)La^{141}$ and $Ce^{142}(p,pn)Ce^{141}$ pose a problem in that the maximum value of r_o obtained for La^{141} (0.67 ± 0.05 fermis) is unreasonably small. The values of r_o obtained from the Ce^{141} production cross section range from less than 0.67 fermis to 1.5 fermis. A possible explanation for the small value of r_o obtained for La^{141} is that there is a strong coupling between the two 2f7/2 neutrons and the 1g7/2 proton hole in La^{141}. Therefore many of the La^{141} parent states are unstable to particle emission. This would decrease the number of available neutrons and increase the value of r_o. A similar strong coupling can also be allowed between the two 2f7/2 neutrons and 1h11/2, 3s1/2, and 2d3/2 neutron-hole states of Ce^{141} if one assumes that the three closely spaced 1h11/2, 3s1/2, and 2d3/2 neutron shells[84] are available. However the effect of this coupling on La^{141} seems unreasonably large when compared to the effect on other nuclei represented in Fig. 20.

There are several other possible explanations of the small maximum value of r_o obtained for La^{141}. The nucleus can be large, with a diffuse surface (only the 2f7/2 neutrons available for Ce^{141} production)

and with the protons strongly concentrated towards the center. This concentration is beyond that already given by the sum over squared harmonic-oscillator wave functions for $N > Z$ [Eq. (22)]. This seems unlikely, because the concentration required to fit the La^{141} cross section is unreasonably large. Also other work shows that the radial neutron and proton density distributions are not too different from one another.[94,95] Another alternative is that the Ce^{142} nucleus is quite small and has relatively little surface. This also seems unlikely in that a half-density radius of 0.6 to 0.8 fermis is an extreme reduction compared to other nuclear radii. A third alternative is that the order of proton-shell filling in Ce^{142} is wrong, and the highest filling proton shell is some shell other than the 1g7/2 shell with just a few protons in it. However, this alternative is contradicted by the observed ground-state spins and parities of the odd-Z, odd-A nuclei from antimony through lanthanum.

It is interesting to examine the possibility that the Ce^{142} nucleus consists of an essentially square-density Ce^{140} core with a diffuse surface generated by the two 2f7/2 neutrons outside the core. Thus the La^{141} production cross section and the Ce^{140}-core contribution to the Ce^{141}-production cross sections can be determined by the square-density results given in Appendix V. By the use of the highest particle-stable excitation energies for Ce^{141} and La^{141} from Table VI and Eqs. (E3), (E4), (E6), and (E7) in Appendix V [for La^{141}, N is replaced by Z in Eq. (E6)] the La^{141} and the Ce^{140}-core part of the Ce^{141} production cross section turn out to be both equal to 3.7 mb (r_o was taken to be 1.3 fermis). The surface contribution of the two 2f7/2 neutrons to the Ce^{141}-production cross section can be estimated from Fig. 17 and Eq. (26) (R_o = 1.3 fermis) and Eq. (34) to be 12.5 mb. These results give cross sections for the reactions $Ce^{142}(p,pn)Ce^{141}$ and $Ce^{142}(p,2p)La^{141}$ of roughly 16 and 4 mb, respectively. These numbers are in satisfactory agreement with the experimental values of 24 and 4.2 mb.[54] The validity of this model can be checked by measuring the $Ce^{140}(p,pn)Ce^{139}$ reaction cross section because this model would predict a cross section about

equal to that for La^{141}. The other alternatives mentioned before all give a larger cross section for Ce^{139} production from Ce^{140} than for Ce^{141} production from Ce^{142}.

D. Nuclear Rearrangement

The approximations used in deriving Eqs. (22) and (32) to (34) and their use with the experimental high-energy p,pn cross sections reveal an interesting result. In this work p,pn reactions have been assumed to occur when a multi-Bev incident proton enters a nucleon and strikes a neutron in a given shell, and the reaction products leave the nucleus all in a time short compared to nuclear rearrangement time. This allows one to consider the nucleus as a container for nucleons whose momenta and shell distribution can be taken to be that of an unperturbed nucleus. After the collision products have escaped, the nucleus is left in any one of a number of excited parent states whose minimum excitation energy is that of the independent-particle neutron-shell hole state. The energy distribution of these states is equal to the excitation energy of the neutron-hole state plus the distribution of the rearrangement energy.[96] In this context, the rearrangement energy consists of all the energy released when the nucleus goes from the ground state of the target minus one neutron from a given shell to the corresponding neutron hole states of the product. This energy comes from such sources as the recoupling of the nuclei in open shells when a neutron is removed, a slight radial shrinkage of the nuclear potential well, etc. The point in this work is that the nuclear rearrangement associated with the snatching of a neutron from an available shell must predominantly populate product states whose excitation energy is less than the highest particle-stable excitation energy of the product nucleus, or about 8 Mev. If the rearrangement were such that all populated product states were more than 8 Mev above the ground state, all p,pn cross sections would be equal to zero.[96]

It is possible in several cases to set the upper limit on the rearrangement energy associated with the states predominantly populated by nuclear reorganization at less than the highest particle-stable excitation

energy of the product nucleus. As has been discussed in Part I, the only particle-stable state of N^{13} is the ground state, the proton binding energy (1.95 Mev) being below the first excited state (2.37 Mev).[21] Further, the low value of the p,pn cross section for N^{14} is explained satisfactorally by the low number of available neutrons (See Table VII and Figs. 19 and 20). Consequently, the nuclear rearrangement associated with the snatching of a 1p1/2 neutron from N^{14} must predominantly populate the ground state of N^{13}. The energy associated with this rearrangement to the N^{13} ground state must be zero Mev.

A similar situation exists for the product O^{15}. From Table VI and Figs. 19 and 20 it can be seen that the $O^{16}(p,pn)O^{15}$ cross section is satisfactorally explained by taking the 1p1/2 and 1p3/2 neutron shells to be available. If one assumes that, because of a large rearrangement energy, the 1p3/2 shell is not available, the density radius parameter, r_o, from Eqs. (26), (29a), and (33) and Fig. 17 would have to be 2.1 fermis to give the p,pn cross section observed. The large discrepancy between this value and others (See Figs. 19 and 20 and ensuing discussion) supports strongly the availability of the 1p3/2 shell. The 1p3/2 neutron-hole state of O^{15} is at 6.14 Mev; there is one more level at 6.82 Mev before the first particle-emitting level at 7.61 Mev is reached (Part I).[21] This part of the level scheme shows that the nuclear rearrangement occurring after a 1p3/2 neutron has been snatched out must predominantly populate either the 6.14-Mev level or the 6.82-Mev level of O^{15}. The respective energies associated with rearrangement to these two levels are zero Mev and 0.68 Mev.

This same argument can be carried into heavier nuclei. It has already been shown how the buried 1f7/2 neutron shell in Cu^{63}, Cu^{65}, and Zn^{64} is probably available, because its exclusion gives unreasonably large values of r_o. Snatching a neutron from the 1f7/2 closed shell of zinc or copper would give a product hole state with appreciable excitation energy (roughly 5 Mev),[84] because it is across both a major and minor (the 2p3/2) shell. Since the highest particle-stable excitation energy for zinc and copper is 8 to 9 Mev (Table VI), there must be no

large population of states whose associated rearrangement energy is greater than 3 to 4 Mev. This figure is quite approximate and is only a rough first guess. This same argument can be applied to other cases such as the 2d5/2 shell of In^{115} and possibly the 1h11/2 shell of Ce^{142}.

E. Further Uses of p,pn Cross Sections

There are other ways in which experimental p,pn cross sections combined with the results of this work can yield more information about nuclei. It has already been shown how the total p,pn cross sections can yield information about the availability of the uppermost shells. A study of those targets that yield p,pn products with isomeric states for which cross sections can be obtained for each isomer allows the group of available shells to be broken into two smaller groups. Under the assumptions of this work, the instantaneous removal of a neutron from an even-N, even-Z target leaves the nucleus in an excited state with the spin and parity of the shell from which the neutron was removed. The strong dependence of the gamma-decay lifetime on the type and multipolarity indicates that neutron-hole states in shells having high angular momentum would decay predominately into high-spin isomers and conversely. This splits the available group into shells of high and low angular momentum which are available to only the high- and low-spin isomers, respectively. This method of studying available shells having high and low angular momentum separately does not apply to odd-Z, even-N targets, because the odd proton can combine with the odd neutron of the p,pn product to give states with a large range of spins, which then decay into the isomers. It is then quite possible for both high- and low-spin neutron-hole states to populate both low- and high-spin isomers, and no such division of the available shells occurs as with the even-N, even-Z targets. The case of In^{115} has already demonstrated this point. If the odd proton is in a low spin state, the situation for even-N, odd-Z targets approaches that of even-N, even-Z targets.

Another way the p,pn cross-section data might be used to give useful information is revealed from examination of Eqs. (32) to (34).

If a sequence of p,pn cross sections is obtained for an isotopic series of targets in which a neutron shell is filling up, Eqs. (32) to (34) predict that a plot of the p,pn cross section vs. the neutron occupation number of the unfilled shell will give a straight line. From Eq. (32) the slope of the straight line would be equal to

$$\sigma M = \sigma_{tot} \left[1 + \left(F \left(\frac{\bar{\sigma}}{\sigma_1} \right)^{1/2} - 1 \right) \right] M_{\text{unfilled neutron shell.}} \quad (35)$$

The intercept would be equal to the sum over available neutron shells exclusive of the one being filled. This assumes that no change in shell availability is occurring throughout the series. Such a change is not likely to occur unless the highest particle-stable excitation energy changes a lot or is close to the excitation energy of a hole state. Neither of these factors would be expected to be very likely. Thus it may be possible to experimentally determine the values of σM for different shells. This argument assumes that the effects of nucleon-nucleon coupling are small. If the distribution in energy of the parent-product states is large, and the value of the sum over the squares of the appropriate fractional parentage coefficients is strongly dependent on the number of neutrons in the unfilled shell, then this argument fails completely.

A good illustration of the ways discussed in which p,pn cross sections might be used exists in the series of tellurium isotopes with an even number of neutrons. The p,pn products of all these isotopes have two isomeric states of spins 11/2- and 1/2+ or 3/2+.[7] Except possibly for Te^{130}, the 1h11/2 neutron shell is filling throughout the series and is probably filled at Te^{128}. Tellurium-130 contains in addition two 3s1/2 or 2d3/2 neutrons.[7,33] If one assumes that the 1h11/2, 1g7/2, and 2d5/2 neutron shells are available but the 1g9/2 shell is unavailable, then the 1h11/2 and 1g7/2 shells are available to the 11/2- isomer and the 2d5/2 shell is probably available to the 1/2+ isomer. If the low-spin isomer is a 3/2+, then the 1g7/2 shell would probably be available to the low-spin isomer. For Te^{130}, the

3s1/2 or 2d3/2 neutrons would be available to the low-spin isomer. The choice from the I^{126} point series for the same set of available shells of $r_o = 0.95$ fermis, the above assumptions, Eqs. (29a) and (33), and Fig. 18 allows the determination of the p,pn cross sections (neglecting nucleon-nucleon coupling effects). The results of these computations are given in Table VIII for 5.7-Bev protons. The cross sections given in column 3 illustrate how the isomer ratio can change depending on the spins of the isomers. It is unlikely that the cross section of the low-spin isomer would be larger than the values given, but it could be smaller if the 2d5/2 neutron shell were partially available to both shells.

Table VIII

Estimated isomer p,pn cross sections for even-N tellurium isotopes

Target isotope	Product isomer spin	Predicted isomer cross section (mb)
Te^{120}	11/2- (?)	22
	1/2+	16
Te^{122}	11/2-	27
	1/2+	16
Te^{124}	11/2-	31
	1/2+	15
Te^{126}	11/2-	36
	1/2+	15
Te^{128}	11/2-	29
	3/2+	25
Te^{130}	11/2-	28
	3/2+	29

For shells such as this one with j values midway between the isomer spins, the availability to one or the other of the isomers would be expected to depend sensitively on the details of the excited-state level scheme. The slope, 2 mb (1h11/2 neutron) is independent of which shells are available.

If the lg9/2 neutron shell were available, the cross section of the high-spin isomer would remain the same, but the cross section of the low-spin isomer would decrease. This conclusion is based on the requirement that the lg9/2 shell would then probably be available in I^{127} also, which necessitates a decrease in r_o. These results given in Table VIII are rather speculative as they depend on several assumptions and are not meant to be quantitatively accurate. Rather, they serve to illustrate the kinds of information which might be obtained from such a study.

VII. POSSIBLE ERROR SOURCES

It has been shown how the results of the theory embodied in Eqs. (32) to (34) and Figs. 17 and 18 may help to understand nuclear structure more clearly by yielding information about nuclear radii and hole-state excitation energies. These results have been derived from a theory based on several simplifying assumptions, such as the impulse approximation, single nucleon-nucleon collisions, and classical nucleon and pion trajectories inside the nucleus. Besides these assumptions and the difficulties inherent in using the independent-particle harmonic-oscillator model to represent real nuclei, there are other implicit approximations in the theoretical results. A discussion of these points will help to put this work in a better perspective.

There are a few sources of possible error in the assumption made that the effective average exit cross section, $\bar{\sigma}$, is a sum of cross sections for pion-nucleon and nucleon-nucleon collisions averaged over event types and particle energies and corrected for the exclusion principle. One source stems from the neglect of the wave properties of high-energy pions and nucleons. If a nucleon and a pion are scattered at an included angle of 20° and 300 Mev kinetic energy each -- not unreasonable figures,[56,57] -- then the nucleon and pion must travel 0.8 and 1.1 fermis respectively before their separation is greater than the pion reduced wavelength. This is an appreciable distance of travel compared to nuclear dimensions. For this part of their paths where the particles are closer than a wavelength apart, the cross section for interaction with nucleons would not be just a sum of individual nucleon-nucleon and pion-nucleon collision cross sections because there would be interference of some sort between the pion and nucleon.

Another source of error which also arises from the neglect of the wave properties of the colliding nucleons is that, depending on the angular distribution of the emitted nucleons and mesons, the momentum transfer to the target nucleon along the incident-particle direction can be very small for high incident energies. The uncertainty principle

then shows that it can be impossible to localize the collision to within a nucleon dimension, or even nuclear dimensions as has been done in Eqs. (10) et seq. This problem has been treated in the literautre and conditions given to determine if the collisions can be localized.[97] The meson energies in the "reconstructed events" used to determine $\bar{\sigma}$, were used in the appropriate condition equation.[97] It appears that on the whole the picture of a collision localized to within nuclear dimensions has approximate validity. For about one half of the $pp\pi^-$ events and many of the $pn\pi^+\pi$ and $pn\pi^+\pi^-\pi^0$ events at $E_N = 3.8 \pm 2.4$ Bev, the collisions are localized to nucleon dimensions.

An error source affecting $\bar{\sigma}$ may exist if the isobar model of pion production from high-energy nucleons is valid inside the nucleus.[44,57] Since the isobar states have small but finite lifetimes, the nucleon-nucleon collision products traverse the first part of the path as isobars which then each decay into pions and a nucleon. Consequently for the first part of the path, $\bar{\sigma}$ consists of cross sections for nucleon isobar - nucleon collisions. No error is introduced only if these cross sections are equal to the sum of the individual cross sections for isobar decay product-nucleon collisions.

The assumption made that the pion-nucleon-collision cross sections used to determine $\bar{\sigma}$ are the same inside the nucleus as out may be a further source of error. Recent theoretical work shows that various parameters describing pion interactions inside a nucleus vary strongly with energy.[98] However, the errors made in assuming the free pion-nucleon cross sections to hold inside the nucleus would be small, except possibly near the resonance.[98] The free n-p scattering data do not show strong peaking in the produced meson intensity at the resonance energy. For this reason and possible similar hard-to-correct errors in "lifting" the free n-p scattering data into the nucleus, no correction was made for this error source.

The magnitude of the error arising from these sources in the approximations used to develop the theory is very difficult to determine.

It is hoped that it is small, possibly through cancellation effects of the individual errors. Perhaps in the future it will be possible to evaluate the uncertainties arising from these sources.

There are several small errors arising from the experimental input p-n collision data and the methods of handling it. A main uncertainty in the input data is that, for $pn \rightarrow pn\pi^+\pi^-\pi^o$ and other less frequent events, the number of neutral pions produced is uncertain.[57] For this work, the number of π^o particles in each event type explicitly stated in the input data was used. There is some evidence that the average π^o multiplicity is somewhat larger than given by the above data.[63] Several errors arising from the method of treatment of the input data include neglecting the few high meson-multiplicity events in the input data (the five-prong and a few of the three-prong events were neglected), letting $A/2 = N = Z$ for all target nuclei, etc. in the determination of $\bar{\sigma}$. These and other errors arising from the method of event reconstruction and estimation of the reduction in $\bar{\sigma}$ due to the exclusion principle should be small.

VIII. SUMMARY AND CONCLUSION

The failure of the model used in the Monte Carlo calculations to predict either the right magnitude or dependence on target element of the p,pn cross sections for Bev protons has been evident for some time. The lack of a nuclear surface and shell structure in the model have been suggested as the most likely reasons for lack of agreement between theory and experiment.

In order to remedy this situation, a theoretical treatment of simple nuclear-reaction cross sections, as exemplified by that of the p,pn reaction, was developed which allows the use of several different nuclear models. The theory is based on several simplifying factors which appear to be valid in the multi-Bev bombarding-energy range. These factors are the impulse and zero-degree scattering-angle approximations, use of classical trajectories for the incident and scattered particles, and quantum mechanical treatment of the target particle. Equations (19) and (20) give the results of the theoretical treatment using the above simplifying approximations.

In order to obtain numerical results, the independent-particle harmonic-oscillator nuclear model with spin-orbit coupling was chosen because it gives a diffuse nuclear surface, shell structure, and analytic wave functions. In the interests of self consistency, the same wave functions were used to give the total nuclear density as well as the probability of finding a nucleon with a given set of quantum labels at a given point. Equation (23) was integrated on the IBM-701 for several shells and target elements over the periodic table for a range of values of the spring constant. Cross sections σ_1 and σ_2 were set equal to 30 mb and 180 mb respectively; $\bar{\sigma}$ was determined from the 4-Bev cloud chamber data. Then for F^{19}, Cu^{65}, and Ce^{142}, $M_{n\ell}$ was determined as a function of $\bar{\sigma}$. The Bev cloud chamber data were reworked using the plots of $M_{n\ell}$ vs $\bar{\sigma}$ to weight the values of Σq_i obtained. The new values of $\bar{\sigma}$ obtained (168 mb for 4-Bev neutrons and 160 mb for 1.72-Bev neutrons) were included in Eqs. (33) and (34) by means of Eq. (29b).

These results and a rather crude approximation for the contribution from the elastic part of the p-n collision give the p,pn cross section as a function of shell availability and nuclear density distribution [Eq. (33) or (34)]. Use of the experimental cross sections and reasonable choices of shell availability give reasonable values for the nuclear size, in contrast to the model used in the Monte Carlo work which requires too large a nucleus to fit the observed p,pn cross sections (Fig. 19). This result confirms the requirement of a diffuse nuclear surface for the explanation of p,pn reaction cross sections.

The low-Z elements for which the available shells are known give values of the nuclear half-density radius parameter of 1.20 ± 0.11 fermis (Fig. 19), larger than the value of 1.03 fermis for the electron-scattering charge distribution using the same nuclear model. Since $\bar{\sigma}$ would have to be reduced rather drastically (to about 100 mb) to bring the radius parameter of the p,pn nucleon density down to that of the electron-scattering charge density, it seems that nuclear matter may extend somewhat beyond nuclear charge.

The results (Fig. 20) show also how the idea of a reasonable value of the nuclear radius parameter may be used with some p,pn cross sections to determine the minimum number of available shells. Coupled with the highest particle-stable excitation energy of the product nucleus, this information can be used to help decide which nuclear models give more appropriate energy eigenvalues. For example, this argument shows that in Zn^{64}, Cu^{63}, and Cu^{65} the 1f7/2-1f5/2 neutron-level spacing must be appreciably less than 8 Mev.

The Ce^{141} and La^{141} data present somewhat of a problem in that the p,pn and p,2p cross sections are low. One possible explanation is that strong nucleon-nucleon coupling reduces the number of available nucleons for the p,pn and p,2p reactions. Other possible explanations are that either the protons are well inside the neutrons -- more than given by the fact that N is greater than Z -- or that the Ce^{140} core has a negligible surface and the two 2f7/2 neutrons generate the Ce^{142} diffuse surface. The Ce^{140} p,pn cross section would allow a choice between these alternatives.

A general consideration of the mechanism of p,pn reactions at high energies shows that the rearrangement energy associated with states predominantly populated by nuclear reorganization after a neutron has been snatched away must be less than the highest particle-stable excitation energy of the product nucleus (roughly 8 Mev). This upper limit on the rearrangement energy of largely populated states can be extended even lower for several target nuclei. In particular, for N^{14} and O^{16} targets the energy associated with the rearrangement to the N^{13} ground state and the O^{15} 6.14- and 6.82-Mev states must be less than zero Mev and 0.68 Mev respectively. A similar conclusion holds for the targets Zn^{64}, Cu^{63}, and Cu^{65} for which it is shown that the buried 1f7/2 neutron shell is very likely available. The appreciable 1f7/2 hole-state excitation energy in these targets depresses the upper limit of the rearrangement energy for populous product states well below the highest particle-stable excitation energy.

The existence of isomeric states of the p,pn products allows the division of the available shells into high and low angular momentum groups and the separate study of each group. Even-even target nuclei are much more suitable for this purpose than are even-odd nuclei. This is due to the fact that there is only one spin and parity possible for a neutron hole in a given shell. For even-N, odd-Z, targets, a wide range of spins is usually possible for a hole in a given neutron shell. A possible series of p,pn cross sections for the even-N tellurium isotopes was computed to show how the isomeric states can be used. The series also shows how further information, such as experimental values of some of the constants [Eq. (35)], can be obtained.

The results of this work indicate that a lot of information may be obtained from p,pn-reaction cross sections in the multi-Bev region. Much more experimental data is certainly needed. Furthermore, all but a small part of this work covered p,pn cross sections, whereas p,2p, $p,p\pi^+$, and $p,p\pi^-$ (or p,n) reaction cross sections can also be treated in the same manner as the p,pn cross sections. Equation (20) holds for p,2p as well as p,pn reactions and, with the inclusion of another factor can be also used for $p,p\pi^+$ and $p,p\pi^-$ reactions.

IX. ACKNOWLEDGMENTS

I want to express my gratitude to Professor Isadore Perlman under whose supervision this work was done. My thanks are extended to Dr. L. Currie who performed the tritium analyses, and to Dr. M. Kalkstein who performed one of the Na^{22} analyses and helped with a few other bombardments. I also want to thank Professors John Rasmussen and Kenneth Watson, and Drs. Lester Winsberg, John Alexander, Jack Uretsky, and especially Dr. Wladyslaw Swiatecki for many helpful and illuminating discussions. I am very grateful to Professor Ben Mottelson for reading this manuscript and offering many helpful suggestions. My sincere thanks are extended to Edward Lofgren and the Bevatron operating group for help with the target bombardments. I am grateful to Alice McMullen for assistance with the computer programming. Ted Ross, Tom Dowd, and the computer-center group were very helpful with the IBM-701 computer operation.

This work was done under the auspices of the United States Atomic Energy Commission.

APPENDIX I

Angular and energy distributions are easily obtained from elastic p-p collisions because the angular dependence of the scattered products at high energies in the c.m. system is known.[65,66] In the absence of experimental data at Bev energies, the angular dependence of the p-n elastic cross section in the c.m. system is taken to be the same as that of the p-p elastic cross section in the forward c.m. hemisphere.[99,100]

In the elastic nucleon nucleon collisions, the recoil energy, T_2, in the laboratory system of the target particle is given by Eqs. (7a) and (13) of Reference 100:

$$T_2 = mc^2 \left(\frac{\gamma-1}{2}\right)(1 + \cos\theta), \tag{A1}$$

where θ is the scattering angle of the target nucleon in the c.m. system, and γ-1 gives the laboratory kinetic energy in units of mc^2. From the same reference, the laboratory scattering angle, θ_2, of the target particle is given by Eqs. (6) and (13) and a trigonometric identity to be

$$\cos\theta_2 = \frac{(\gamma-1) + (\gamma+3)\cos\theta}{(\gamma+3) + (\gamma-1)\cos\theta} . \tag{A2}$$

The numbers of neutrons from elastic p-n collisions ... scattered per unit scattering c.m. angle into the solid angle $2\pi\sin\theta d\theta$ and normalized to one incident proton, is given by

$$\frac{dN}{d\theta} = (n+1)\cos^n\theta \sin\theta . \tag{A3}$$

This result is obtained from the $\cos^n\theta$ dependence of the p-p differential scattering cross section in the forward c.m. hemispheres.[65]

The fraction of collisions, F_T, which scatter target neutrons with a laboratory recoil kinetic energy of T or less is obtained by integrating Eq. (A3) between the limits π and θ_M. The value of θ_M is obtained from Eq. (A1) with T_2 set equal to T. These operations give

$$F_T = \left[1 - \left(1 - \frac{2T}{mc^2(\gamma-1)}\right)^{n+1}\right] . \tag{A4}$$

APPENDIX II

The totally antisymmetric nuclear wave functions for the ground state of a stable nucleus with two open shells and A j-j coupled nucleons is given by[69,101]

$$\Psi_A(JM_J TM_T) = \mathcal{S} \prod_{i=1}^{p-2} \Psi_i(j_i^{n_i}\tau^{n_i}0000) \sum_{M_J'} C(J_1J_2J;M_J',M_J-M_J') \Psi_{p-1}(j_{p-1}^{n_{p-1}}\tau^{n_{p-1}}J_1M_J'T_1M_T') \Psi_p(j_p^{n_p}\tau^{n_p}J_2M_J-M_J',T_2M_T-M_T'). \quad (B1)$$

The first p-2 shells are the closed shells with spin and iso spin, and their respective projection quantum numbers, J, T, M_J, and M_T all equal to zero. The Clebsch-Gordan coefficient uncouples the spins of the (p-1)th and pth open shells. A similar C coefficient uncoupling the isotopic spins of the two unfilled shells has been left out. This is (due to the fact that) for all stable nuclear ground states, the C coefficient uncoupling the isotopic spin of any shell, filled or unfilled, from the rest of the nucleus is in its stretched condition,[69] $(T_1+T_2=T)$, and consequently we have $|C|^2 = 1$. This holds for any number of shells in the ground-state configuration with respect to nuclear charge states. For this reason and the fact that nuclear ground states (configuration mixing excluded) contain at most two unfilled shells with respect to the spin states, Eq. (B1) will give, in this work, the same results as a more general wave function that represents all stable nuclear ground states with any number of open $T = M_T$ shells.

The antisymmetrizing operator, $\mathcal{S}$, is given by[101]

$$\mathcal{S} = \left(\frac{n_1!n_2!\cdots n_p!}{A!}\right)^{1/2} \sum_Q (-1)^q . \quad (B2)$$

The sum is over all permutations of nucleons between shells, q is the number of nucleon exchanges required to give a permutation Q, and $A = \sum_{i=1}^{p} n_i!$. The number of nucleons in the ith shell is given by n_i. The normalization factor is the square root of the number of possible intershell permutations.

It is useful to repeat Eq. (13) of the text here:

$$P_k = \int \Psi_A^* \, \Psi_A \, d\tau \ , \tag{B3}$$

where the integration is over all coordinates of all nucleons except the space coordinates of the kth nucleon. Here P_k is the probability that the kth nucleon is at a given space point. Substitution of Eqs. (B1) and (B2) into Eq. (B3), performing the antisymmetrizing operation, and taking account of the orthonormality of all the shell wave functions except for the ith shell in each term of the i sum gives the result,

$$P_k = \sum_{i=1}^{p-2} \frac{n_i}{A} \int \Psi_i^* \, (j_1^{n_i} \tau^{n_i} 0000) \ \Psi_i (j_i^{n_i} \tau^{n_i} 0000) d\tau_i$$

$$+ \sum_{M_J' \mu_J'} C(J_1 J_2 J; M_J', M_J - M_J') C(J_1 J_2 J; \mu_J', M_J - \mu_J') \delta_{\mu_J', M_J'}$$

$$\left[\frac{n_{p-1}}{A} \int \Psi_{p-1}^* (j_{p-1}^{n_{p-1}} \tau^{n_{p-1}} J_1 \mu_J' T_1 M_T') \ \Psi_{p-1} (j_{p-1}^{n_{p-1}} \tau^{n_{p-1}} J_1 M_J' T_1 M_T') d\tau_{p-1} \right.$$

$$\left. + \frac{n_p}{A} \int \Psi_p^* \, (j_p^{n_p} \tau^{n_p} J_2, M_J - \mu_J', T_2 M_T') \ \Psi_p (j_p^{n_p} \tau^{n_p} J_2 M_J - M_J', T_2, M_T - M_T') d\tau_p \right] , \tag{B4}$$

where $d\tau_i$ refers to all the ith shell nucleon coordinates except the space coordinates of the kth nucleon. The factor n_i/A arises from the following considerations. Out of all the $A!/(n_1! n_2! \cdots n_p!)$ nucleon permutations between shells there are $(A-1)!/(n_1! n_2! \cdots (n_i - 1)! \cdots n_p!)$ permutations in which the kth nucleon in the ith shell does not take part, i.e., it occupies the same place in the ith shell. Each one of these permutations contributes an identical term in Eq. (B4). The summation over all of these permutations, for which the kth nucleon is fixed in the ith shell, and combination with the normalization factor obtained from Eq. (B2) give n_i/A.

In order to simplify the writing from here on, the isotopic-spin quantum numbers and coordinates will be dropped from Eq. (B4). The requirement that the struck nucleon be a neutron for p,pn reaction can be fulfilled, as is done in the main part of the text, by replacing n_i by N_i, the number of neutrons in the ith shell. One obtains the same result by keeping the isotopic-spin formalism and inserting the operator

$$\frac{1}{n_i} \sum_{j=1}^{n_i} (\tau_{zj} + 1/2)$$

between the Ψ^* and Ψ terms in Eq. (B4). Here $\tau_{zj}+1/2$ gives unity if the exposed nucleon is a neutron and zero if it is a proton. Transformation of the wave functions in Eq. (B4) to linear combinations of single-particle wave functions and integrations over the isospin coordinates of all nucleons, using the above operator, results in the factor N_i/n_i inside the i sum. The combination of this factor with the n_i/A gives the same result as the replacement of n_i by N_i given above.[102]

The wave functions in Eq. (B4) have to be transformed so that the coordinates of a single nucleon appear explicitly. The terms in the i sum for closed shells will be treated first. We have[69] (the isospin quantum numbers are all suppressed)

$$\Psi_i (j_i^{n_i} 00) = \sum_{M_i', m_\ell} C(J_i' j_i 0; M_i', -M_i') \; C(\ell_i s j_i; m_\ell, -M_i' - m_\ell)$$

$$\psi (j_i^{n_i - 1} J_i' M_i') T_{r_i \ell_i j_i} Y_{\ell_i, m_\ell} \chi_{s, -M_i' - m_\ell} . \qquad \text{(B5)}$$

Here the last nucleon has been split out of the shell by use of the first C coefficient. The second C coefficient allows the separation of the spin and space parts of the single-nucleon wave function. The fractional-parentage coefficient is unity for a closed shell. The radial part of the single nucleon wave function is $T_{r\ell j}$, $Y_{\ell m_\ell}$ is a spherical harmonic, and

$\chi_{s,M_i'-m_\ell}$ is a spin function. The first and second C coefficients in Eq. (B5) are equal to[69]

$$\frac{(-1)^{J_i'+s-2M_i'-m_\ell}\,\delta_{J_i'j_i}}{(2J_i'+1)^{1/2}}\left(\frac{2j_i+1}{2\ell_i+1}\right)^{1/2} C\,(j_i s\ell_i;\, M_i', -m_\ell - M_i') \ .$$

Substitution of this expression into Eq. (B5) and the result into Eq. (B4) and integrating over all nucleon coordinates except the space coordinates of the kth nucleon gives for the closed shells

$$P_{k\,(\text{closed shells})} = \sum_{i=1}^{p-2} \frac{n_i}{A(2\ell_i'+1)} \sum_{\substack{M_i' m_\ell \\ \mu_i' \mu_\ell}} (-1)^x\, C(j_i s\ell_i;\mu_i', -\mu_\ell - \mu_i')$$

$$C(j_i s\ell_i;M_i', -m_\ell - M_i')\ \ T^2_{r_i \ell_i j_i}\, Y^*_{\ell_i m_\ell}\, Y_{\ell_i m_\ell}\, \delta_{\mu_i', M_i'}\, \delta_{\mu_\ell, m_\ell} \qquad \text{(B6)}$$

$x = 2(J_i'+s-M_i'-\mu_i')-m_\ell-\mu_\ell$ = even integer. Taking account of the delta functions and the unitary properties of the C coefficients gives

$$P_{k\,\text{closed shells}} = \sum_{i=1}^{p-2} \frac{n_i}{A(2\ell_i+1)}\ T^2_{r_i \ell_i j_i}\ Y^*_{\ell_i m_\ell}\ Y_{\ell_i m_\ell} \ ,$$

which, by the spherical-harmonic addition theorem,[70] gives finally

$$P_{k\,\text{closed shells}} = \frac{1}{4\pi A} \sum_{i=1}^{p-2} n_i\ T^2_{r_i \ell_i j_i} \ . \qquad \text{(B7)}$$

This result also holds for open shells if $J = 0$.

The treatment for open shells with $J \neq 0$ is more complex than for the closed shells. Considering the pth open shells, one has, from Eq. (B4), a relation similar to Eq. (B5):[69,103]

$$\sum_{M_J'} C(J_1' J_2 J; M_J', M_J - M_J') \, \Psi_p(j_p^{n_p} J_2 M_J - M_J') = \sum_{\substack{J' M_J' \\ M_J'' m_\ell}} F_{J'} C(J_1 J_2 J; M_J', M_J - M_J')$$

$$C(J' j_p J_2; M_J'', M_J - M_J' - M_J'') \; C(\ell_p s j_p; m_\ell, M_J - M_J' - M_J'' - m_\ell)$$

$$\psi(j_p^{n_p - 1} J' M_J'') T_{r_p \ell_p j_p} Y_{\ell_p m_\ell} \chi_{s, M_J - M_J' - M_J'' - m_\ell} , \qquad \text{(B8)}$$

where $F_{J'}$ is a fractional parentage coefficient. The C coefficients on the right-hand side of Eq. (B8) are not in a suitable form for their removal. They can be brought into such a form by use of the symmetry relations of the C coefficients[69] and relationships between Clebsch-Gordan and Racah coefficients.[104] After use of Eqs. (3.16b),[69] (6.4b),[104] (3.16b), (6.4b), (3.16b) twice, (3.17a),[69] and finally (3.16b) again, in the order given (the equation numbers refer to the references given), one gets the cumbersome expression

$$\sum_{M_J'} C(J_1 J_2 J; M_J', M_J - M_J') \; \Psi_p \, (j_p^{n_p} J_2 M_J - M_J') = \sum_{J' J'' J'''} F_{J'}$$

$$\left[\frac{(2j_p+1)(2J''+1)(2J_2+1)(2J'''+1)(2J+1)}{2\ell_p+1} \right]^{1/2} W(\ell_p s J_2 J'; j_p J'') \; W(\ell_p J'' J J_1; J_2 J''')$$

$$\sum_{M_J' M_J'' m_\ell} C(J J''' \ell_p; M_J, m_\ell - M_J) C(J_1 J'' J'''; M_J', M_J - m_\ell - M_J') C(J' s J''; M_J'', M_J - M_J' - m_\ell - M_J'') (-1)^x$$

$$\psi(j_p^{n_p - 1} J' M_J'') \, T_{r_p \ell_p j_p} \, Y_{\ell_p m_\ell} \; \chi_{s, M_J - M_J' - M_J'' - m_\ell} , \qquad \text{(B9)}$$

where $x = 2J_1 + 2J'+s+j_p - J''' + M_J-m_\ell-\ell$ is an integer. The W coefficients are the Racah coefficients. There is a similar expression for the conjugate pth-shell wave function. If Eq. (B9) and its conjugate are substituted into the pth-shell term of Eq. (B4), and the integrations performed, the result is a form which allows the M''_J and M'_J sum to be done over the third and second C coefficients, respectively.[69] One then gets for the pth-shell term in Eq. (B4) $[(-1)^{2x}=1]$

$$P_{kp} = \frac{n_p}{A} \sum_{J'J''J'''} F^2_{J'} \left[\frac{(2j_p+1)(2J''+1)(2J_2+1)(2J'''+1)2J+1)}{2\ell_p+1} \right] \tag{B10}$$

$$W^2(\ell_p s J J'; j_p J'') \, W^2(\ell_p J'' J J_1; J_2 J''') \sum_{m_\ell} C^2(JJ''' \ell_p; M_J, m_\ell - M_J) T^2_{r_p \ell_p j_p} Y^*_{\ell_p m_\ell} Y_{\ell_p m_\ell} .$$

The substitution of Eq. (B10), a similar expression for the (p-1)th shell, and Eq. (B7') into Eq. (B4) gives a result which can now be substituted into Eq. (12) of the main text. However, this result refers to a target nucleus whose spin projection on the quantization axis has a certain value M_J. Equation (12) must be averaged over all the possible orientations of the nucleus with respect to the coordinate axis (here taken to be the beam direction). Since the nucleus is in an essentially field-free region, each value of M_J is equally probable, and the averaging operator for Eq. (12) is

$$\frac{1}{2J+1} \sum_{M_J=-J}^{J} .$$

From Eqs. (B10) and (12) it can be seen that the integrand does not depend on M_J or J. The averaging over M_J may then be brought inside the integral to operate on P_{kp} and P_{kp-1} in Eq. (B10). The remaining C coefficient in Eq. (B10) is the only factor depending on M_J, and so the M_J sum can be done to give

$$\frac{1}{2J+1}\sum_{M_J} P_{kp} = \frac{n_p}{A}\sum_{J'J''J'''} F^2_{J'}\left[\frac{(2j_p+1)(2J''+1)(2J_2+1)(2J'''+1)}{2\ell_p+1}\right]$$

$$W^2(\ell_p s J_2 J'; j_p J'')\, W^2(\ell_p J'' J J_1; J_2 J''')\, T^2_{r_p \ell_p j_p} \sum_{m_\ell} Y^*_{\ell_p m_\ell} Y_{\ell_p m_\ell}. \qquad (B11)$$

The unitarity of the Racah and fractional-parentage coefficients allows the J''', J'', and J' sums to be done in turn to give the much simplified expression

$$\frac{1}{2J+1}\sum_{M_J} P_{kp} = \frac{n_p}{A(2\ell_p+1)}\, T^2_{r_p \ell_p j_p} \sum_{m_\ell} Y^*_{\ell_p m_\ell} Y_{\ell_p m_\ell}.$$

The spherical-harmonic addition theorem[70] gives the final result

$$\frac{1}{2J+1}\sum_{M_J} P_{kp} = \frac{n_p}{4\pi A}\, T^2_{r_p \ell_p j_p}, \qquad (B12)$$

where r_p is the principal quantum number of the pth shell. Substitution of Eq. B12), a similar equation for the (p-1)th shell, and Eq. (B7) into Eq. (B4) gives

$$\underline{P_k} = \frac{1}{2J+1}\sum_{M_J} P_k = \frac{1}{4\pi A}\sum_{i=1}^{p} n_i\, T^2_{r_i \ell_i j_i}. \qquad (B13)$$

Comparison of this equation with Eq. (17) of the main text shows that P_k from Eq. (B13) equals P_k from Eq. (17). This result shows that Eq. (18) of the text is the same whether or not j-j coupling is taken into account. This neglects the fact that, under j-j coupling, the density terms in the exponent of Eq. (18) would be composed also of j-j coupled wave functions like those given in Eq. (B4). Here one can't remove the C and W coefficients by summing over M_J, becuase they are in the exponent. However the effect of this would be expected to be small because of both some smearing

out of the differences by averaging over M_J and the large contribution to the nuclear density from the closed J shells for which no such effect exists. Furthermore this effect is nonexistent for even-even nuclei because J equals zero.

APPENDIX III

Equations (25) and (26) can be derived by considering the nucleus as a degenerate Fermi gas. Then the nuclear density, ρ, is given by[105]

$$\rho = \frac{16\,(2m)^{3/2}}{3h^3}\,T^{3/2}\,, \tag{C1}$$

where T is the Fermi kinetic energy of the nucleons, and m is the nucleon mass.

For a harmonic-oscillator nuclear well, T is given by

$$T = T_o - \frac{1}{2}\,m\,\omega^2\,r^2\,, \tag{C2}$$

where T_o is the Fermi energy at the center of the nucleus and ω is the oscillator frequency. If R_o is the classical turning point of a nucleon with the Fermi energy [obtained from Eq. (C2) by setting T equal to zero] then it can be seen from Eqs. (C1) and (C2) that we have

$$\frac{\rho}{\rho_o} = \left(1 - \frac{r^2}{R_o^2}\right)^{3/2}\,, \tag{C3}$$

where ρ_o is the central nuclear density. Normalization of Eq. (C3) to require that A nucleons are contained in a sphere of radius R_o gives

$$\rho_o = \frac{8A}{\pi^2 R_o^3}\,. \tag{C4}$$

Since Eq. (C1) also gives a relation between ρ_o and T_o, use of Eqs. (C4) and (C2) (at T = 0) and Eq. (C1) gives

$$\omega = \left(\frac{3}{2}\right)^{1/3}\frac{2A^{1/3}\,\hbar}{m\,R_o^2}\,. \tag{C5}$$

Since we have[71]

$$\beta = \left(\frac{m\,\omega}{\hbar}\right)^{1/2}\,,$$

we obtain

$$\beta^2 = \left(\frac{3}{2}\right)^{1/3}\frac{2A^{1/3}}{R_o^2}\,. \tag{C6}$$

For later use it is preferable to give β^2 in terms of the half-density radius, R, rather than the turning-point radius. From Eq. (C3) it can be seen that $R^2 = R_o^2 (1 - (1/2)^{2/3})$. Writing $r_o = R/A^{-1/3}$ and evaluating the numerical constants gives finally

$$\beta^2 = \frac{0.847}{A^{1/3}} = \frac{g}{A^{1/3}}, \tag{C7}$$

where g is given by

$$g = \frac{0.847}{r_o^2}. \tag{C8}$$

In spite of the approximations involved in using Eq. (C1),[105] Eqs. (C7) and (C8) give fairly accurate values of the half-density radius parameter, r_o. This was checked by plotting the actual nuclear density distribution as a function of the radius for a few values of g by using Eq. (24) and the entries in Table V for three nuclei, F^{19}, Cu^{65}, and Ce^{142}. Table IX gives the results.

Table IX

Comparison of half-density radius parameters

Element	g (fermis)$^{-2}$	Half-density radius parameter, r_o (fermis) from Eq. (C8)	from Eq. (24) and Table V
F^{19}	0.60	1.19	1.16
	0.80	1.03	1.00
Cu^{65}	0.50	1.30	1.37
	0.80	1.03	1.06
Ce^{142}	0.80	1.03	1.12
	0.90	0.97	1.06

A comparison of the results in columns 3 and 4 shows that r_o obtained from Eq. (C8) varies from being 3% too large for F^{19} to 9% too small for Ce^{142} when compared to the correct values of r_o obtained from Eq. (24) and Table V.

Appendix IV

The effective barrier against nuclear emission of particles (S-wave neutrons excluded) when gamma decay is the only competing process can be roughly estimated in the following manner.

The partial width for emission of a particle with energy E_p from a compound state of excitation energy, W, leaving a residual nucleus in state, α, is given by Eq. (33) of Reference 106:

$$\Gamma_{p\alpha}(W) = \frac{g_R \sigma_{p\alpha}(E_p)}{2\pi^2 \rho_c(W) \lambda\!\!\!^{-2}}, \qquad (D1)$$

where p refers to the emitted particle, $\rho_c(W)$ is the level density of the compound state, g_R is the statistical weight of the residual nuclear state, and $\sigma_{p\alpha}(E_p)$ is the cross section for formation of the compound state c from particle p and nuclear state α. The total width Γ_p is obtained by summing $\Gamma_{p\alpha}$ over all states α whose excitation energy is less than $W-B_p$, where B_p is the binding energy of particle p. For the cases under discussion, the energy of the emitted particle, E_p, is always well below the barrier. The strong dependence of the barrier penetrability on E_p effectively limits the sum over α to the ground state and in some cases the first excited states of the residual nucleus. Consequently, the sum over α will be limited in most cases to one residual nuclear state. The cross section $\sigma_{p\alpha}$ is given by Eq. (49) of Reference 106 to be

$$\sigma_{p\alpha} = (2\ell+1)\,\pi \lambda\!\!\!^{-2}\, P_\ell(E_p)\, \xi_{p\ell\alpha}, \qquad (D2)$$

where $\lambda\!\!\!^{-}$ is the reduced particle wavelength, $P_\ell(E_p)$ is the penetrability, and $\xi_{p\ell\alpha}$ is the sticking probability for the particle p, and ℓ is the minimum value of the angular momentum which p must carry away from the compound state c to give the residual state α. The sum over ℓ has been neglected in Eq. (D2) due to the strong dependence of the barrier penetrability on ℓ for small values of E_p. The barrier penetrability is found by setting the gamma-ray width equal to the particle width:

$$\Gamma_\gamma = \Gamma_{p\alpha}(W),$$

which gives, with Eqs. (D1) and (D2)

$$\Gamma_\gamma = \frac{(2\ell+1)\, g_R\, P_\ell(E_p)}{2\pi\rho_c(W)}\xi_{p\ell\alpha}$$

If the level density is written in terms of the level spacing $D(W) = 1/\rho_c(W)$, and $\xi_{p\ell\alpha}$ is set equal to unity,[106] then one gets

$$P_\ell(E_p) \simeq \frac{2\pi\, \Gamma_\gamma}{(2\ell+1)\, g_R\, D(W)}. \qquad (D3)$$

Here g_R, the statistical weight of the residual nuclear state, equals $2j+1$, where j is the spin of the residual nuclear state α that gives the lowest value of W satisfying Eq. (D3), and α is usually either the ground or first excited state. The residual nucleus is the p,pn product minus particle p.

The values of $\Gamma_\gamma/D(W)$ for W = 6 to 9 Mev can be obtained from the 1-Mev neutron-capture cross sections by use of Eq. (4-7) Reference 107:

$$\sigma_{n\gamma} = \frac{2\,\pi^2\,\lambda\!\!\!^{-2}\,\Gamma_\gamma}{D},$$

where $\lambda\!\!\!^{-}$ is the reduced wavelength of a 1-Mev neutron. Substitution of this equation into Eq. (D3) gives

$$P_\ell\,(E_p) \simeq \frac{1.5\,\sigma_{n\gamma}}{(2\ell+1)g_R} \qquad (D4)$$

where $\sigma_{n\gamma}$ is given in barns, and $\sigma_{n\gamma}$ can be taken from the literature data.[107] Since the values of $\sigma_{n\gamma}$ are not given for the radioactive targets under consideration here, the values for a stable target can be used. The stable target is chosen to give an $n\gamma$ compound nucleus whose mass, excitation energy, and number of nucleons or holes removed from a closed shell are similar to those of the given radioactive target. Since ℓ is different for each neutron hole state of the p,pn product and only rough estimates of the effective Coulomb barrier are needed, ℓ was set equal to zero in Eq. (D4) (S-wave proton or alpha emission) to give

$$P_o(E_p) \simeq \frac{1.5\,\sigma_{n\gamma}}{g_R} . \qquad (D5)$$

The effective Coulomb barrier given in Table VI was obtained from Eq. (D5) and published formulas and graphs[108] which give the penetrability in terms of the ratio E_p/B.

APPENDIX V

The p,pn cross sections as a function of r_o for each model of the nucleus used in the Monte Carlo calculations[52] can be computed easily under the assumptions made in this work, since all the necessary integrations can be performed analytically. The nuclear model used for the Monte Carlo calculations was that of a degenerate Fermi Gas with a uniform radial density distribution out to $R_o = r_o A^{1/3}$. For R greater than R_o, the density was set equal to zero.

These characteristics can be easily put into Eq. (20) of the main part of this work. Since the radial distribution is independent of the position and momentum of the nucleons, the n, ℓ, subscript can be removed from $T^2_{n,\ell,j}(r^2 + z^2)$, and we can write for the normalized single-nucleon distribution

$$T^2 = \frac{3}{r_o^3 A}, \tag{E1}$$

where the factor of 1/2 is outside the integrals in Eq. (20). In this model, the two density factors, $\rho(R)$ and $\rho'(R)$, will be set equal to one another because the one nucleon less in $\rho'(R)$ will have even a smaller effect than for the harmonic-oscillator model. Normalization of $\rho(R)$ to contain A nucleons in a sphere of radius $R_o = r_o A^{1/3}$ gives

$$\rho(R) = \frac{3}{4\pi r_o^3}. \tag{E2}$$

Substitution of Eqs. (E1) and (E2) into Eq. (20) and changing the infinite limits to limits on the surface of the sphere gives

$$M = \frac{3}{2r_o^3 A} \int_o^{R_o} r\,dr \int_{-\sqrt{R_o^2-r^2}}^{\sqrt{R_o^2-r^2}} \exp\left[-\frac{3\sigma_1}{4\pi r_o^3} \int_z^{\sqrt{R_o^2-r^2}} dy - \frac{3\bar{\sigma}}{4\pi r_o^3} \int_{-\sqrt{R_o^2-r^2}}^{z} dy \right] dz .$$

Evaluation of the integrals gives

$$M = \frac{8\pi^3 r_o^6}{9A(\bar{\sigma}-\sigma_1)} \left[\frac{1 - (1 + 2a_1)e^{-2a_1}}{\sigma_1^2} - \frac{1 - (1 + 2\bar{a})e^{-2\bar{a}}}{\bar{\sigma}^2} \right], \quad \text{(E3)}$$

where

$$a_1 = \frac{3\sigma_1 A^{1/3}}{4\pi r_o^2},$$

and

$$\bar{a} = \frac{3\bar{\sigma} A^{1/3}}{4\pi r_o^2}.$$

For $A \gg 1$, the sum over the allowed shells in Eqs. (33) and (34) can be replaced by an integral over the Fermi-gas density distribution from the Fermi energy T_F to a depth E_b down from the top of the Fermi sea. Here E_b is the highest particle-stable excitation energy (Table VI). Because M given by Eq. (E3) is independent of the integration variable in Eqs. (33) and (34), it can be removed outside the integration. Then one has

$$n_a = \int_{T_F - E_b}^{T_F} \left(\frac{dn}{dT}\right) dT, \quad \text{(E4)}$$

where n_a is the number of allowed neutrons.

The neutron density per unit energy, dn/dT, for a Fermi gas is found from Eq. (C1) of Appendix III[105] to be

$$\frac{dn}{dT} = \frac{4\pi (2m)^{3/2} T^{1/2}}{h^3} \left(\frac{4\pi r_o^3 A}{3}\right), \quad \text{(E5)}$$

where the last factor on the right converts dp/dT into dn/dT. The Fermi energy is obtained from Eq. (E5) by the requirement that

$$\int_0^{T_F} (dn/dT)\, dT = N, \qquad \text{where N is}$$

the total number of neutrons in the nucleus. Substitution of Eq. (E5) into Eq. (E4) along with the normalization condition for T_F gives, after rearrangement,

$$n_a = N\left[1 - \left(1 - \frac{32\, m\, r_o^2\, E_b}{h^2}\left(\frac{\pi^2 A}{18N}\right)^{2/3}\right)^{3/2}\right]. \qquad \text{(E6)}$$

Equations (33) and (34) give

$$\sigma_{ppn} = \bar{\sigma}\, n_a M, \qquad \text{(E7)}$$

where $\bar{\sigma}$ = 36 mb for 3-Bev protons and 33 mb for 5.7-Bev protons. The substitution of Eqs. (E6), (E3), and (E4) into Eq. (E7) allows one to find what values of r_o are necessary to give the observed p,pn cross sections for different target elements. The value of E_b is taken from Table VI. As before, σ_1 for 3- and 5.7-Bev protons is 36 ± 3 mb and 32 ± 3 mb, respectively, and $\bar{\sigma}$ was determined in the same manner as before but for T_F = 20 Mev and was found to be 150 mb for 4 Bev neutrons on hydrogen. If r_o is set equal to 1.3 fermis, as was done in the Monte Carlo calculations,[52] σ_{ppn} from Eq. (E7) for 3-Bev protons on Cu^{65} and Ce^{142} turns out to be 5.3 ± 0.5 mb and 3.7 ± 0.4 mb, respectively. These values are in satisfactory agreement with the actual Monte Carlo calculations which give values of σ_{ppn} for 1.8-Bev protons on Cu^{64} and Ce^{140} of 7 ± 3 mb and 10 ± 5 mb respectively.[27]

REFERENCES

1. R. Peierls, Sci. American 200, 75 (1959).

2. The spallation reactions of some of these elements have been extensively studied. See for example References 15, 26, 27, and 43.

3. Bernardini, Booth, and Lindenbaum, Phys. Rev. 85, 826 (1952).

4. Currie, Libby, and Wolfgang, Phys. Rev. 101, 1557 (1956).

5. Gerhart, Carlson, and Sherr, Phys. Rev. 94, 917 (1954).

6. Marvin Kalkstein, University of California Radiation Laboratory, private communication.

7. Strominger, Hollander, and Seaborg, Revs. Mod. Phys. 30, 585 (1958).

8. William Biller, The Characteristics of Bismuth Fission Induced by 340-Mev Protons (thesis), UCRL-2067, January 1953.

9. Frederic Benson, Chem. Revs. 41, 1 (1947).

10. M. Kalkstein and J. Hollander, A Survey of Counting Efficiencies for a 1-1/2-Inch-Diameter by 1-Inch-High Sodium Iodide (Thallium Activated) Crystal, UCRL-2764, October 1954.

11. Donald Barr, Nuclear Reactions of Copper Induced by 5.7-Bev Protons (thesis), UCRL-3793, May 1957.

12. Blaedel, Meloche, and Ramsey, Chem. Ed. 28, 643 (1951).

13. Robley Evans, The Atomic Nucleus (McGraw-Hill Book Co., New York, 1955), pp. 757-771.

14. R. Dean and W. Dixon, Anal. Chem. 23, 636 (1951).

15. Cumming, Friedlander, and Swartz, Phys. Rev. 111, 1386 (1958). This work reviews the $C^{12}(p,pn)C^{11}$ cross-section data in references 16, 26, 37, 38, and 40.

16. Horwitz, Murray, and Crandall, Bull. Am. Phys. Soc. 1, No. 4, 225 (1956); Nahmin Horwitz, University of California Radiation Laboratory, private communication.

17. D. White, Jr. and J. Burk, The Metal Beryllium (American Society for Metals, Cleveland, Ohio, 1955), p. 658.

18. R. Koch and A. Turkevich, Bull. Am. Phys. Soc. 1, No. 2, 95 (1956).

19. Luiz Marquez, Phys. Rev. 86, 405 (1952); L. Marquez and I. Perlman, Phys. Rev. 81, 953 (1951).

20. Robert Deutsch, Phys. Rev. 97, 1110 (1955).

21. F. Ajzenberg and T. Lauritsen, Revs. Mod. Phys. 27, 77 (1955).

22. M. Rich and R. Madey, Range Energy Tables, UCRL-2301, March 1954.

23. Nelson Jarmie, Phys. Rev. 98, 41 (1955).

24. R. Mckeague, Proc. Roy. Soc. (London) A236, 104 (1956).

25. Beverly Willis, High Energy Particle Data, UCRL-2426, October 1953.

26. Burcham, Symonds, and Young, Proc. Phys. Soc. (London) A68, 1001 (1955). Symonds, Warren, and Young, Proc. Phys. Soc. (London) A70, 824 (1957).

27. Markowitz, Rowland, and Friedlander, Phys. Rev. 112, 1295 (1959).

28. Considerations similar to these have been advanced concurrently by Dr. James Grover in a private communication.

29. Tyren, Hillman, and Maris, Nucl. Phys. 7, 10 (1958).

30. Hagedorn, Mozer, Webb, Fowler, and Lauritsen, Phys. Rev. 105, 219 (1957). E. Warburton and J. McGruen, Phys. Rev. 105, 639 (1957).

31. E. Bennett, Bull. Am. Phys. Soc. 3, No. 1, 26 (1958); Kuehner, Almquist, and Bromley, ibid, p. 27; F. El Bedewi and I. Hussein, Proc. Phys. Soc. (London) A70, 233 (1957).

32. P. Endt and C. Braams, Revs. Mod. Phys. 29, 683 (1957).

33. M. Mayer and J. Jensen, Elementary Theory of Nuclear Shell Structure (John Wiley and Sons, Inc., New York, 1955), p. 74.

34. D. Salter and L. Bird, Phil. Mag. (7) 44, 1305 (1953).

35. J. Dickson and T. Randle, Proc. Phys. Soc. (London) A64, 902 (1951).

36. Crandall, Millburn, Pyle, and Birnbaum, Phys. Rev. 101, 329 (1956).

37. Rosenfeld, Swanson, and Warshaw, Phys. Rev. 103, 413 (1956).

38. R. Wolfgang and G. Friedlander, Phys. Rev. 96, 190 (1954); ibid 98, 1871 (1955).

39. Chackett, Reasbeck, Symonds, and Warren, Proc. Phys. Soc. (London) A69, 43 (1956).

40. Iu. Prokøshkin and A. Tiapkin, J. Exptl. Theoret. Phys. U.S.S.R. 32, 177 (1957). [Translation: Soviet Phys. JETP 5, 148 (1957)].

41. Baker, Friedlander, and Hudis, Phys. Rev. 112, 1319 (1959).

42. Hicks, Stevenson, and Nervik, Phys. Rev. 102, 1390 (1956).

43. Friedlander, Hudis, and Wolfgang, Phys. Rev. 99, 263 (1958).

44. S. Lindenbaum, Ann. Rev. Nuclear Sci. 7, 317 (1957).

45. James Grover, The Reactions of Tantalum with 5.7-Bev Protons (thesis), UCRL-3932, September 1957.

46. Rex Shudde, Fission of Uranium with 5.7-Bev Protons (thesis), UCRL-3419, June 1956.

47. David Nethaway, Excitation Functions for Reactions of Bev Protons on Indium (thesis), UCRL-3628, January 1957.

48. Inge-Maria Ladenbauer, Interactions of High Energy Protons and Alpha Particles with Iodine-127, UCRL-8200, March 1958.

49. Gösta Rudstam, Spallation of Medium Weight Elements (thesis), Uppsala, Sweden, 1956.

50. David Templeton, Ann. Rev. Nuclear Sci. 2, 93 (1952).

51. M. Goldberger, Phys. Rev. 74, 1269 (1948).

52. Metropolis, Bivins, Storm, A. Turkevich, Miller, and Friedlander, Phys. Rev. 110, 185 (1958); 110, 204 (1958).

53. Dostrovsky, Rabinowitz, and Bivins, Phys. Rev. 111, 1659 (1958).

54. A. Caretto and G. Friedlander, Phys. Rev. 110, 1169 (1958).

55. Maris, Hillman, and Tyren, Nuclear Phys. 7, 1 (1958).

56. Fowler, Shutt, Thorndike, and Whittemore, Phys. Rev. 95, 1026 (1954).

57. Fred Holmquist, Pion Production in Neutron-Proton Collisions at Bevatron Energies (thesis), UCRL-8559, December 1958. The author also wishes to thank Dr. Holmquist for providing unpublished data.

58. Block, Harth, Cocconi, Hart, Fowler, Shutt, Thorndike, and Whittemore, Phys. Rev. 103, 1484 (1955).

59. Kalbach, Lord, and Taso, Phys. Rev. 113, 325, 330 (1959).

60. Geoffrey Chew, Phys. Rev. 80, 196 (1950).

61. W. Selove, Phys. Rev. 101, 231 (1956).

62. Wilson Powell, University of California Radiation Laboratory, private communication.

63. D. King, Phys. Rev. 109, 1344 (1958).

64. N. Duller and W. Walker, Phys. Rev. 93, 215 (1954).

65. Cork, Wenzel, and Causey, Phys. Rev. 107, 859 (1957).

66. Lester Winsberg, University of California Radiation Laboratory, private communication.

67. Fernbach, Serber, and Taylor, Phys. Rev. 75, 1352 (1949).

68. M. Mayer and J. Jensen, Elementary Theory of Nuclear Shell Structure (John Wiley and Sons, Inc., New York, 1955), Ch. IV.

69. M. Rose, Elementary Theory of Angular Momentum (John Wiley and Sons, Inc., New York, 1957), Ch. III.

70. E. Condon and G. Shortley, The Theory of Atomic Spectra (Cambridge University Press, London, 1957), Ch. III and IV, pp. 53, 178.

71. M. Mayer and J. Jensen, Elementary Theory of Nuclear Shell Structure (John Wiley and Sons, Inc., New York, 1957), p. 236.

72. Robert Hofstadter, Ann. Rev. Nuclear Sci. 7, 231 (1957).

73. Wilmot Hess, University of California Radiation Laboratory, private communication.

74. Wilmot Hess, Revs. Mod. Phys. 30, 368 (1958).

75. E. Clementel and C. Villi, Nuovo cimento 2, 176 (1955).

76. I. Ivanter and L. Okum, J. Expt'l. Theoret. Phys. U.S.S.R. 32, 402 (1957). [Translation: JETP 5, 340 (1957)].

77. R. Sternheimer, Phys. Rev. 106, 1027 (1957).

78. M. Mayer and J. Jensen, Elementary Theory of Nuclear Shell Structure (John Wiley and Sons, Inc., New York, 1955) pp. 40,41.

79. W. Frahn and R. Lemmer, Nuovo cimento 6, 1221 (1957).

80. The author wishes to thank Dr. Frank Stephens for supplying the occupation numbers of the upper shells of U^{238}.

81. S. Unna and I. Talmi, Phys. Rev. 112, 452 (1958).

82. G. Rakavy, Nuclear Phys. 4, 375 (1957).

83. J. Blatt and V. Weisskopf, Theoretical Nuclear Physics (John Wiley and Sons, Inc., New York, 1952), Ch. VII, pp. 340 to 342.

84. Ross, Mark, and Lawson, Phys. Rev. 102, 1613 (1956). The legends on Figs. 1 and 4 are interchanged in this reference: R. Lawson, Enrico Fermi Institute of Nuclear Studies, Chicago, Illinois, private communication.

85. Way, King, McGinnis, and van Lieshout, Nuclear Level Schemes A = 40 to A = 92. Nuclear Data Project, National Research Council, Washington D.C., USAEC TID 5300, June 1955, pp. 186, 187.

86. A. Wapstra, Physica 21, 367 (1955).

87. J. Ridell, A Table of Levy's Empirical Atomic Masses, Chalk River Project, Ontario, CRP 654, AECL 339, July 1956; A. Cameron, A Revised Semiempirical Atomic Mass Formula with Appended Table, Chalk River Project, Ontario, CRP 690, AECL 433, March 1957. Whenever particle binding energies could not be obtained from reference 86, the average of the values taken from the above two tables was used.

88. W. Johnson, Jr. and A. Nier, Phys. Rev. 105, 1014 (1957).

89. The author wishes to thank Dr. Lester Winsberg of this laboratory for allowing the use of his results before publication.

90. Stephen Moskowski, Beta and Gamma Ray Spectroscopy, K. Siegbahn, Ed., (Interscience Publishers Inc., New York, 1955) Ch. XIII.

91. Blatt and Weisskopf, Theoretical Nuclear Physics (John Wiley and Sons, Inc., New York, 1952), Ch. IX, pp. 482 to 483, 488 to 492.

92. Alfred E. Glassgold, Revs. Modern Phys. 30, 419 (1958).

93. Sidney Fernbach, Revs. Modern Phys. 30, 414 (1958).

94. L. Elton, Revs. Modern Phys. 30, 557 (1958).

95. Lawrence Wilets, Revs. Modern Phys. 30, 542 (1958).

96. The author is indebted to Dr. Ben Mottelson for pointing out this extra source of excitation energy and that it must contribute less energy than the binding energy of the least bound particle in the product nucleus.

97. E. Feinberg, J. Expt'l. Theoret. Phys. U.S.S.R. 28, 241 (1955). [Translation: JETP 1, 176 (1955)].

98. K. Watson and C. Zemach, Nuovo cimento 10, 452 (1958).

99. The author is indebted to Professor Kenneth Watson for suggesting the following possible angular dependence for elastic collisions of Bev protons incident on neutrons. The proton differential scattering cross section in the forward c.m. hemisphere can be taken to be the same as that from p-p elastic collision data. This is the forward diffraction peak. Superimposed on this is an inelastic differential scattering cross section. For p-n collisions this can be considered equal to the 90° c.m. differential scattering cross section from elastic p-p collisions. At multi-Bev energies, this differential scattering cross section is very small (Reference 65) and has been neglected by the author.

100. Philip Morrison, Experimental Nuclear Physics, Vol. II, E. Segre, Ed. (John Wiley and Sons, Inc., New York, 1953), Part VI, pp. 3 to 11.

101. E. Condon and G. Shortley, The Theory of Atomic Spectra, (Cambridge University Press, London, 1957) Ch. VIII.

102. The author is indebted to Dr. Ben Mottelson for a valuable discussion about this point.

103. M. Rose, Elementary Theory of Angular Momentum (John Wiley and Sons, Inc., New York, 1957), Ch. XII.

104. M. Rose, Elementary Theory of Angular Momentum (John Wiley and Sons, Inc., New York, 1957), Ch. VI.

105. Wladislaw Swiatecki, Proc. Phys. Soc. (London) A68, 285 (1955). The author is indebted to Dr. Swiatecki for a valuable discussion about the points covered in Appendix III.

106. Philip Morrison, Experimental Nuclear Physics, Vol. II, E. Segre, Ed. (John Wiley and Sons, Inc., New York, 1953), Part VI, pp. 45 to 64.

107. Donald Hughes, Pile Neutron Research (Addison Wesley Publishing Co., Cambridge, Mass., 1953), Ch. 4, pp. 109 to 114.

108. Philip Morrison, Experimental Nuclear Physics, Vol. II, E. Segre, Ed. (John Wiley and Sons, Inc., New York, 1953), Part VI, pp. 179, 193 to 198.